UNIVERSITY OF TURKU

The activity of FGFR and AR inhibitor combinatorial treatment in organotypic *in vitro* models of prostate cancer

Institute of Biomedicine
MDP Programme in Biomedical Sciences, Drug Discovery and Development
Master´s thesis

Author:
Vladyslav Melnyk

Supervisors:
Adjunct Professor Matthias Nees
Docent Malin Åkerfelt
PhD student Syeda Afshan
Institute of Biomedicine, University of Turku

18.5.2024
Turku, Finland

Master's thesis

Subject: Institute of Biomedicine, MDP Programme in Biomedical Sciences, Drug Discovery and Development
Author: Vladyslav Melnyk
Title: The activity of FGFR and AR inhibitor combinatorial treatment in organotypic *in vitro* models of prostate cancer
Supervisors: Adjunct Professor Matthias Nees, Docent Malin Åkerfelt, PhD student Syeda Afshan
Number of pages: 85 pages
Date: 18.05.2024

Androgen deprivation therapy (ADT) and androgen receptor (AR) antagonists, such as darolutamide remain as the first-line pharmacological strategy against prostate cancer (PC). Despite this, it has been estimated that 10-20 % PC patients progress to castration-resistant prostate cancer (CRPC), which is associated with a poor therapeutical response to treatment and resulting in less than 5-year survival. CRPC maintains its growth by switching AR-independent signalling pathways particularly, fibroblast growth factor receptor (FGFR)-signalling. Tumour microenvironment (TME), a physiologic 3D-environment of PC with tumour-stroma interaction and extracellular matrix (ECM), is known to contribute to the development of CRPC and AR-independence. The aim of the current thesis was to investigate the effectiveness of combining clinically utilized AR-inhibitor, darolutamide with a second-generation FGFR-inhibitor FIIN1. The second aim was to develop an *in vitro* PC model with key TME characteristics and evaluate the impact of 3D organotypic modelling, ECM and stromal component on treatment effectiveness. VCaP cell line was utilized as tumour and PF179T GFP cancer-associated fibroblasts (CAFs) as a stromal component. FIIN1 and darolutamide combination was studied in 2D, 3D and CAF-included co-culture models by evaluating proliferation, viability, and morphology of PC in response to treatment. The combination of inhibitors did not result in a distinct effect compared to inhibitors given separately. However, it was found that treatment effectivity decreased when given to more physiologic PC models. Specifically, 3D co-culture was associated with the lowest sensitivity to treatment, whereas simplistic 2D model was the most sensitive. All in all, results suggest the importance of combining both 3D modelling, ECM as well as tumour-stroma interaction in PC already *in vitro*, for achieving a good predictability in early-stages of drug screening. Furthermore, the developed 3D co-culture could be optimized for greater applicability and TME could be studied in-depth as a potential PC drug target.

Key words: Prostate cancer, Cancer-associated fibroblasts, 3D organotypic culture, FGFR inhibitor, AR inhibitor

Table of contents

1 Introduction

1.1 Pathophysiology and management of Prostate Cancer

1.1.1 Prostate cancer disease burden

Prostate cancer (PC) is estimated to be the second most frequently diagnosed type of cancer worldwide in men, surpassed only by the lung cancer. According to the Global Cancer Observatory from World Health Organization (GLOBOCAN) estimates for 2020, there were 1.414 million new PC diagnoses and 0.375 million mortalities in 2020 worldwide. In comparison to other cancer types among men in 2020 worldwide, PC is estimated to be the second by the incidence and 5th by the cause of death (Sung et al., 2021). Moreover, prostate cancer was the most diagnosed type of cancer and the second by the cause of death among men in United States and European Union in 2020 (European Union, 2023 ; Sung et al., 2021).

Meanwhile since 1990s there has been a solid progress in disease management, such as novel diagnostical screening or targeted therapies, significant changes in global incidence and mortality trends in recent decades could not been confirmed (Wang, Lu and He, 2022). As example, introduction of prostate-specific antigen (PSA) as a novel screening marker in 1990s has been suggested to be associated with increased disease incidence, decreased metastatic findings and disease-specific mortality in countries it was initially introduced, the effects of PSA screening on long-term trends remain debated (Hu et al., 2017). Introduction of novel hormonal therapies (e.g abiraterone), antiandrogens (e.g enzalutamide), taxanes (e.g docetaxel), therapies targeting alternative pathways as well as their combinations, improved overall survival (OS) of a patient indeed (Teo et al., 2019). Currently, PC has one of the most favourable 5-year prognosis among cancers when localized or regional cancer sites (Siegel et al., 2019). However, despite the progress in therapy alternatives as well as improved disease management, challenges remain for the advanced stages of the disease. Specifically, castration-resistant prostate cancer (CRPC), which is associated with an estimated OS less than 30 months despite treatment given (Aly et al., 2020). According to a meta-study published in 2011 (Kirby et al., 2011), it is estimated that 10-20 % of PC patients progress into the CRPC stage of the disease within 5 years.

1.1.2 Biology of healthy prostate

The prostate gland is a secretory organ and part of the reproductive system in males. It secretes fluids that builds up approximately one third of the ejaculate. Together with enzymes, such as (PSA), which helps to liquify semen, prostate fluid is a promoting factor in fertilization (McPhee & Hammer, 2014). Secretion of prostate fluid occurs from the luminal cells in epithelium of the prostate gland and is dependent on various factors including growth factors and androgens. The prostatic fluid is secreted into a cavity surrounded by luminal cells called acini or more specifically lumen, which is the central clear cavity of acini (Aaron et al., 2016) as portrayed in the Figure 1.

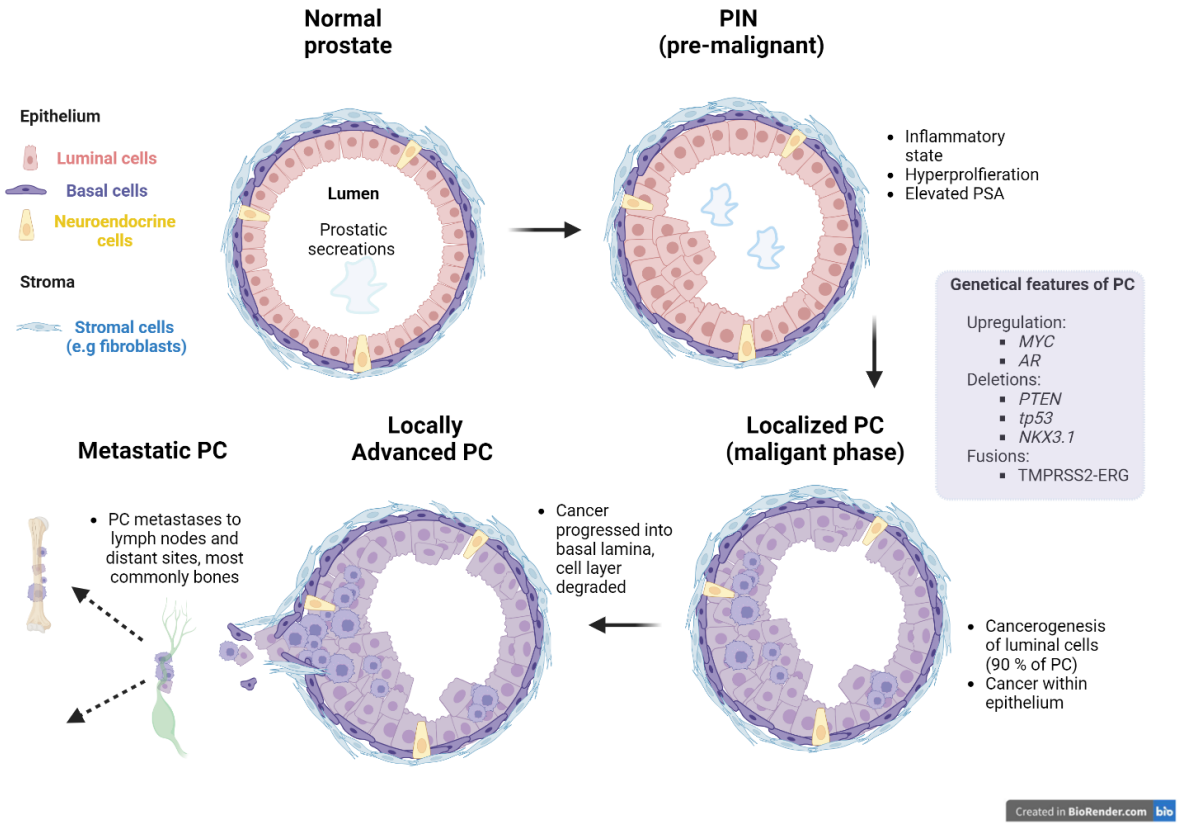

Figure 1. Main phases of prostate adenocarcinoma progression from the healthy state. In general, carcinogenesis of normal prostate begins with pre-malignant, hyperproliferative, inflammatory phase where luminal cells proliferate into acinar lumen of prostate (PIN). Next phase is considered malignant, which initially is localized within epithelium (Localized PC), but subsequently progression ruptures the cell layer and progresses into basal extracellular space of epithelium (Locally Advanced PC). In early-phase of Metastatic PC, cancer progresses to lymph nodes, providing potential to distant site metastases, which are most prevalently in bones. Genetically, PC features *MYC, AR* upregulations, *NKX3.1, PTEN and tp53* deletions as well as TMRSS2-ERG fusions. Figure created with BioRender.com.

Subsequently the fluid is collected into prostatic ducts from which it reaches the prostatic urethra (Aaron et al., 2016). In addition to luminal cells, basal and neuroendocrine cells are also part of the prostate epithelium. Meanwhile luminal cells of epithelium have mainly secretary function and are terminally differentiated, they are surrounded by basal cells, which are actively proliferating and can differentiate into secretory luminal cells when required. Basal cells are bridging the basement membrane with the luminal cells of prostate epithelium. In addition to providing luminal cell survival and cell integrity, basal cells are hypothesized to serve as a protective barrier for luminal cells in case of oncogenic event from the basolateral part of the epithelium (Xin, 2013). Neuroendocrine cells (NE) are building up the smallest part of the epithelium, around 1 %, they are elongated, tiny, microscopic cells, which function in prostate is not fully understood yet. However, it was suggested that NE cells are secreting various peptides, which enable communication with other epithelial cells. (Butler & Huang, 2021).

1.1.3 Carcinogenesis of prostate

The transformation of healthy prostate into malignant state occurs by a multi-step process, involving distinct changes in histology, commonly started as proliferative inflammatory atrophy (PIA) followed by prostatic intraepithelial neoplasia (PIN). While PIAs could be identified as overall inflammatory state of prostate, PINs are already seen as pre-malignant neoplastic developments of prostate (Packer & Maitland, 2016). These neoplastic changes or enlargements of epithelial cells in acini or ducts are also sharing some of the molecular and genetical phenotypes with prostate cancer. PINs are considered as an intermediate state between healthy and malignant prostate, as well as clinically accepted precursor for prostate carcinogenesis in specifically adenocarcinomas (Brawer, 2005).

Approximately 90 % of PC occur as adenocarcinomas, which arise from mucus-producing epithelial cells with secretory function, so luminal cells of prostate (Alizadeh & Alizadeh, 2014). However, it remains debatable whether luminal, basal, their progenitor stem cells, or other cell types could be the cell of origin in adenocarcinoma oncogenesis (Zhang et al., 2018). Moreover, several hypothetical mechanisms for the cell of origin in PC were proposed. In particular, tumour initiation from immune cells where malignant changes are induced into prostate stromal cells, resulting in reactive – stromal microenvironment and subsequent tumour initiation in prostate epithelium. (Barron & Rowley, 2012).

Another hypothetical mechanism suggests tumour initiation from prostate stem cells (PSCs) that can be both luminal as well as basal cell progenitors. In a particular process, tumorigenic

mutations in PSCs could generate a malignant epithelium progenitor which would eventually cover the prostate epithelium. Interestingly, PSCs were also found to promote the tumour progression in later disease stages. PSC- model could also partially explain the heterogenic cellular and histological nature of PC, as different mutations in PSCs would generate different malignant clones by a sub-clonal expansion of cancerous stem cells. The possible link between histological heterogeneity of PC and the type of PSCs initiating the tumour is an active topic of speculation. It is unclear whether PC progresses transitionally; from one phenotype to another, or clonally; histological phenotype of cancer is dependent on the type of cell of origin in carcinogenesis. (Packer & Maitland, 2016). Nevertheless, to date, it is known that histological phenotypes could not always explain the cell of origin of cancer, as genetical expression could vary significantly between even a similar histological phenotype (Xin, 2013).

1.1.4 Pathophysiology and genetics of PC

PC is commonly associated with chromosomal rearrangements, which might cause implications, leading to carcinogenesis (Packer & Maitland, 2016). The most common chromosomal rearrangements found in PC are genetical fusion of transmembrane protease serine 2 (TMPRSS2) with ERG. TMPRSS2-ERG fusions were found in 50 % of PC cases, and they are considered as a common marker of in the earliest stages of prostate adenocarcinoma. PC cases with TMPRSS2-ERG fusions were also detected to have deletions targeting tumour suppressors; *PTEN, tp53*. Additionally, loss of *NKX3.1,* overexpression of *MYC* and mutations of androgen receptor encoding gene (*AR*) were found to be overrepresented in prostate adenocarcinoma (Rebello et al., 2021 ; Wang & Zhao, 2018).

In general, initially developed PINs of prostate proliferate at first within the epithelium, which is referred as a localized adenocarcinoma. Sequentially, localized adenocarcinoma progresses into the basal part of epithelium, degrades the cell layer, and invades the basal lamina of basement membrane (Wang & Zhao, 2018), which is illustrated also in the Figure 1. This stage is often referred as a locally advanced PC. Locally advanced adenocarcinoma also possesses a potential to metastasize into lymph nodes and in turn, distant organs. The most frequent site of distant metastases in PC are bones, however also liver and lung metastases is not uncommon (Wang & Zhao, 2018). Meanwhile adenocarcinomas are commonly asymptomatic, with an exclusion of moderately common urinary incontinence in early stages of prostate neoplasms and cancer progression (Parsons et al., 2009), bone metastases in PC are accompanied with

osteoblastic lesions, bone destruction, hypercalcemia, significant pain, and frequent fractures (Wang & Zhao, 2018).

1.1.5 Diagnostic markers of cancer progression

In the clinics, prostate cancer diagnosis is confirmed by a prostate tissue needle biopsy (Litwin et al, 2017). The histological features of biopsy samples are investigated by a light microscopy, utilizing haematoxylin and eosin tissue-staining method for detection of PIAs, PINs, and other tissue architecture abnormalities (Sehn, 2018). Histopathological results are in turn classified according to the Gleason grading system. The grading system is based on a scoring within 1-10 range, in which a larger score denotes a lesser extent of differentiated cells, larger malignant changes in tissue architecture as well as poorer survival prognosis. (Packer & Maitland, 2016). The scale is divided into separate severity groups from 1 to 5 where the first group collects findings with a Gleason score ≤ 6 and is associated usually with favourable survival prognosis (Sehn, 2018). Up to date there are several hypothetical interpretations of Gleason grading on cancer progression. For example, it remains unclear whether histopathological changes are transitional, progressing from one histological phenotype to another more malignant state of PC and as a result, increasing Gleason score. Or could they be clonal, where different Gleason score is associated with different type of progenitor cells promoting malignant changes of prostate (Packer & Maitland, 2016). Nevertheless, it is well known that a higher Gleason score correlates with more aggressive cancer and poorer survival prognosis (Wang & Zhao, 2018). In addition to microscopical investigation of prostate histology, several immunohistochemical markers are also utilized for biopsy analysis. Particularly, basal cell layer specific antibodies, such as high molecular weight cytokeratin or cytokeratin 5 are sensitive markers of cancer progression since destruction of basal layer and its absence is a common feature of invasive PC (Bjartell et al., 2011).

1.1.6 Diagnostical challenges in PC

A confirmation of cancer and its severity assessment by a Gleason or immunohistochemistry, all based on histopathology have their clinical limitations. Arguably the main limitation is the timing, as biopsy samples are often taken already after significant cancer progression, in response to symptomatic evidence. In the clinics today, this issue is tackled by the recruitment of prostate-specific antigen (PSA) testing from blood. PSA is encoded by the *(KLK3) Kallikrein Related Peptidase 3* and is secreted by the luminal cells of prostate. In response to a prostate

neoplasia, growth as well as cancer progression, PSA serum levels are significantly increased (Figure 1) compared to the levels from a normal prostate. Due to its non-invasiveness and sensitivity PSA-tests are also part of a populational screenings, aimed for early cancer detection. However, due to its sensitivity to both benign as well as cancer progressions, it is not utilized independently but in a combination with histopathological evaluations (Bjartell et al., 2011). Moreover, risk stratification of PC is in general done by combining Gleason scoring with PSA levels of a patient (Litwin et al., 2017).

1.2 AR-signalling and treatment strategies in PC

1.2.1 Prerequisites for the AR-signalling

The function and survival of healthy prostate, such as growth, fluid secretion and enzyme synthesis, as example PSA are dependent on male sex hormones called androgens. It is evident that the main prerequisite of prostatic cellular regulation by androgens or also known as androgen-signalling (AR-signalling) axis, is the binding of androgens to the androgen receptor (AR) in the cell cytoplasm and resulting in initiation of AR target gene expression. The process can be initiated by both testosterone and dihydrotestosterone (DHT), which is the more potent form of testosterone. DHT is the product of conversion of testosterone in prostate and testes by 5α-reductase. DHT is estimated to have a 10-fold more potent stimulation of AR target genes in prostate compared to testosterone. Meanwhile both molecules can initiate the transcription of AR products, the enzymatic conversion of testosterone into DHT and sufficient concentrations of DHT, have a crucial role in healthy prostate development (Dai et al., 2017). Among the prostate cell types, ARs are expressed in both prostatic epithelial as well as stromal cells (Xie et al., 2017).

From the larger perspective, around 95 % of testosterone in men are synthetized and released from the Leydig cells of testes and remaining 5 %, from the zona reticularis of adrenal cortex (Choi et al., 2022). Steroidogenesis of androgens is regulated by the hypothalamic–pituitary–gonadal axis. The biosynthesis is activated by the hypothalamic gonadotropin-releasing hormone (GnRH), which is released via the hypothalamic neurons into anterior part of the pituitary and activates the secretion of luteinizing hormone (LH) from the gland. Secreted LH hormone in turn, targets testes and adrenals for steroidogenesis activation. Subsequently, released testosterone acts as a negative-feedback mechanism of the axis (Dai et al., 2017).

In molecular studies, synthetic androgens are preferred over DHT, as they possess significantly higher stability and binding affinity to AR compared to naturally occurring androgens. Particularly R1881 a stable, high affinity synthetic androgen is widely utilized in analytical studies involving AR and its binding with ligands (Attardi et al., 2010; Chen et al., 2006).

1.2.2 Treatment strategies against localized PC

Surgical removal of the malignant prostate gland also known as prostatectomy, followed by radiation therapy were historically the first medical intervention against PC (UroToday, 2012). Active surveillance, prostatectomy and radiation therapy remain up today as a standard of care in newly diagnosed, localized and non-metastatic PC. However, their effectivity is limited to primary stages of PC (Litwin et al., 2017). Therefore, a clinical demand for second-line therapies in case of cancer recurrence were recognized (Choi et al., 2022).

1.2.3 Therapies against PC recurrence: depleting serum androgen

The evidence of hypothalamic-pituitary-gonadal axis and androgen function on a prostate physiology served as an inspiration for first therapies against advanced PCs. The discovery of oestrogen analogue called diethylstilbesterol (DES) in 1938 as the inhibitor of hypothalamic GnRH production, as well as an evidence of orchiectomy effectiveness in depleting serum androgen, leading to suppressed PC activity introduced a new strategy against PC, known today as an androgen deprivation therapy (ADT). The drawbacks of the initial ADT were their side-effects associated with blood clotting and cardiovascular issues. Introduced in 1980s GnRH agonists and antagonists were effective as initial ADT but provided safer cardiovascular outcomes (Choi et al., 2022).

Alternative to hypothalamic-pituitary-gonadal axis inhibition was introduced with a drug class of steroidogenesis inhibitors, such as CYP17A1 or 17α-hydroxylase enzyme inhibitors. These drugs inhibit the testosterone production specifically within testes. Currently, GnRH agonists and antagonists as well as abiraterone - CYP17A1 inhibitor, remain a standard ADT against recurrent PC. Suppression of androgens and steroidogenesis proved to be effective, but due their effect being non-limited to PC, they are accompanied with health complications, such as cardiovascular, bone mineral density issues and sexual dysfunction. Also, majority of patients in their advanced stages of PC and despite ADT, developed an androgen deprivation-resistant or so-called castration-resistant prostate cancer (CRPC) with no response to the therapy (Choi et al., 2022).

1.2.4 Androgen Receptor structure

ADT is an extracellular androgen-lowering method, which is not cell-specific to prostate cancer cells and cannot target its intracellular processes. In fact, the biologically active DHT initiates the cell-specific cellular response by targeting to the AR that is found in androgen-targeting tissues, such as prostate (Davey & Grossmann, 2016). AR structure comprises of four important regions with distinct functions: N-terminal domain (NTD), DNA-binding domain (DBD), ligand-binding domain (LBD) and hinge region connecting DBD with LBD. In the absence of androgens, AR is in the cell cytoplasm and is associated particularly with the heat-shock proteins. The binding to ligand occurs in LBD region and the binding of AR to DNA occurs in the DBD area via specific zinc fingers of the AR. DBD is also thought to be the most conserved and stable to mutations, whereas NTD is prone to mutations and variations, particularly in PC. The two transcriptional factors required for the AR activity are the activation function 1 (AF-1) and 2 (AF-2). The AF-1 is located in NTD and modulates the ligand-independent AR-signalling, whereas AF-2 is located in LBD and is activated in the presence of androgens, thus responsible for ligand-dependent pathway (Dai et al., 2017 ; Davey & Grossmann, 2016), which is also illustrated in the Figure 2.

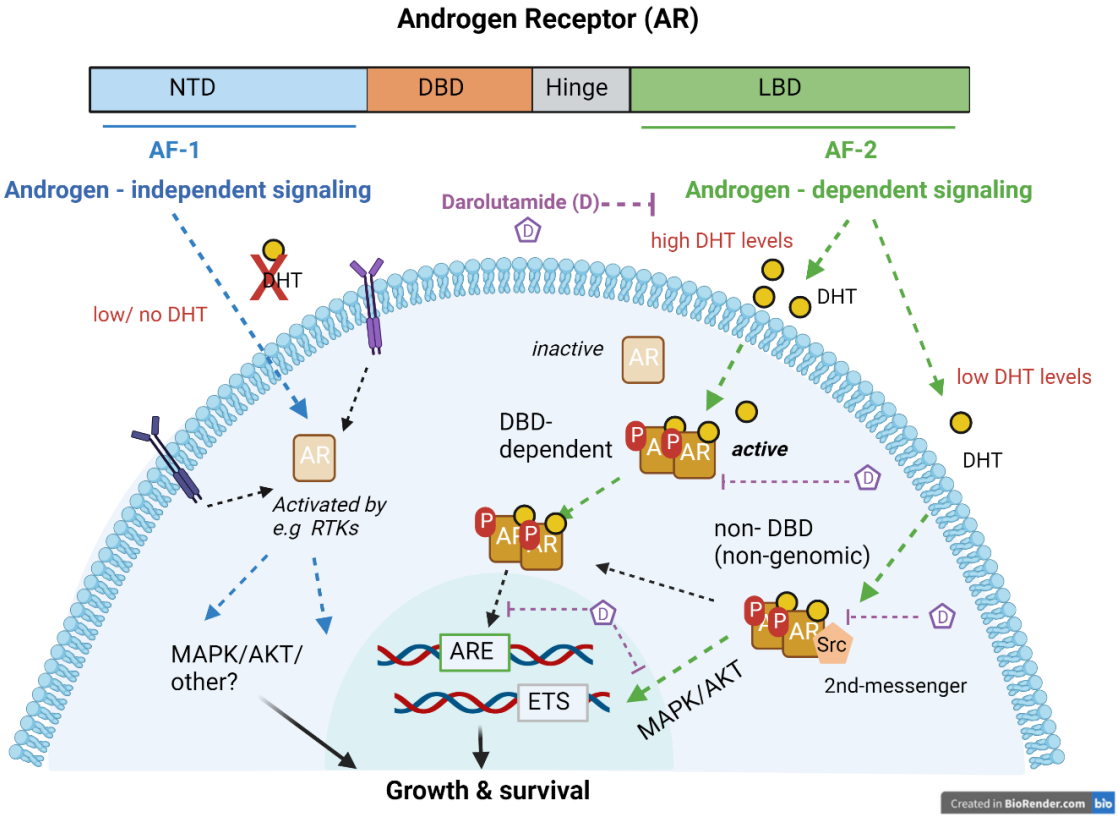

Figure 2. Androgen Receptor (AR) structure, signalling pathways in PC and darolutamide inhibition. Structurally AR is comprised of four main regions, which have individual functions, such as NTD and LBD regions, regulating specific downstream pathways. The ligand/androgen-dependent signalling is activated by AF-2 transcriptional factor, and it activates two distinct intracellular pathways, which are operational depending, on availability of androgens. Both DBD and non-DBD activated genes promote growth and survival of the cell. AF-1-activated ligand/androgen-independent signalling can operate even without available androgens, for example by AR-RTKs crosstalk and AR activation resulting in MAPK/AKT signalling initiation, which promote cell growth and survival responses in PC. Darolutamide inhibitory effects are based on two major mechanisms. First, inhibiting the nuclear translation of AR and secondly, blocking the AR-DNA binding inside the nucleus. The inhibitory effect of darolutamide on AF-1-activated signalling is not known. Figure created with BioRender.com.

1.2.5 Androgen- dependent and- independent signalling

AF-2-activated or ligand-dependent signalling is transduced towards DNA in two distinct downstream pathways; canonical-DBD domain dependent or non-canonical where the signal is transduced independently from DBD via second messenger molecules (Dai et al., 2017 ; Davey & Grossmann, 2016). Upon binding with the ligand, conformation changes occur in AR, enabling interaction with the coregulators, and dimerization. In canonical ligand-dependent pathway, AR-ligand complex translocate into the nucleus. Subsequentially, AR phosphorylates and binds into androgen response elements (AREs) found within promoter sites of AR gene

targets. It is estimated that the cell response to this canonical pathway occurs in several hours after signalling initiation (Dai et al., 2017).

In DBD-independent or non-genomic pathway, AR-ligand complex in the cytoplasm interacts with the second messenger of the mitogen- activated protein kinases (MAPKs) by binding to Src kinase and protein kinase B (AKT)- regulator p85α. Phosphorylated Src and p85α activate MAPK and AKT pathways resulting in activation of alternative factors, such as ETS, activating also non-AR target genes. Non-genomic pathway is suggested to promote also the genomic or AREs-targeted signalling (Figure 2). All in all, non-genomic pathway was shown to maintain cell proliferation and cell survival within minutes from the activation and even in the presence of lower availability of androgens (Leung & Sadar, 2017).

The non-canonical, AF-1-activated ligand-independent AR-signalling pathway is up today not fully understood. One of suggested mechanisms is the AR activation via crosstalk with receptor tyrosine kinases (RTKs) and their ligands, which results in MAPK/AKT pathway initiation (Makino et al., 2021) as portrayed in the Figure 2. Ligand-independent AR-signalling was also detected in healthy tissues and cells, however in PC it is associated with cancer progression (Davey & Grossmann, 2016 ; Dai et al., 2017).

1.2.6 AR-signalling inhibition and clinical utilization

The key role of Androgen Receptor (AR) in modulating cellular response to androgens, provided alternative and prostate gland -specific drug target. Introduced in 1980s and 1990s flutamide and bicalutamide were a potent AR-inhibitors, without interfering with serum hormonal levels and reproduction system. They introduced into clinics a novel class of therapy, called antiandrogens or AR-antagonists (Choi et al., 2022). Bicalutamide was one of the first-generation nonsteroidal antiandrogens (NSAAs). NSAAs are AR-specific, in contrast to previous steroidal antiandrogens, which targeted several distant steroidal receptors. The development of enzalutamide in the early 2000s provided the clinics with a more effective second-generation NSAAs. Enzalutamide is a potent, selective AR-antagonist, which inhibits both nuclear translocation of AR, as well as AR binding into DNA, which was not inhibited by bicalutamide (Helsen et al., 2014).

Darolutamide, which was approved by Food and Drug Administration (FDA) in 2019 is the most recent AR-inhibitor for PC. The mechanism of action (MoA) of darolutamide is similar to enzalutamide and it is also considered as a second-generation NSAA. Despite their similar

mechanism, darolutamide was observed to have lower probability of adverse events and especially lower risk of seizures. This could be explained by the fact that darolutamide was found to have lower penetrance of blood-brain barrier compared to enzalutamide (Rice et al., 2019). In addition to wild-type androgen binding domains, darolutamide was shown to target several mutated variants of AR, such as T878A and F877L that were detected in majority of enzalutamide-resistant CRPC patients (Borgmann et al., 2018). Despite its potent AR inhibition, darolutamide is targeting mainly the LBD region of AR, and its effect on AF-1-activated ligand-independent signalling is unknown (Antonarakis et al., 2016).

1.2.7 CRPC stage: limited cure from current therapies

Despite surgical castration, radiation, ADT, or antiandrogens, 10 % of treated PC advance into castration-resistant stage (CRPC) with an estimated average survival of less than 30 months due to rapid advance of cancer and distal metastases (Aly et al., 2020). CRPC is defined as recurrent prostate cancer that continues to progress despite castration therapies. Nevertheless, CRPC has still shown to rely on androgens and AR by various adaptive mechanisms and it is suggested that majority of CRPC phenotypes are AR-dependent, meaning that CRPC is still targetable by ADT and AR-inhibition.

In non-metastatic CRPC, second-generation antiandrogens are recommended, particularly darolutamide, enzalutamide and apalutamide. Moreover, enzalutamide was shown to prolong OS in also metastatic stages of CRPC (Parker et al., 2020; Vellky & Ricke, 2020). Nonetheless, specific phenotypes, including cases with ARV7 mutation have shown to be unresponsive to second-generation antiandrogens. Another currently utilized drug-class in CRPC are taxanes. Specifically, microtubule inhibitors docetaxel and cabazitaxel were shown to prolong OS regardless of CRPC phenotype. Radium-223 have also shown effectiveness but only limited to bone metastases (Parker et al., 2020). Additionally, combination of microtubule inhibitors with ADT have suggested synergistic effect in metastatic but non-CRPC cases. (Mohler et al., 2019). On the other hand, combinations of ADT with second-generation antiandrogens in metastatic CRPC have shown only minor improvement in OS but a high adverse-effect outcomes. Recent most drug-class that was clinically approved for the CRPC treatment is immunotherapy, such as Sipuleucel-T that was shown effective in early- stages of CRPC (Mohler et al., 2019 ; Parker et al., 2020).

1.2.8 Mechanisms of CRPC and alternative signalling pathways

The current understanding is that CRPC maintain the growth and survival by mechanisms as follows: AR-signalling overexpression from *AR* amplifications, constitutively active splice variants of AR and other mutations, retention of intra-tumoral steroid synthesis, as well as AR-independent pathways (Leung & Sadar, 2017; Vellky & Ricke, 2020). AR-signalling overexpression is often the result of *AR* gene amplifications. Splice variants of AR, such as ARV7 are receptor alterations where the LBD is absent, allowing the receptor to be constitutively active independently from androgens. Also point mutations in LBD region enable PC to escape castration therapies by decreasing AR-DHT-specificity (Vellky & Ricke, 2020).

On the other hand, the AR-independent phenotypes are becoming more prevalent due to systemic clinical utilization of AR-inhibition and ADT. The most common phenotypes are NE PC (NEPC), AR-low PC (ARLPC) and double-negative PC (DNPC), which is characterized with both absence of NE cells as well as AR-negative phenotype (Vellky & Ricke, 2020). As part of a natural adaptation, PC was shown to switch to alternative signalling pathways as well as de-differentiate into distinct cell type, resulting in heterogeneity of CRPC. De-differentiation of PC is commonly found as transitions of epithelial cells into stromal or mesenchymal tissue, known as epithelial-to-mesenchymal transition (EMT), which is particularly frequent in DNPC (Makino et al., 2021 ; Vellky & Ricke, 2020).

One of observed AR-independent signalling pathways in PC are downstream pathways mediated by RTKs and their ligands, such as epidermal (EGF) - and fibroblast growth factors (FGF). Specifically, it has been found that EGFs and FGFs are able to activate AR target genes without androgens and interaction with AR. Moreover, FGFs were found to be clinically overexpressed in DNPC according to *in vivo* and *in vitro* studies. According to the studies FGF/MAPK pathways were responsible for PC progression and specifically MAPK, in development of poorly differentiated PC (Bluemn et al., 2017 ; Makino et al., 2021). Overexpression of N-MYC with *PTEN* loss, as well as Lysine-specific demethylase 1 (LSD1) were also shown to promote PC progression *in vitro* and *in vivo* (Makino et al., 2021). All in all, supporting the role of AR-bypass mechanisms in CRPC and underlying the importance of novel therapies targeting these alternative signalling pathways.

1.3 FGFR inhibition and alternative treatment strategies for CRPC

1.3.1 Families of FGFs and associated pathologies

FGFs and their receptors (FGFRs) are among the most promising targets in PC and its AR-independent stage. Their association in CRPC development, cancer survival and progression could be interpreted by their role in healthy cells' physiology. FGFs have a potent mitogenic and angiogenic activity in cells, and they are regulating processes, such as tissue development and homeostasis, regeneration and repair, liver metabolic activities and inflammatory reactions. Alterations in FGF- signalling have been associated to various diseases including birth defects such as, congenital craniosynostosis, dwarfism syndromes as well as chronic kidney disease, insulin resistance and cancer (Xie et al., 2020).

Based on the way of action, FGF proteins could be categorized into intracrine, paracrine and endocrine subfamilies. Intracrine are distinct among all due to their activity being limited to intracellular space as well as in a receptor-independent manner (Teishima et al., 2019). In turn, paracrine and endocrine subfamilies of FGFs are initiating their signalling by binding into extracellular site of FGFRs, more specifically to the heparin/ heparan sulphate proteoglycan (HSPG) site of the receptor. While both paracrine as well as endocrine FGFs can act through FGFR homologs, paracrine FGFs have a higher affinity to HSPGs, whereas endocrine FGFs have lower affinity to HSPGs and their signalling activity is dependent on co-receptors, such as alfa/beta-Klotho transmembrane proteins (Teishima et al., 2019 ; Xie et al., 2020). It is suggested that endocrine FGFs are modulating the metabolic activities, such as energy metabolism, whereas paracrine FGFs are regulating angiogenesis, cell proliferation and differentiation (Teishima et al., 2019). Regarding prostate physiology, it is suggested that specifically paracrine FGF7 and FGF10 that are like majority of FGFs, synthesized in prostate mesenchymal cells, are the essential factors for prostate gland development (Giacomini et al., 2021).

1.3.2 Targets of FGFs

Structurally, the FGF targets, so FGFRs are transmembrane RTKs with extracellular, transmembrane, and intracellular domains as can be seen in the Figure 3a. Extracellular domain is built by three immunoglobulin like parts (D1-D3), acidic part, heparan and co-proteins. The transmembrane domain (TMD) is a helix-like protein that initiates the receptor dimerization and contains the alfa/beta - Klotho proteins. The intracellular part - juxtamembrane domain of

FGFR is responsible for receptor dimerization, as well as serves as attachment site for adaptor proteins, which affects the further signal transduction pathway. Among FGF-family, there are four canonical FGF-receptors (FGFR1-4) with two major splicing variants (b/c) of D3-immunoglobulin domain present in each receptor type, and a Tyrosine Kinase (TK) domain lacking FGFR5/FGFR-like 1 (FGFRL1) receptor (Giacomini et al., 2021 ; Teishima et al., 2019 ; Xie et al., 2020).

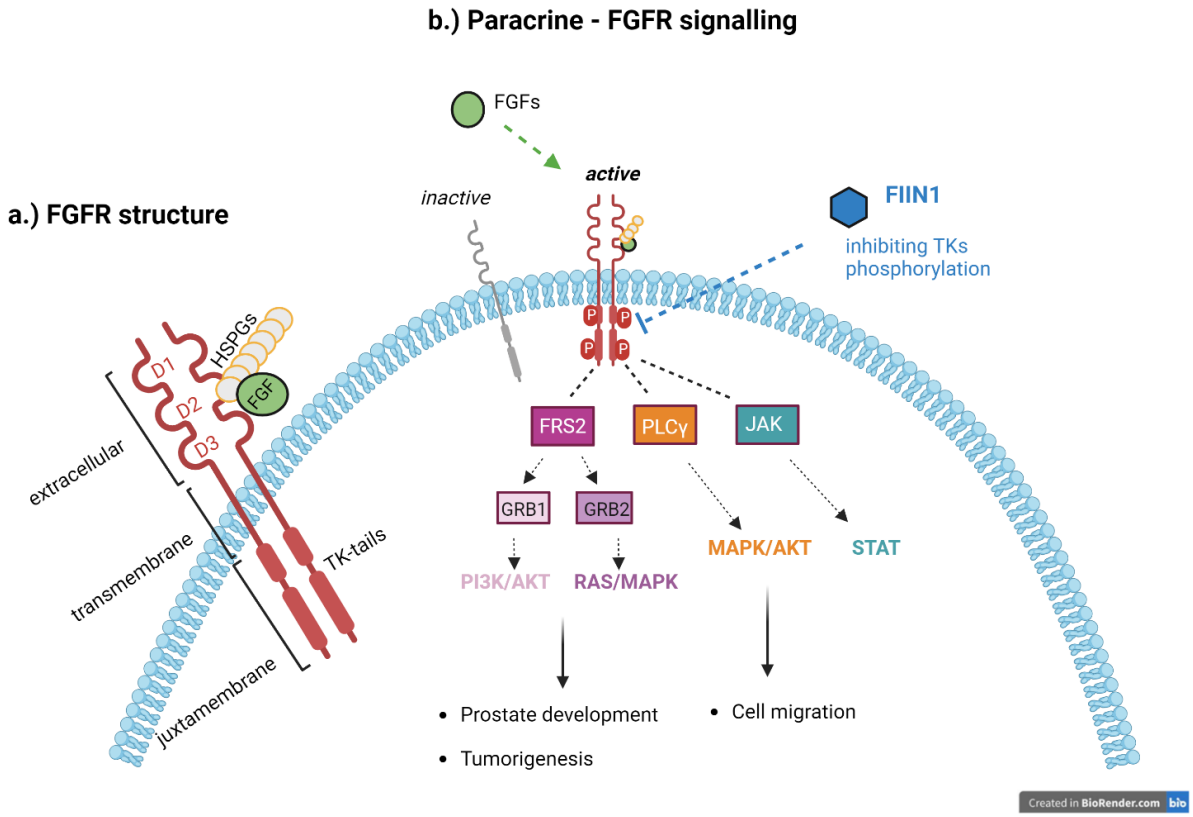

Figure 3. FGFRs structure and paracrine- signalling pathways. a.) FGFR is structurally divided into extracellular, transmembrane, and juxtamembrane/intracellular domains. FGFs binding occurs on HSPGs between D2 and D3 immunoglobulin-domains. b.) Paracrine-FGFR signalling can undergo via four major pathways depending on the recruited adaptor protein. FRS2 adaptor-linked pathways are associated with prostate development and tumorigenesis regulations, whereas PLCγ is suggested to regulate cell migration. FIIN1, a potential FGFR- inhibitor was shown in preclinical studies to covalently bind to FGFRs and block the phosphorylation of their TKs. Figure created with BioRender.com.

1.3.3 Downstream signalling pathways

In paracrine signalling, FGF-binding into HSPG occurs between D2-D3 immunoglobulin domains. FGF-FGFR binding initiates conformational changes to FGFR, receptor dimerization, phosphorylation of TKs in the cytosol and subsequently attachment of adaptor proteins. The

major FGFR-adaptor proteins or signal transducers are FGFR-substrate-2 (FRS2), phospholipase C-γ (PLCγ) and janus kinase (JAK)- activated STAT-signalling (Giacomini et al., 2021). In event of FRS2 activation, at least two distinct pathway involvement were identified: the Ras/Raf-MEK-MAPKs and PI3K/AKT pathways. The first is initiated by FRS2 binding into GRB2, which binds to SOS- and activates Ras/Raf-MEK-MAPK- signalling. The PI3K/AKT pathway is initiated by FRS2 binding with GRB1. In turn, PLCγ signal transduction is associated with MAPK/ AKT and JAK-activation on STAT-reliant signalling, which is also illustrated in the Figure 3b. These different adaptor-specific downstream pathways were found to have a closer association with specific cell functions. In particular, PLCγ activated MAPK/ AKT associates with cell migration, and FRS2 activation regulates prostate development as well as tumorigenesis (Giacomini et al., 2021 ; Teishima et al., 2019). Additionally, several intracellular modulators were found to regulate the intracellular signal transduction via inhibition. These modulators, such as SEF or Sprouty proteins, (e.g SHP2) are capable of blocking the signal transduction further from TK phosphorylation, initiated by FGF-ligand activation of FGFR, which allows formation of negative-feedback loops for the signalling (Giacomini et al., 2021 ; Xie et al., 2020).

1.3.4 FGFR- signalling in primary PC

FGFR alterations were found to be closely associated with various cancers, such as breast, lung, head and neck, bladder, endometrial and PC. In PC the specific malignant processes FGFR were found to be responsible for were tumorigenesis, EMT, cell proliferation and cell invasion (Teishima et al., 2019). It was detected that specifically paracrine FGF-1, -2, -8, -9, -10,-13, -17, endocrine FGF-19 and -23 growth factors, as well as FGFR-1 and -4 receptors were upregulated in PC (Yu Lan et al., 2016 ; Teishima et al., 2019 ; Giacomini et al., 2021). In contrast to FGFR-1 and -4, FGFR2 expression, specifically FGFR2-IIIb- variant might correlate with inhibition of PC growth and progression, potentially, via maintenance of stromal – epithelium signalling balance (Giacomini et al., 2021).

1.3.5 FGFR/FGFs promoting metastasis and CRPC

Particularly, *in vivo* studies discovered that FGF2 and FGF8 were overexpressed in PC bone metastases and associated with increased invasive properties of cancer. FGF2 was also found to increase tumour progression, and post-operative cancer recurrence. In murine models, FGF9 formed reactive stroma and bone metastases in specifically, AR-negative CRPC and high-grade

PC phenotypes (Giacomini et al., 2021). Evidence suggest FGFR1 overexpression in bone metastases of CRPC patients as well as induction of PC metastases progression (Labanca et al., 2022). In another study, cytoplasmic and nuclear localisation of FGFRL1/FGFR5 was indicative of PC progression (Yu Lan et al., 2022). Furthermore, endocrine FGF19 was found to induce several EMT – linked biomarkers in hormone-sensitive PC, and in human- derived PC, intracellular accumulation of FGF19 was elevated. It is also suggested that FGF23 is linked with PC, as it was overexpressed in PC cell lines and associated with induced proliferation and invasion of cells (Teishima et al., 2019).

Even though majority of PC-linked FGFs, such as FGF2, FGF7, and FGF10 are secreted by a prostate stroma, epithelial cells were also found to be involved in tumour development via FGF-signalling. FGF8b was found to be released by epithelial cells, and responsible for driving hyperactivation of prostate stroma and PC development. Self-stimulation of PC cells via autocrine FGF-signalling has also been detected. In addition to specifically FGF/FGFR activity, alterations of FGFR-adapter or modulator as well as Extracellular matrix (ECM) proteins can also promote PC progression (Giacomini et al., 2021).

1.3.6 Targeting FGFRs and FGFs in clinics

The discovered association of FGF/FGFR-signalling in PC, has led to development of novel class of cancer therapies, FGFR-inhibitors. These inhibitors are capable in inhibiting the function of FGFR activation and its downstream signalling pathway transduction. The current available FGFR-signalling inhibitors could be divided into two three main groups; so-called small-molecule inhibitors or tyrosine kinase (TK) inhibitors, targeting the catalytic activity of kinase tail, antibody/peptide antagonists that inhibit the receptor binding with FGFs and so-called ligand traps, targeting the growth factors instead. Two types of small-molecules FGFR inhibitors are currently under clinical trials: selective and non-selective inhibitors. Meanwhile selective inhibitors bind specifically to subtype of FGFRs, non-selective can bind to multiple RTKs, such as vascular endothelial growth factor (VEGF) or platelet-derived growth factor (PDGFR) receptors. Nevertheless, non-specific FGFR inhibitors were found to possess a strong antitumour as well as angiogenesis property due to their affinity to several RTKs, they are found to have more severe toxicity profiles and weaker FGFR-signalling-specific inhibition compared to their selective relatives. Lenvatinib, is an example of non-selective inhibitor, which was also approved by FDA in 2015 for treating radio-iodine refractory thyroid carcinoma. Lenvatinib targets particularly FGFR1-4, VEGFR1-3, PDGFR-β and other kinases. (Chae et al, 2017).

Despite the initial anti-tumour efficiency of the first-generation FGFR inhibitors, drug resistance was further observed in several cancers. Non-selective RTK-specificity enabled alternative by-pass mechanisms of signalling. In turn, binding to non-conserved regions of the receptors, such as hinge regions in FGFRs, arise in gatekeeping mutations, which resulted in treatment challenges to even more advance, selective-FGFR inhibitors (Tan et al., 2014).

1.3.7 Selective and pan- FGFR inhibitors

Subsequentially, more selective inhibitors were developed including AZD4547, BGJ398 and JNJ-42756493, which are currently under evaluation in clinical trials. BGJ398 and JNJ-42756493 inhibitors are also so-called pan- FGFR- inhibitors, since they are FGFR-specific but able to target several FGFR-subtypes (Chae et al., 2017). Pemigatinib is so far the only selective FGFR inhibitor, that was clinically approved for treating cholangiocarcinoma. *In vivo* studies have also suggested its effectivity in treating CRPC (Chiodelli et al., 2022). Despite promising preclinical results of pemigatinib, evidence of FGFR- inhibitors effectively treating PC and especially its progressed, CRPC state are limited. One of challenges in clinical utilization of the inhibitions arise from gatekeeping mutations which were shown to assist FGFRs to confer resistance to previous FGFR-inhibitors including also FGFR-selective AZD4547. One of the clinically promising agents are FIIN1 and FIIN2, which are pan-FGFR- inhibitors with a high binding affinity due to irreversible covalent binding to FGFR 1-4 subtypes, inhibiting their TK phosphorylation (Figure 3b) and as a result, signalling transduction. Additionally, *in silico* models suggested their effectivity against gatekeeping mutations due to targeting highly conserved regions of FGFR (Tan et al., 2014). Interestingly, results from cell and animal models suggest that FGFR- signalling inhibition might have also an indirect anti-tumour effect, particularly increased sensitivity of cancer cells to conventional chemotherapy, such as taxane-drugs (Chae et al., 2017).

1.3.8 FGFR- and AR-signalling interplay in PC and CRPC

The possible crosstalk between androgen/AR- and FGF/FGFR- signalling is not an extensively studied topic yet. However, recent studies have suggested a possibility of AR/FGFR interplay in a two-way manner. In particular, it has been found that epithelial and stromal secretions of FGF-1, -2, -8, -10 are regulated by AR- signalling. Moreover, cancerous stromal/mesenchymal cells in PC, also known as cancer-associated fibroblasts (CAFs), were found to express AR. Whereas, AR-silencing in CAFs resulted in their decreased FGF7 and FGF10 expression,

suggesting that AR and FGFR-signalling can induce positive-feedback loops in PC and CAFs in both paracrine and autocrine manner. Inversely, there is evidence that expression of AR can be regulated by FGFR-signalling. A particular *in vitro* study suggests that overexpression of AR increased FGF2 secretion by PC cells, whereas stimulation by FGF2, decreased cellular AR-expression in a specific PC model (Giacomini et al., 2021).

As previously mentioned, FGFR-signalling might also maintain PC progression in DNPC and phenotypes with low or null AR expression. Moreover, FGFR inhibitors were found to inhibit the PC growth in AR-null cell- and xenograft models (Bluemn et al., 2017 ; Makino et al., 2021). All in all, suggesting a potential drug target for PC phenotypes that do not respond to ADT or AR-targeted therapy. Moreover, evidence of AR and FGFR-signalling interplay in PC survival and growth (Giacomini et al., 2021) as well as direct and indirect anti-tumour effect of FGFR inhibitors (Chae et al., 2017) suggest a potential for a novel therapeutical approach. Specifically, a simultaneous inhibition of AR and FGFR- signalling as a combinatorial drug therapy. This could be achieved by the advanced versions of FGFR-inhibitors, such as second-generation covalent binding- FGFR- inhibitors, e.g, FIIN1 (Tan et al., 2014) combined with a second-generation antiandrogen that are able to target mutated versions of AR, like darolutamide (Borgman et al., 2018).

1.4 Tumour microenvironment and In vivo-like model engineering

1.4.1 TME in prostate cancer

To study the potential of anti-tumour drug therapy *in vitro*, it has to be acknowledged that cancer cells communicate and cooperate with other cell and tissue components by forming an optimal tumour-supportive environment, which is known as tumour microenvironment (TME). Similarly, as healthy cells demand the optimal cell-cell communication and microenvironment, however in cancer this balance is altered and switched into malignant growth. Depending on a cancer type, TME is comprised of various cell types, connective proteins, and particular signalling molecule expression pattern, which maintains the crosstalk between the TME components (Bonollo et al., 2020). Primary TME of PC constitutes of epithelial cells, fibroblasts as a stromal tissue, which are de-differentiated into CAFs, as well as neuroendocrine, nervous and blood cells. These cells are supported by extracellular connective tissue, which is built by extracellular matrix (ECM) (Ellem et al., 2014).

TME enables sufficient nutrient and gas exchange between cells stromal-epithelium crosstalk, promotes de-differentiation and EMT, maintains structural integrity and polarity of cells, all in all, regulating cancer growth and sensitivity to chemotherapy (Bonollo et al., 2020 ; Ellem et al., 2014). In addition to previous functions, it is suggested that TME itself, particularly its stromal components might also serve as a tumorigenesis promoter of non-cancerous cells (Bissell et al., 2011). Potentially, ECM, blood vasculature, immune cells and nerve cells were can also regulate tumorigenesis, either by promoting it alone or by co-operating with malignant components of TME (Ellem et al., 2014).

1.4.2 Transformation into CAFs

CAFs are transformed malignant cells with fibroblast-like functions, but with tumorigenic phenotype. In majority, cellular origin of CAFs are healthy fibroblasts but they can also originate from bone marrow- derived mesenchymal stem cells, adipocytes and epithelium cells via EMT. Likely because of their cell of origin variations, CAFs are highly heterogenic in PC, which gives a challenge to accurate identification or CAF-marker development. Nevertheless, according to biopsies CAFs could be defined by cells within TME with elongated morphology, absence of endothelial, epithelial and leukocyte markers, and lack of mutations that are present in primary PC cells (Bonollo et al., 2020).

1.4.3 CAFs as a key driver of PC progression

Preclinical studies suggest that CAFs can additionally regulate the tumour growth, invasiveness, de-differentiation of cells as well as drug treatment resistance of PC. Increasing evidence suggest that CAFs are among the key component in TME and can drive de novo tumorigenesis of PC solely on their own (Bonollo et al., 2020 ; Ellem et al., 2014 ; Ehsani et al., 2021). In particular, CAFs that were derived from PC were shown to transform originally healthy epithelial cells into cancer *in vitro* (Bissell et al., 2011).

Regulation of PC and TME by CAFs is supported by their secretion of various cytokines and growth factor such as, Interleukins (IL-6 and IL-8), Transforming growth factor-beta (TGF-β), FGFs, VEGFs, Hepatocyte growth factors (HGFs), Matrix metalloproteinases (MMPs) and others. Specifically, CAFs can transform ECM composition via secretion of Collagens that are building components of ECM, allowing tissue repair and regeneration processes, which however in TME stimulate solely invasiveness, metastasis, and growth. CAFs communicate with other cancer cells via paracrine signalling by FGFs, ILs, TGFβ, VEGFs. They can recruit

more CAFs by transforming other cell types into CAFs via EMT, particularly by secreting MMPs. Several studies have also suggested that CAFs are the key factors in PC transformation into CRPC. Particularly, CAFs were shown to activate AR target genes of primary PC in the absence of androgens by secreting IL-6, which altered MAPK, STAT3 and PI3K/AKT signalling of PC (Bonollo et al., 2020 ; Erdogan & Webb, 2017). *In vitro* studies demonstrated that CAFs decreased sensitivity to enzalutamide and bicalutamide of PC when two cell types were grown together as a co-culture (Bonollo et al., 2020 ; Fontana et al., 2020).

1.4.4 The role of cell-tissue architecture

Inclusion of a key co-culture, so CAFs into TME is only one of the steps for simulating a natural in vivo-like microenvironment of PC. Mimicking a natural shape and polarization of co-culture structure would be the next key considerations for recapitulating TME. Apical-basal polarization of prostate gland epithelium is essential for prostatic secretions from apical side into lumen, as well as nutrient exchange and epithelium-stromal bridging provided by basal cells. Moreover, in both healthy prostate as well as PC microenvironments, single cells are not exposed to nutrients uniformly, and as a result, cells are highly differentiated with individual cell cycles, which results in different specializations within microenvironment. In PC, an example of a particular phenomenon could be seen by formation of a hypoxic core in the middle of tissue, lacking sufficient gas and nutrient exchange, which results in inactive and necrotic cells in the middle, however highly proliferative and viable cells in the outer surfaces of a tissue. Such consideration is also important in disease modelling since drug molecule exposure and potential resistance development are occurred in a non-uniform manner. The polarization and organization of cells in TME or normal prostate is maintained by ECM. By producing a scaffold-like connective proteins, such as collagen, ECM can build so-called scaffolding tracks, which can modulate cell organization as well as potential distant invasion of PC cells. These ECM- processes are in turn mediated by CAFs (Fontana et al., 2020 ; Erdogan & Webb, 2017 ; Joseph et al., 2018).

1.4.5 *In vivo*-like cellular disease modelling

To simulate PC *in vitro*, previous TME components would need to be present within a plastic dish. However, up today *in vitro* models in PC remain simplistic and recapitulate only a minor portion of TME, which limits the translatability of drug screening results. Currently, majority of models are based on epithelial PC- monocultures grown as a 2D-monolayer, which lacks

TME- processes, such as cell-stromal interaction, cell-ECM interaction, individual cell differentiation and polarization and variability in nutrient and drug exposure as presented in the Figure 4 (Ellem et al., 2014 ; Joseph et al., 2018).

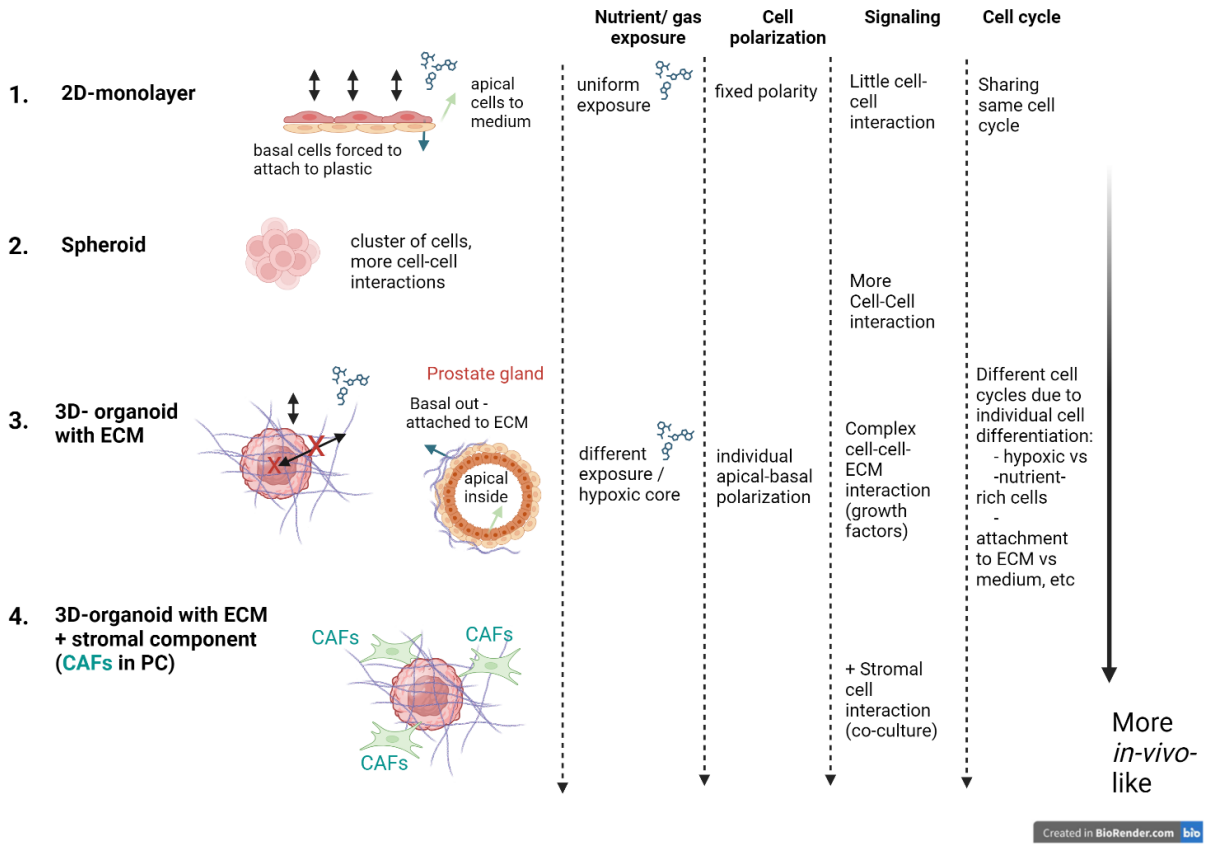

Figure 4. Significance of 3D organotypic model with stromal component for physiologic *in vivo*-like TME cell culture environment. Four major *in vitro* models are illustrated in the figure based on the extent of TME-characteristics they are harbouring shown in ascending order from 1 to 4. The most basic model, 2D-monolayer has forced/fixed polarity, uniform exposure to pharmacological or nutrient agents, uniform gas exchange, minor cell-cell interaction, and low differentiation of cells. In the most advanced and *in-vivo*-like model, 3D modelling combined with CAFs could instead simulate TME-characteristics that are absent in 2D models. Specifically, apical-basal polarity, variations in nutrient exposure, complex cell-cell interactions, high differentiation of cells, tumour-stroma interactions, and other features. Figure is created in BioRender.com.

Recently, several more sophisticated *in vitro* models were introduced, which are simulating TME in a larger extent than canonical 2D-monolayer PC models (Figure 4). Particularly 2D co-culture models with monolayer cell growth but inclusion of stromal culture to enable epithelial-CAF interaction. ECM-cell interaction as well as individual cell polarization and differentiation simulating 3D organotypic model is a further evolution of PC models. In 3D organotypic model, cells are grown in scaffolding-protein such as Matrigel or Collagen containing growth medium

suspensions. As a result, providing cells with structural support for formation a three-dimensional tumour clusters or organoids, which harbour several features of TME including several cell-cell interactions, hypoxic core, nutrient exposure, and differentiation variability as well as interactions between ECM and cells (Ellem et al., 2014 ; Fontana et al., 2020 ; Joseph et al., 2018 ; Åkerfelt et al., 2015). An advanced and less studied model would be combination of 3D organotypic and co-culture models into 3D co-culture, which could recapitulate the key features of TME, serving as a valuable drug response prediction model for PC (Åkerfelt et al., 2015).

1.4.6 Cell line applicability for AR and FGFR inhibitor studies in PC

Several PC cell lines that express AR and are androgen-sensitive were developed for preclinical research, such as LNCaP, CWR-R1, VCaP, LAPC4 (Sampson et al., 2013). These cell lines are originated from distant or local PC sites of a patient, and therefore possess individual histology and phenotype. In the previous study of the research group, second-generation FGFR- and AR inhibitor combinations were assessed in LNCaP and CWR-R1 providing evidence of combinatorial treatment effectivity in 2D as well as 3D models (Kim, Yu, 2021). However, LNCaP and CWR-R1 have limitations specifically in terms of AR subtype, as they are not expressing the wild-type of the receptor. In contrast, VCaP and LAPC4 are one of the only cell lines that are androgen sensitive with a wild-type AR. In addition, VCaP s were found to possess AR splice isoforms that lack LBD and are constitutively active in a ligand independent manner, also suggesting their applicability for studying CRPC (Sampson et al., 2013). Moreover, studies involving VCaP modelling into 3D organotypic culture, instead of commonly utilized spheroid-cultures, remain limited. Thus, *in vivo*-like 3D models constituting of VCaP could be a valuable tool for preclinical drug studies in PC.

2 Aims and hypotheses

Taking in count the evidence that FGFR-signalling may promote PC survival and progression when the availability of androgens is low and AR-signalling is blocked, the hypothesis was that inhibition of both AR- and FGFR-downstream pathways simultaneously in PC *in vitro* would be more efficient than inhibition of only one of the pathways. It was speculated that PC sensitivity to combinatorial inhibition would be different in simplistic 2D models compared to co-cultures with CAFs as well as 3D organotypic models. Hypothetically, inclusion of TME into the model was expected to improve the survival of PC in response to the treatment.

The aim of the Master´s thesis project was to investigate the efficacy of second-generation antiandrogen and second generation-pan-FGFR-inhibitor combination on PC- *in vitro* models and study if treatment efficacy was affected in response to inclusion of more TME-characteristics *in vitro*. The underlying goal of the project was to develop an *in vivo*-like model that could feature both 3D- as well as stromal-epithelium interaction- characteristics, so 3D co-culture.

The experimental questions were following:

1. The potential effect of (darolutamide and FIIN1) combinatorial treatment compared to inhibitors given separately as a single treatment on PC proliferation (2D models), morphology (3D models) and cell/organoid (2D and 3D models) viability

2. Influence of CAF-inclusion (co-culture) into VCaP -monocultures on a response to combinatorial treatment

3. Influence of 3D- and ECM-inclusion (3D monoculture) into VCaP on a response to combinatorial treatment

4. The role of CAF-inclusion compared to 3D- and ECM (2D co-culture vs 3D monoculture), as well as when both are combined (*in vivo*-like 3D co-culture), in a response to combinatorial treatment

3 Results

3.1 Validation of AR presence and activity in VCaP cells

Prior to the main drug sensitivity studies, western blotting was conducted in order to confirm the presence and activity of AR in VCaP cells. The experimental plan was to investigate whether the AR and PSA expression was increased in response to ascending amount of VCaP lysate in the sample. Western blotting was conducted on VCaP lysates that were collected and lysed after growing in an adherent cell culture dish until reaching 70-80 % confluence. BCA assay was then performed to measure the protein amount. The fluorescent signal expression of normalized and relative to alfa-tubulin loading control of AR and PSA was then quantified by the Li-Cor Odyssey® platform.

Results from western blotting provided evidence that VCaP cells have both AR expression as well as androgen-dependant signalling due to expression of PSA. As can be observed from the Figure 5a, AR and PSA expression increased in response to ascending loading amount of lysate. In terms of protein expression relative to loading control, so alfa-tubulin, AR was found to be similar within the dose range (Figure 5b), but PSA expression increased in response to ascending loading amount of lysate with significant expression starting from the 40 µg/well dose and the highest when loaded 50 µg/ well (Figure 5c). Particularly PSA expression quantifications (Fig. 5c) represent increased protein signal in response to a higher lysate loading, thus serving as a quality control of our initial western blotting results.

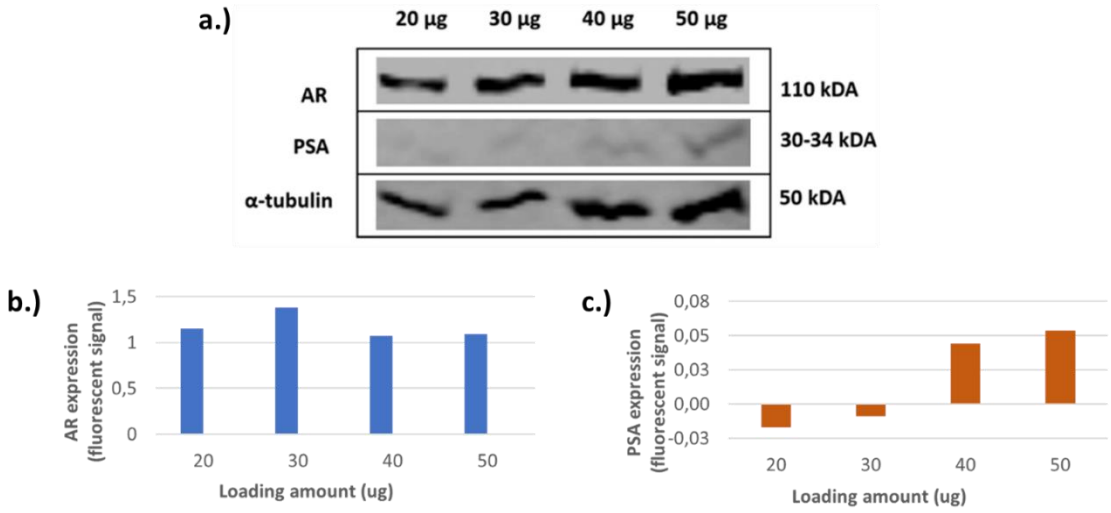

Figure 5. VCaP cells express both AR and PSA protein. Ascending amount (20-50 µg) of VCaP lysate was tested to investigate the AR and PSA presence in lysates. a.) The expression of AR (110 kDA), alfa-tubulin (50 kDA) and PSA (30-34 kDA) was detected by western blotting. b.) The AR and c.) PSA were calculated as relative to alfa-tubulin expression as shown in fluorescence signal that was quantified by Li-Cor Odyssey® platform.

3.2 AR presence in VCaP and CAF cells illustrated by Immunofluorescence

To illustrate the AR presence in both prostate tumour VCaP cells as well as in their stromal component, CAFs, Immunofluorescence- staining of AR with nuclear staining was performed in 2D-cell cultures of VCaP and PF179T GFP CAFs.

AR staining was present in both VCaP and CAFs (Figure 6). However, images could not provide clear information about the localization of AR, whether it is primarily localized inside the nucleus or cytoplasm. The illustrated GFP expression represents the PF179T CAFs, as they express the green fluorescent protein (GFP). Prior to individual imaging channel acquisitions, presence of all cells was validated by phase contrast microscopy.

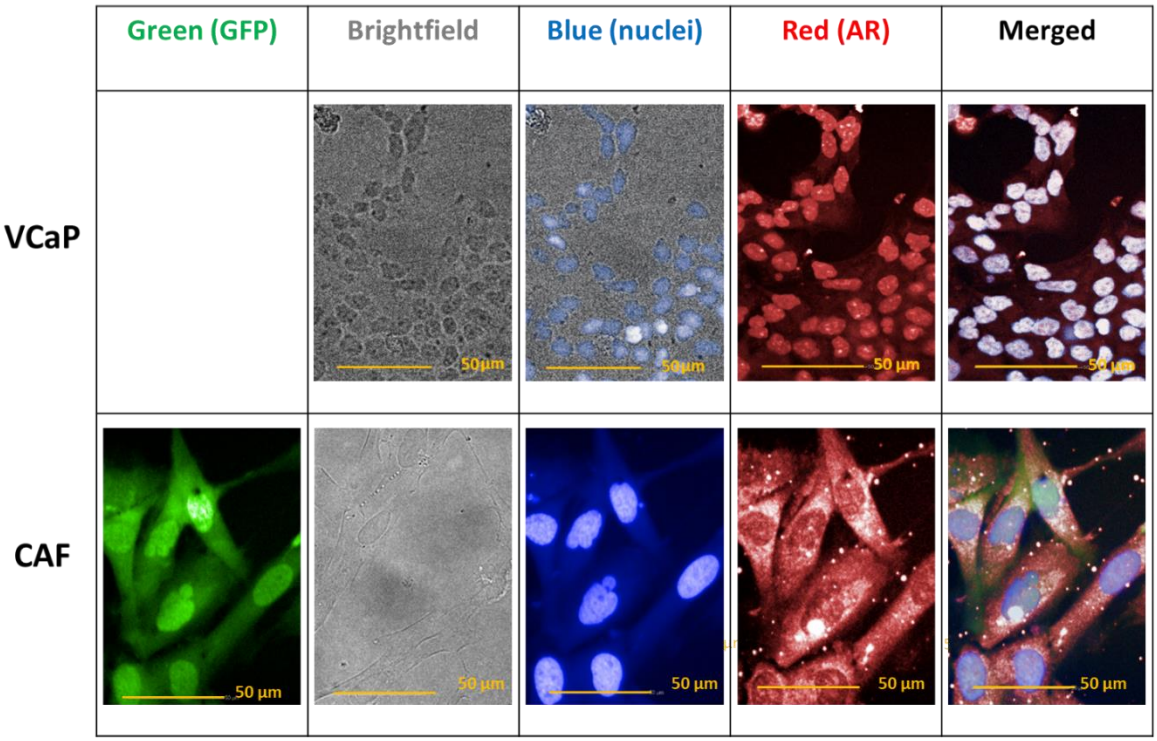

Figure 6. AR is present in both VCaP and CAFs according to the Immunofluorescence staining. Immunofluorescence staining of VCaP (top row) and PF179T GFP CAFs (bottom row) performed after 72-hour treatment of Enzalutamide 1 µM and fixation/ permeabilization. Images were acquired by the *Operetta High Content Imaging System* (PerkinElmer, Inc.) with 60X magnification. Green Fluorescence Protein (GFP) utilized for validating CAFs seen as green. Brightfield images were used for visualizing all cells. Nuclei staining illustrated as blue/ UV was stained by *Hoechst 33342*. Scale bar is representing 50 µm.

3.3 Cell viability and proliferation decreased in response to 1 µM single treatment of darolutamide

In order to determine the minimal required FGFR- and AR-inhibitor concentration for further combinatorial treatment studies, drug sensitivity studies were performed separately for each inhibitor in most simple 2D monoculture model of VCaP. The objective was to assess at which drug concentration the effect is biologically relevant. Specifically, which doses affect the proliferative activity and viability of the cells. VCaP sensitivity was investigated in 3-fold single dose escalation (0.3 – 10 µM) of darolutamide (antiandrogen) and FIIN1 (FGFR-inhibitor). After single inhibitor treatment initiation, proliferation of cells was monitored by the Phase contrast image-scanning utilizing IncuCyte S3 and confluence was quantified by the IncuCyte 2020A software for the proliferation trend generation. At the endpoint of 72-hour inhibitor treatment, cell viability was performed. Comparison between Dimethyl Sulfoxide (DMSO) -control and ascending doses of inhibitors was analysed and calculated for statistical significance. DMSO 0.1 % was utilized as the negative control.

Darolutamide treatment decreased VCaP proliferation starting only from 1 µM (15 % confluence at 71h), since 0.3 µM treatment had similar effect on confluence as DMSO-control (17% at 71 h time-point) (Figure 7a). Nevertheless live-cell imaging did not illustrate clear difference between these drug concentrations in terms of confluence, their difference between DMSO-control was clear (Figure 7c). Cell viability results (Figure 7b) showed statistically significant difference between 1 µM treatment (34%) and the DMSO-control. Additionally, 3 µM treatment showed statistically significant difference compared to the control, but with slightly lower effect compared to the previously mentioned 1 µM. Interestingly, 10 µM treatment affected the cell viability on similar level as 0.3 µM.

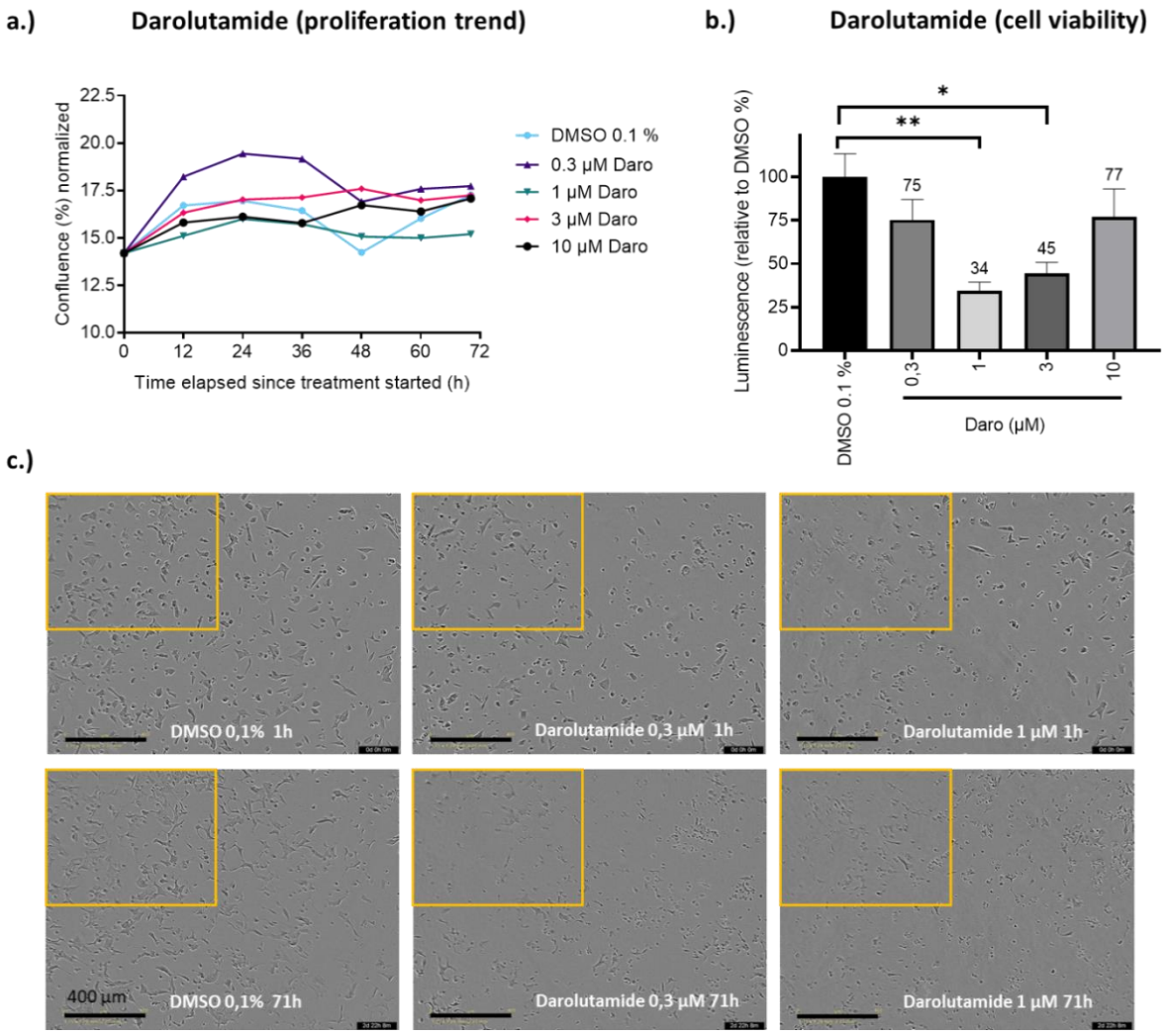

Figure 7. Darolutamide 1 µM single treatment significantly reduced VCaP viability with mild effect on proliferation in 2D monoculture. Darolutamide (Daro) was given as a 3-fold dose-escalation (0.3-10 µM). a.) Normalized proliferation trend of cells by confluence measurements (%) in response to treatment quantified by IncuCyte S3 2020A software. b.) Cell viability results at the treatment endpoint are shown above each bar as the mean relative to DMSO-control (%) luminescence signal. Each drug treatment sample as well as control was represented as triplicates. Comparison between control and inhibitor samples was statistically analysed by Kruskal-Wallis and Dunn's post-hoc test. * = P ≤ 0.05, ** = P ≤ 0.01. c.) Illustrative Phase contrast images by IncuCyte S3 for representative wells of control, 0.3 µM and 1 µM drug doses taken 1 hour after drug treatment start and 1 hour before the endpoint. Error bars illustrated as standard error of mean. Scale bar; 400 µm.

On the contrary, FIIN1 single treatment was associated with more potent inhibitory effects compared to darolutamide. In terms of the drug effect on proliferative activity of VCaP (Figure 8a), interestingly, no significant differences were detected between the DMSO-control and 3 µM dose at the 70h time-point. However, the lower doses; 0.3 and 1 µM reduced the confluence to 15 % and 16 % respectively. 10 µM of FIIN1 reduced the proliferation of VCaP the highest, as expected (11 %). While the statistical analysis of cell viability results (Figure 8b) detected significant difference between the DMSO- control only starting from 1 µM FIIN1, which decreased the viability to 34 %,

relative to the control, it is evident that lower 0.3 µM dose (38 % viability relative to the control) showed similar effects. Higher FIIN1 concentrations, such as 3 and 10 µM reduced cell viability to 18 % and 0.1 % respectively. The latter cell viability result shows that most cells were dead after 10 µM treatment. The live-cell images (Figure 8c) confirmed the significant difference between the FIIN1 doses and the DMSO-control at the 71h time-point, as can be observed with significant cell death starting already from the 0.3 µM dose of FIIN1.

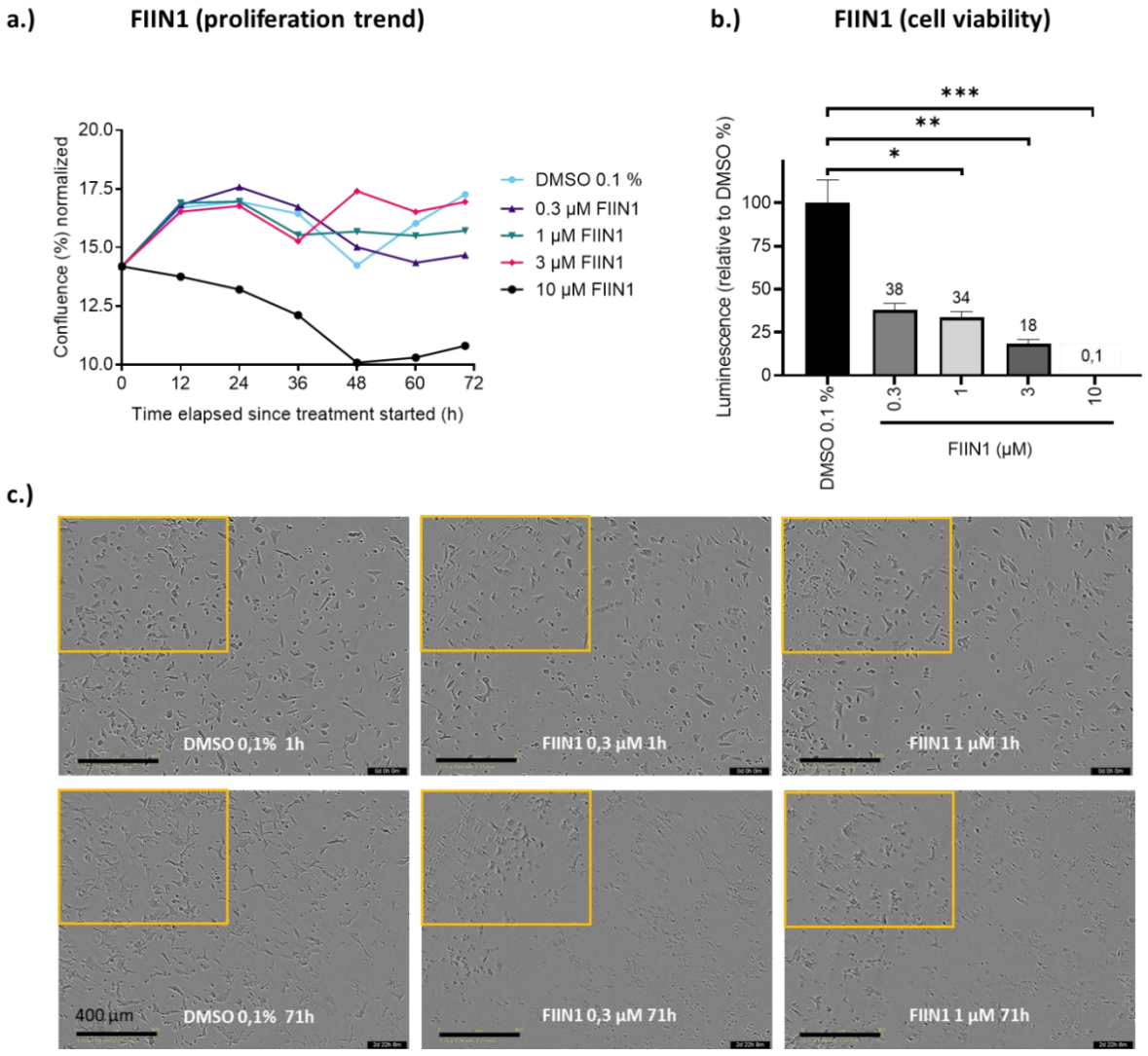

Figure 8. FIIN1 single treatment reduced VCaP viability more potently compared to darolutamide, with reduced cell viability and proliferation starting from 0,37 µM in 2D monoculture. FIIN1 was given as 3-fold dose-escalation. DMSO 0.1 % was served as the negative control in our experiment. a.) Normalized proliferation trend of cells by confluence (%) was quantified by IncuCyte S3 2020A software b.) Cell viability results at the treatment endpoint are shown above each bar as the mean relative to DMSO control (%) luminescence signal. Each drug treatment sample as well as control was represented as triplicates. Comparison between control and inhibitor samples was statistically analysed by Kruskal-Wallis and Dunn's post-hoc test. * = P ≤ 0.05, ** = P ≤ 0.01, *** = P ≤ 0.001. c.) Illustrative Phase contrast images by IncuCyte S3 of representative wells of control, 0.3 µM and 1 µM drug doses taken 1 hour after drug treatment start and 1 hour before the endpoint. Error bars illustrated as standard error of mean. Scale bar; 400 µm.

Based on the results (Figure 7), for the following combinatorial treatment experiments 1 µM of datrolutamide was selected as the fixed dose for antiandrogen. Given the potency of FIIN1 and its highly cytotoxic effect from the 10 µM (Figure 8), 0.3, 1 and 3 µM doses of FIIN1 were selected to be utilized for the combinatorial treatment.

3.4 No significant effect from the darolutamide + FIIN1 combination compared to their single treatment in 2D monoculture

After determination of minimal effective dose for darolutamide, and effective dose range for FIIN1 in VCaPs, the actual combinatorial treatment experiments were performed, starting with the standard 2D-monoculture model. The main objective was to assess the potential effect of AR- and FGFR-inhibitor combinations compared to the inhibitor single treatment. The concentrations of antiandrogen darolutamide was set to be 1 µM and the FGFR-inhibitor FIIN1 was tested on 3-fold dose-escalation manner excluding the 10 µM dose (0.3-3 µM) in combinatorial treatment. Additionally, single treatments of 1 µM darolutamide and 1 and 3 µM of FIIN1 were assessed separately for comparison with the combinatorial treatment. The proliferation (Figure 9a) as well as the cell viability (Figure 9b) assays were performed. The phase contrast images were obtained from the representative wells of control wells (Figure 9c) that were illustrated for comparison with the combinatorial treatment images (Figure 9d).

The proliferation of cells was significantly decreased starting from the 0.3 µM FIIN1 + Daro combinatorial treatment where the confluence was around 7.5 % compared to 14 % of DMSO-control at 71h time-point (Figure 9a). The highest concentration, 3 µM of FIIN1 + Daro combinatorial treatment, clearly decreased the confluence to 2.5 % at the endpoint. The rest of the treatments resulted in similar result as the 1 µM FIIN1 + Daro combinatorial treatment, showing no obvious difference between the single and combinatorial drug treatments in terms of cell proliferation. On the contrary to proliferation, the cell viability results suggested a minor effect from combination treatment compared to single treatment, as the Daro 1 µM alone resulted in 45 % cell viability, FIIN1 1 µM alone (40 %), but the combinatorial Daro + FIIN1 1 µM treatment resulted in 25 % cell viability compared to the DMSO-control (Figure 9b). Likely due to the high variation within DMSO-control triplicates, the statistical analysis did not confirm the difference between combinatorial and single treatments to be significant. According to the live-cell imaging results (Figure 9c), cell confluence decreased in response to drug treatment compared to DMSO-control, which associated with confluence growth, as expected. No significant differences in cell proliferation when single treatment images (Figure 9c) compared to Daro + FIIN1 1 µM combinatorial treatment (Figure 9d) could be

suggested. However, differences between single treatment and control as well as combinatorial treatment and control was observed (Figure 9c-d). In addition, phase contrast images of combinatorial treatments did not suggest differences between 1 and 3 µM FIIN1 combinations (Figure 9d).

Nevertheless, the quantified difference in cell viability between the 1 µM FIIN1 (40%) as well as darolutamide (45%) single treatments compared to combinatorial treatment (25%) in the figure, statistical analysis of cell viability, as well as the proliferative trend (Figure 9a), and phase contrast images, did not support this finding. All in all, we can conclude that there was no biologically significant difference between the single and combinatorial treatment in VCaP 2D monoculture model (Figure 9).

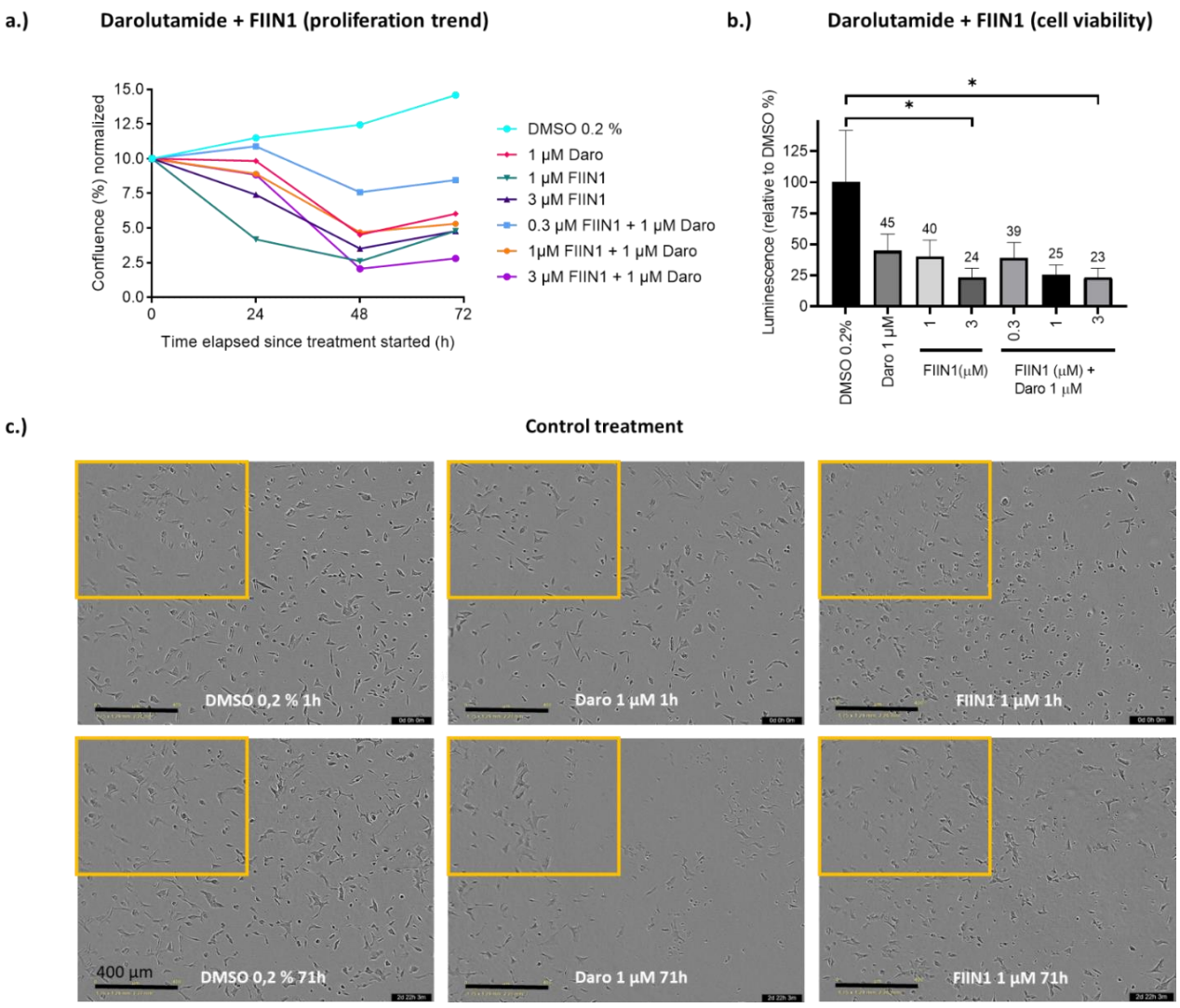

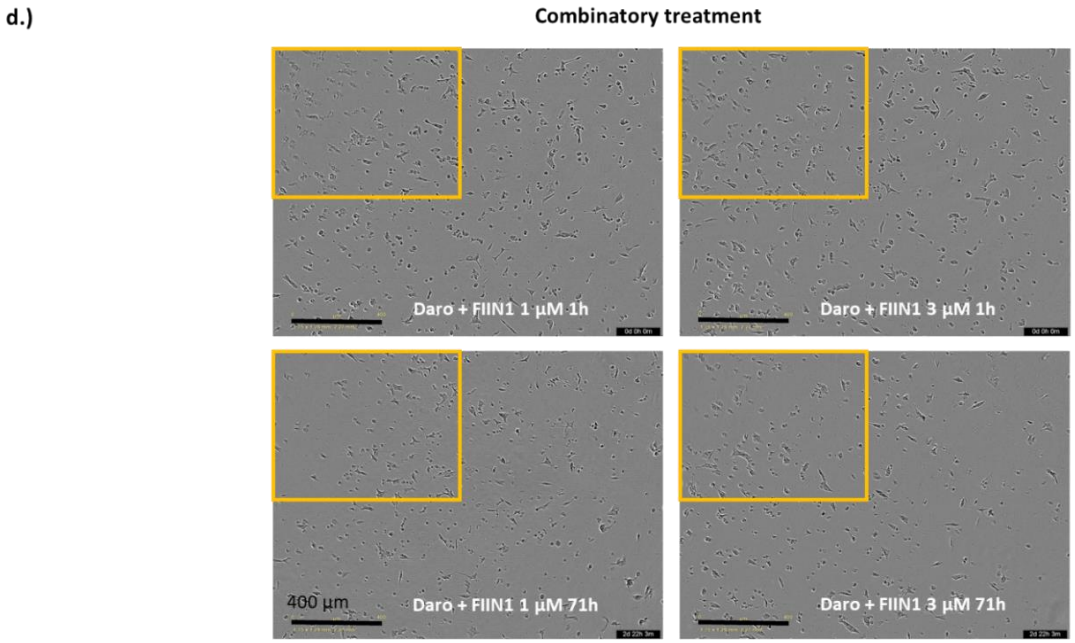

Figure 9. In the 2D monoculture model, combinatorial treatment of darolutamide with FIIN1 did not have significantly higher effect compared to the drugs in single treatment. Darolutamide/Daro was given as 1 µM in all combinatorial treatments. a.) Normalized cell proliferation trend shown as confluence (%) quantified by the IncuCyte S3 2020 A software. b.) Cell viability measured at 72h after initial drug treatment, shown as the mean relative (%) to DMSO-control luminescence signal (value above bar). Each drug treatment sample as well as control was represented as triplicates. Statistical analyses performed by Kruskal-Wallis and Dunn's post-hoc test of drug treatment in comparison to DMSO-control, Daro and FIIN1 single treatments. * = $P \leq 0.05$. c.) and d.) Illustrative Phase contrast images by the IncuCyte S3 taken 1 hour after drug treatment start and 1 hour before the endpoint for representative wells of d.) 1 µM and 3 µM FIIN1 + Daro combinatorial treatments. Error bars illustrated as standard error of mean. Scale bar; 400 µm.

3.5 Addition of CAFs to VCaP 2D culture model did not affect the effectiveness of drug combinations compared to single treatment.

As was previously described, it was suggested that including CAF- component in 2D culture model for drug sensitivity tests could lead to more biologically relevant results compared to standard monoculture 2D models. Therefore, the combinatorial treatment effect of darolutamide and FIIN1 in 2D co-culture model consisting of both VCaP tumour as well as stromal CAF cells, was assessed. Due to CAFs are labelled with GFP, they can be visualized under the green channel for the live-cell imaging (Figure 10).

Proliferation analysis of the 2D co-culture in Figure 10a, detected the highest cell growth for the DMSO-control (15 %), which was confirmed by the cell viability results (Figure 10b) as well as imaging results (Figure 10c). The combinatorial treatment of Daro + FIIN1 1 µM was not associated with significantly higher inhibitory effects according to proliferative curve and imaging results when

compared to FIIN1 or darolutamide 1 μM single treatments. On the contrary to darolutamide, FIIN1 1 μM single treatment showed higher cell proliferation compared to combinatorial treatment (Figure 10a, 10c-d). Unexpectedly, single treatment of darolutamide was associated with the lowest proliferative trend (7 % confluence at the endpoint) and confluence in imaging results, nevertheless its higher cell viability (66%) compared to Daro + FIIN1 1 μM combinatorial treatment cell viability (56%) (Figure 10a-d). Meanwhile Figure 10b suggested slight differences of co-culture viability between Daro (68%) or FIIN1 (66%) 1 μM single doses and their corresponding combinatorial treatment (56%). These differences could not be confirmed statistically, neither by other experimental methods (Figure 10). Comparison of FIIN1 3 μM with its Daro + FIIN1 3 μM combination did not detect significant differences in proliferation (Figure 10a) and confluence (Figure 10d). However, slight differences in cell viability were detected (Figure 10b).

Taken together, current experiments did not detect any significant differences between single and combinatorial drug treatments in terms of their effect on proliferative capability and viability of the co-culture.

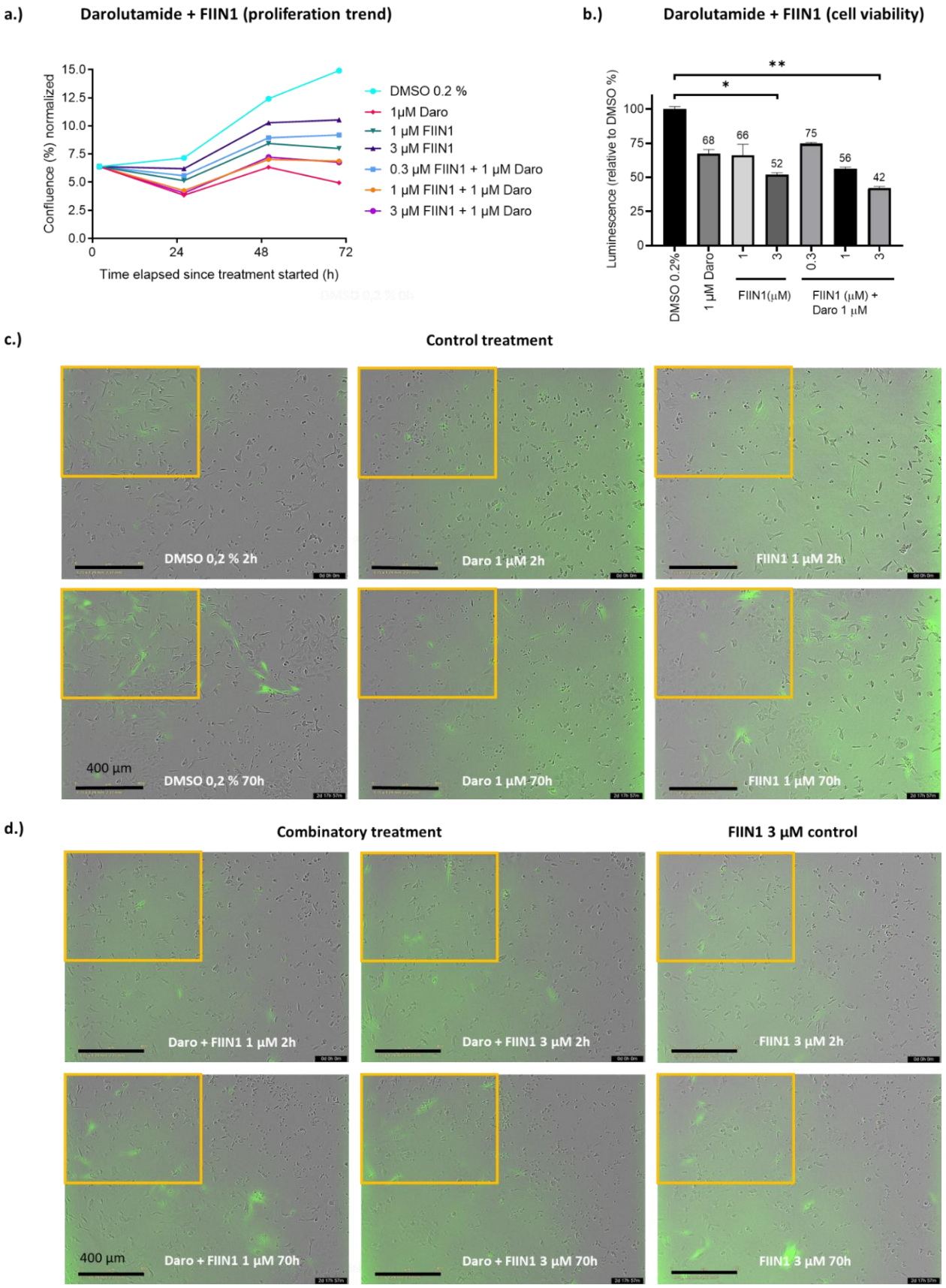

Figure 10. Addition of CAFs to VCaP 2D culture model did not significantly affect the effectivity of combinatorial treatment compared to single treatment. Darolutamide/Daro was given as 1 µM in all combinatorial treatments. a.) Normalized cell proliferation trend shown as confluence (%) quantified by the

IncuCyte S3 2020A software. b.) Cell viability measured at 72h after initial drug treatment, shown above each bar as the mean relative (%) to DMSO-control luminescence signal. Each drug treatment sample as well as control was represented as triplicates. Statistical analyses performed by Kruskal-Wallis and Dunn's post-hoc test of drug treatment in comparison to DMSO-control, Daro and FIIN1 single treatments. * = P ≤ 0.05, ** = P ≤ 0.01. c.) and d.) Illustrative Images from the IncuCyte S3, acquired by Phase contrast and Green- channel filter where CAFs are detected as green and tumour cells as grey. Images were taken 2 hours after drug treatment start and 2 hours before the endpoint for representative wells of c.) DMSO-control, 1 µM single treatments. and d.) 1 µM and 3 µM FIIN1+ Daro combinatorial treatments and FIIN1 3 µM single treatment. Error bars illustrated as standard error of mean. Scale bar; 400 µm.

3.6 3D organotypic model optimization

Due to specific features of the cell line, conventional way of cell seeding, such as seeding VCaP cell suspension directly into the gel would not be an option. Therefore, alternative VCaP growing methods were studies at first. VCaP pre-growth in a U-Shape plate and in a non-adherent Petri dish prior to the gel seeding was studied.

Non-adherent surfaces of both U-shape and Petri dish enabled formation of freely floating clusters from the single cells. These floaters subsequently formed long clusters in Petri dishes, which required regular mixing by pipetting up and down as can be observed in the Figure 11. In the current optimization experiment the mixing was initiated on the second day of pre-growth. After optimal spheroid and cluster formation, they were seeded with different organoid densities into Angiogenesis µ-slide plate with Matrigel.

The optimization experiment revealed that both pre-growth platforms yielded 3D organoids that were able to grow and stay alive for up to 17 days, since seeding into Matrigel (Figure 11). It was also found that tested 20 and 40 organoid/well seeding densities were likely too little for actual experimental morphological image analysis, as illustrated in the Figure 11. Regarding the gel protocol, Matrigel and the generally utilized in the lab gel protocol with the 2:1 bottom, and upper gel density proved to be optimal, thus was kept for the future 3D monoculture. Petri dish was chosen as a pre-growth platform due to its ability to generate larger number of organoids than U-shape plate.

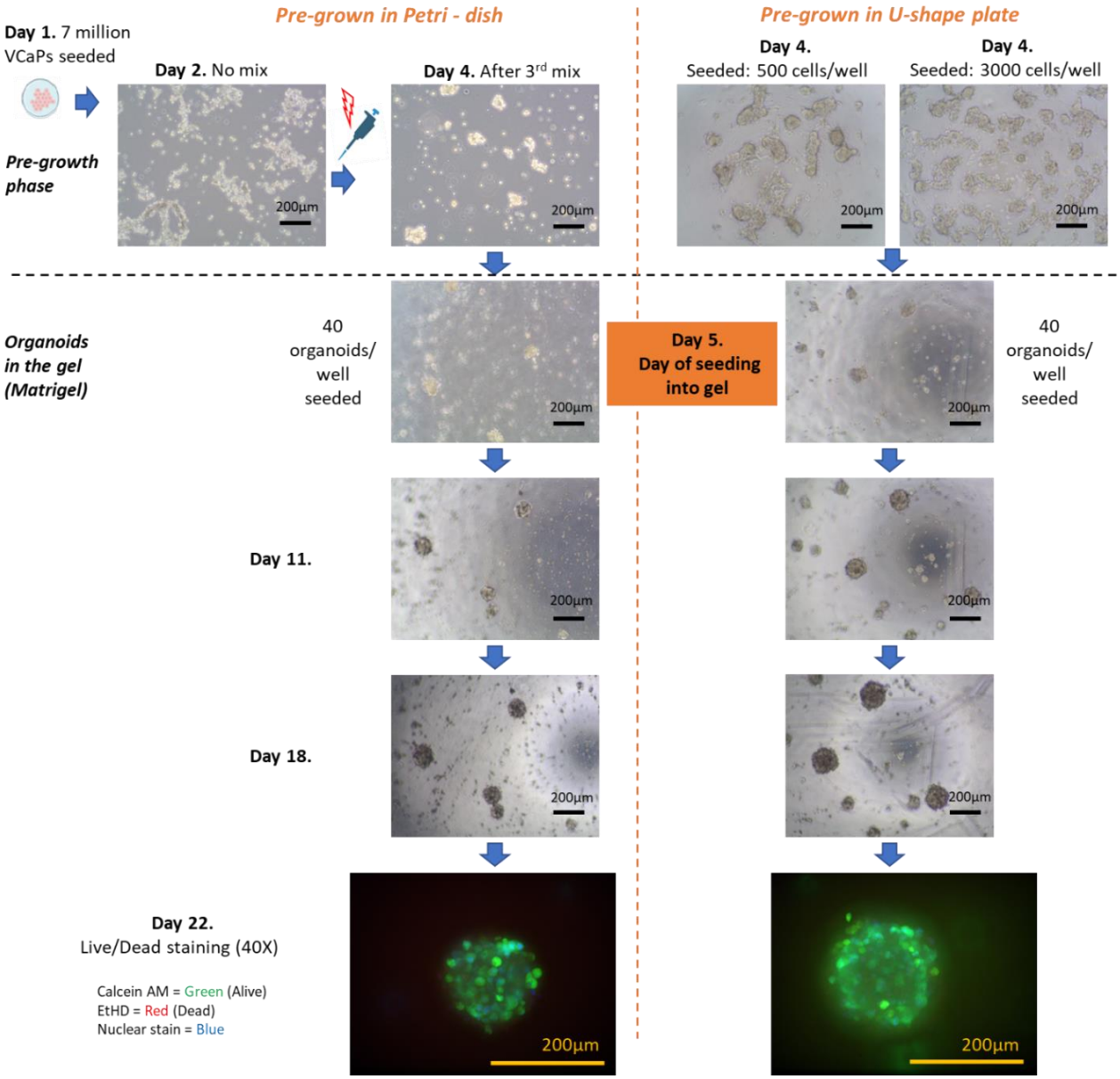

Figure 11. Optimization experiment with 40 organoids/well seeded into Matrigel, utilizing different pre-growth platforms suggested organoid growth, and organoid viability up to 17 days for both platforms. Platform type is indicated column-wise and experiment stage (pre-growth/Matrigel stage) row-wise. Clusters in Petri dish was mixed to avoid cluster chain formation. Pre-growth of clusters utilizing U-shape plate is illustrated with two different seeding densities. Organoid growth was monitored by the Inverted phase contrast microscope (Olympus, Japan). The endpoint of the experiment (Day 22) was detection of alive and dead cells by Calcein AM for alive cells and Ethidium Homodimer (EtHD) for dead cells (both Invitrogen, Thermofisher Scientific, USA). Nuclei were detected by the Hoechst 33342 stain. Results were visualized by Spinning disk confocal microscope (Zeiss Axiovert-200M, microscope,) utilizing the CSU22 spinning disk confocal unit (Yokogawa, Japan). Under fluorescence stains were excitated as following; Calcein AM as green, EtHD as red and nuclear stain as blue. Confocal images were magnified 40X. Scale bar; 200 µm.

3.7 3D organotypic VCaP model suggests therapeutical effect of higher treatment concentrations on organoid size and viability

To evaluate the therapeutical potential of antiandrogen and FGFR-inhibitor drug combination in *in vivo*-like environment, inclusion of CAFs is not enough. As a natural behaviour of PC would require TME- characteristics, including but not limited to 3D- differentiation of cells (Åkerfelt et al., 2015). Therefore, combinatorial treatment was further studied in 3D organotypic model, at first in a monoculture.

Initially, VCaPs were pre-grown in non-adherent Petri dish before seeding into an angiogenesis 96-well µ-Plate with Matrigel. Based on the previous optimization, seeding density was set to be as 80 VCaP organoids/well and general gel protocol was utilized. As several features of 3D organoid, develop slower compared to the 2D (Fontana et al., 2020 ; Joseph et al., 2018), the time of the experiment had to be extended. Therefore, organoids were treated starting only from the 5th day from organoid seeding into the gel, and combinatorial treatment duration was set to be 6 days. Experiment was monitored with live-cell imaging by IncuCyte S3. At the end of the drug treatment, live-cell staining was performed with Calcein AM, and organoid were imaged by confocal microscopy. After confocal imaging, cell viability measurements were performed. Morphological analysis was run by the Automated Morphometric Image Analysis (AMIDA) software (Härmä et al., 2014). Two morphological parameters were investigated: 1) Area of organoids shown as average area of segmented structures in pixels and 2) Roughness, which indicates the average roughness of segmented structures in percentage. The area is a marker of tumour growth and organoid roughness as depicts cell stress and cytotoxicity in response to drug treatment.

As can be observed from the Figure 12, VCaP 3D-organoids expanded in the DMSO-control and lower drug concentrations between the 1st and 6th days of drug (Figure 12). Regarding the 1 µM combinatorial treatment, the difference in organoid area compared to single treatment was not clear. However, the 3 µM combinatorial treatment indicated reduced growth of organoids in response to drug treatment compared to control and lower drug treatment concentrations (Figure 12.). The green Calcein AM staining confirmed the viability of the VCaP-organoids in the experiment (Figure 12). Intriguingly, the core of the organoids was suggested to be non-viable according to the Calcein AM staining, which might suggest non-alive cells in the middle of the organoid, and hypothetically, one of the *in-vivo* characteristics of 3D tumours, a hypoxic core (Fontana et al., 2020).

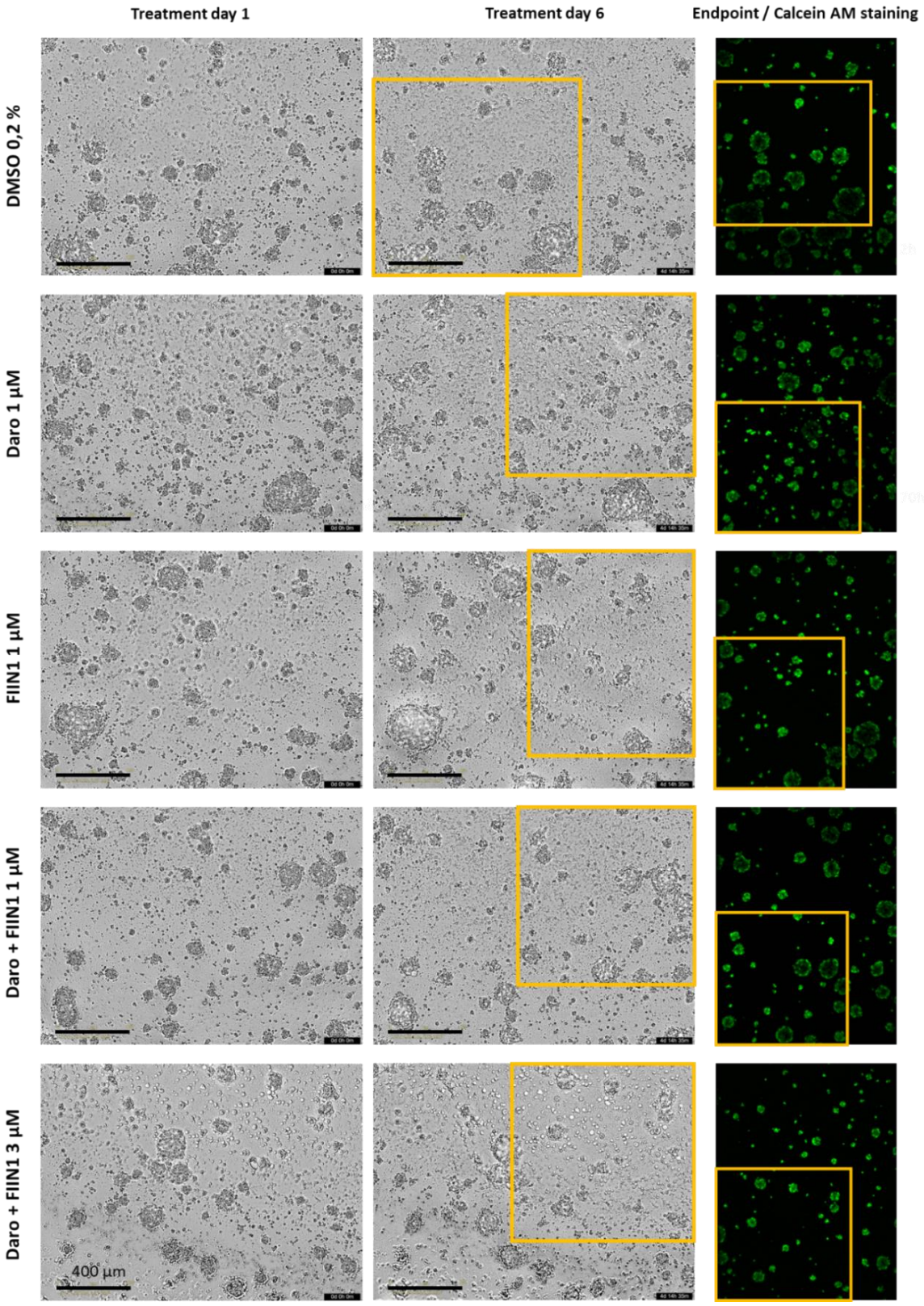

Figure 12. Live-cell imaging detects inhibition of 3D organoid growth in response to 3 µM FIIN1 + Daro. Confirmation of organoid viability by Calcein AM staining. Representative images of DMSO-control and single as well as combinatorial treatments at day 1 and day 6 of treatment. Live-cell phase contrast imaging performed by IncuCyte S3. Calcein AM staining (viable organoids, green) of the representative images is shown (right-most column). Fluorescence images were captured by the spinning disc confocal microscope. Scale bar; 400 µm. Same area in the Calcein AM and live-cell images is indicated with yellow lines.

The AMIDA software detected reduced area of VCaP 3D-organoids in response to 3 µM FIIN1+ Daro combination and 3 µM FIIN1 single treatment compared to DMSO-control (Figure 13a). Similar drug treatment combination also significantly increased proportion of surface roughness (%) compared to DMSO-control. This indication of rougher edges in organoids in response to 3 µM combinatorial treatment, could suggest a possible indication of increased organoid apoptosis and cytotoxicity from the drug treatment (Figure 13b). Cell viability was significantly reduced by 3 µM FIIN1 + Daro combinatorial treatment with resulted 25 % relative to DMSO-control viability and FIIN1 3 µM single treatment (40 %) (Figure 13c). However, no significant difference between 3 µM single and combinatorial treatment was detected. Interestingly, 1 µM single treatment of darolutamide and FIIN1 reduced viability only until 92 % relative to DMSO-control, however their combination reduced viability until 59 %, which was not statistically significant (Figure 13c).

In conclusion, VCaPs grown in 3D monoculture, did not have any significant drug response differences between single and combinatorial darolutamide and FIIN1 treatments. The significant biological effect from the drug treatment itself was only detected with 3 µM FIIN1 treatment and 3 µM FIIN1 + Daro combination, as was observed with decreased area of organoid and lower viability in response to drug treatment as well as increased organoid roughness, which was more evident in 3 µM combinatorial treatment.

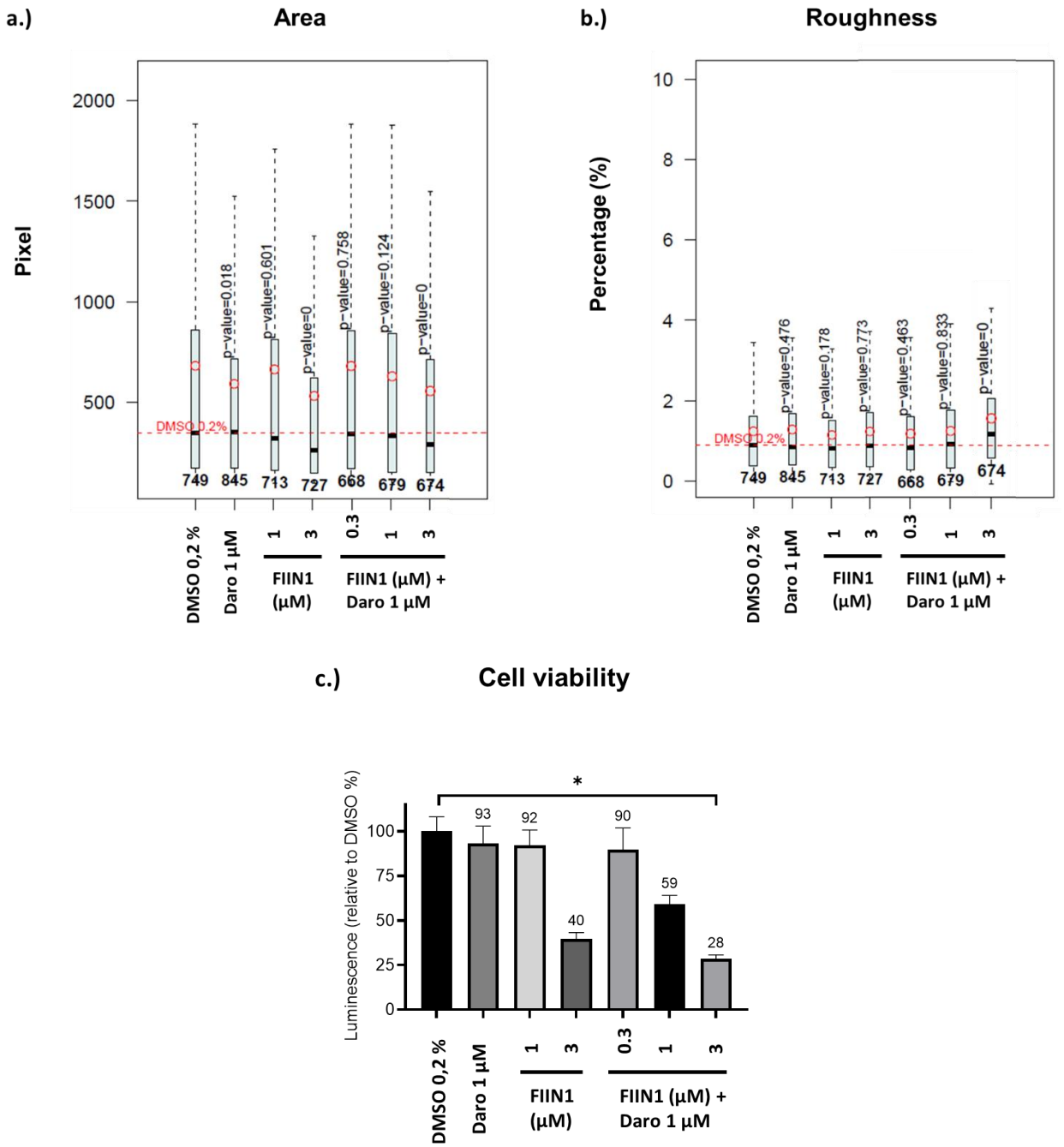

Figure 13. Area, roughness, and cell viability of organoids were significantly affected by 3 µM FIIN1 + Daro 1 µM compared to control. Morphological data was quantified, segmented by AMIDA, and visualized as box (half of cases) and whisker (quartiles) plots with median (cross line) average (circle) presentation by RStudio. Each drug treatment sample as well as control was represented as triplicates. Significance was calculated by Mann- Whitney U test with Bonferroni correction in comparison to DMSO-control. *P*= 0 equals to *P* < 0,001. a.) Size of organoids calculated as area of surface in pixels of segmented objects. b.) Cell stress and cytotoxicity of cells presented as roughness in percentage (%) of segmented objects. c.) Cell viability with significance calculation by Kruskal-Wallis and Dunn's post-hoc tests of drug treatment in comparison to DMSO-control, Daro and FIIN1 single treatments. Mean luminescence represented above each bar. Significancy level is represented as following * = P ≤ 0.05. Error bars illustrated as standard error of mean.

3.8 3D co-culture optimization and its preliminary results suggest no effect from combinatorial treatment

Inclusion of CAFs into 3D organotypic VCaP culture would result in a complex, almost complete set of TME- characteristics, including tumour-stroma interaction (Bonollo et al., 2020). As a result, this was suggested to be the most in vivo-like VCaP cell model system for investigating the combinatorial treatment potential in PC *in vitro*.

To grow both cell cultures together as an organotypic model, the ECM composition was modified into Matrigel and Collagen type 1 mixture. The treatment experiment was monitored by the IncuCyte S3. At the endpoint, Calcein AM staining, and cell viability experiments were performed.

Optimization of 3D co-culture resulted in two issues. First, the uneven seeding of organoids at the seeding day resulted in higher density in the peripheral area of the wells and only few tumour organoids in the centre area (Figure 14, left most column). Thus, whole well imaging was conducted by the IncuCyte S3 to confirm the presence of organoids in each well. Secondly, gel contraction occurred between the treatment days 3 and 5, depending on the drug treatment (Figure 14), and even earlier in initial 3D co-culture optimization. Due to these two issues, morphological analysis by AMIDA was not performed. Nevertheless, the 3D co-culture was still able to grow and form a tumour-stromal network with majority of organoids managed to stay structured and viable together with CAFs, as confirmed by the Calcein AM staining (Figure 14). It can be also noted how fibroblast-VCaP organoid network formation was inhibited in response to Daro + FIIN1 3 μM combination. The potential difference between a 1 μM single treatment and their combination, could not be detected in the figure (Figure 14).

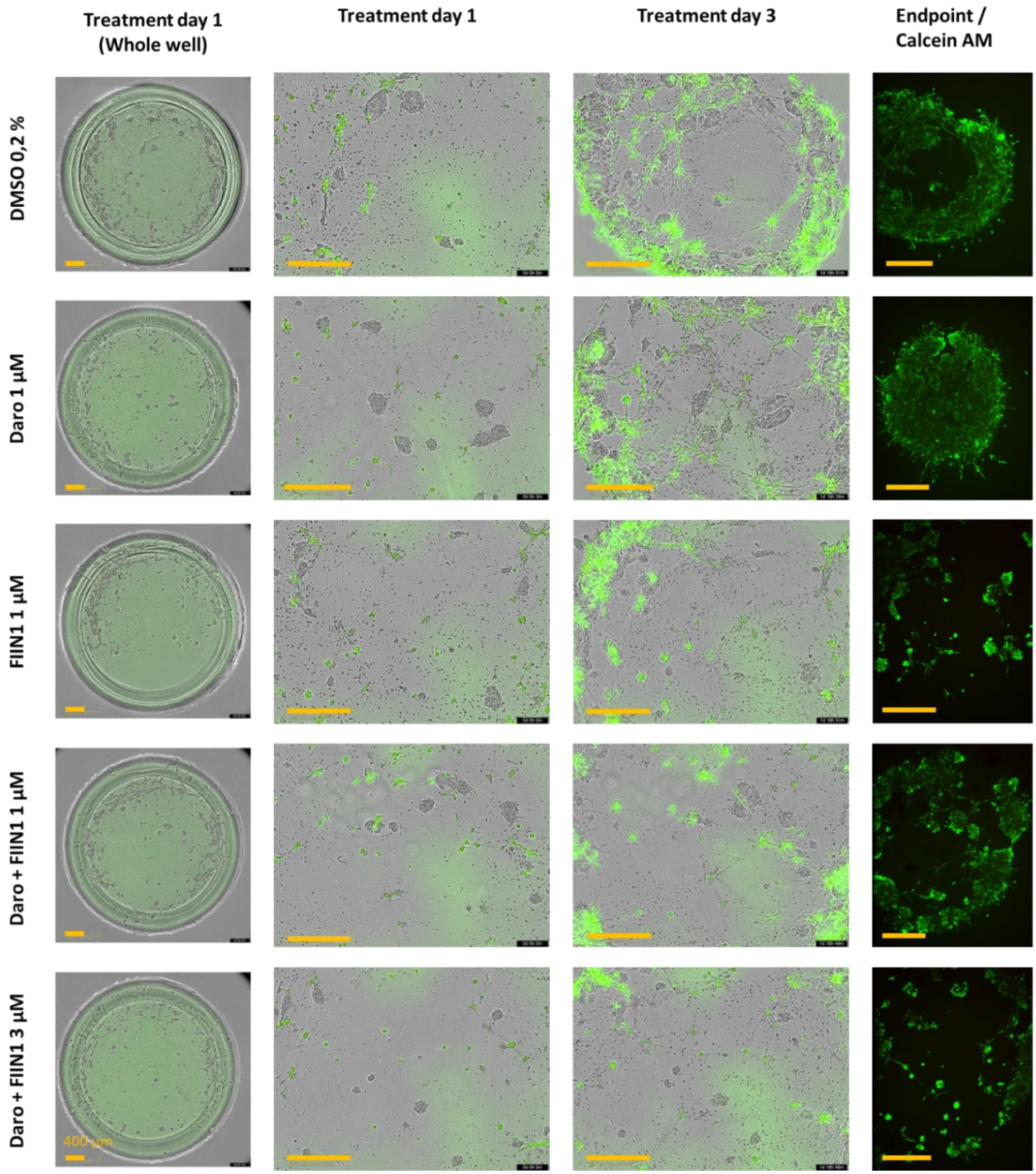

Figure 14. Addition of CAFs into VCaP 3D organotypic model facilitated co-culture development and ECM contraction. Representative wells of DMSO-control and selected single and combinatorial treatments of 3D co-culture; whole well imaging (left-most column) illustrating the seeding density of the well at the first day of drug treatment. Magnified live-cell imaging (second and third columns) illustrating single organoid/CAFs growth before major gel contraction. IncuCyte S3 imaging where CAFs were detected as green and tumour cells as grey. Calcein AM staining was conducted (right-most column) and fluorescence captured by spinning disc confocal microscope at the endpoint/ treatment day 6 for confirming viability (green, viable). Scale bar; 400 µm.

Viability analysis of tumour and CAF co-culture did not display any significant differences between DMSO-control or single and combination treatments (Figure 15). Mean values of each treatment

also suggest that there was no effect from either darolutamide single treatment or its combination with FIIN1 1 µM (131 % vs 104 %) (Figure 15).

It can be concluded that 3D co-culture optimization was shown to be still reliable in investigating the co-culture viability response drug treatment. Preliminary 3D co-culture results suggest that Daro + FIIN1 1 µM and 3 µM combination treatment were not superior to a single treatment in terms of effectivity, as can be concluded from the figures 14 and 15.

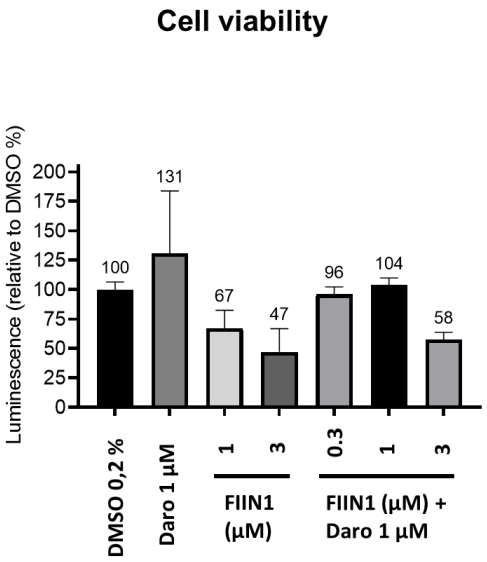

Figure 15. 3D co-culture viability results did not display any significant differences between drug treatment and DMSO-control. Relative luminescence to DMSO-control of co-culture in percentage (shown as mean values above each bar) with significance calculation by Kruskal-Wallis and Dunn's post-hoc tests of drug treatment in comparison to DMSO-control, darolutamide (Daro) and FIIN1 single treatments. Each drug treatment sample as well as control was represented as triplicates. Error bars illustrated as standard error of mean.

3.9 3D co-culture model was the least sensitive to drug treatments and significantly different from the 2D monoculture.

The final study objective was to investigate whether there are significant differences in drug responses between cell culture models. In specific, to analyze the differences of PC viability in response to inhibitor treatments in simplistic 2D monoculture compared to more in vivo-like cell models. Sample luminescence values normalized to each cell culture model's DMSO-control values (%) were utilized for the model comparison analysis.

The analysis demonstrated the following results: 1) difference between 3D co-culture and 2D monoculture in Daro + FIIN1 1 µM (104 % vs 25 %) and 3 µM (58 % vs 23 %) combinations (104 % vs 25 %), 2) difference between FIIN1 1 µM single treatment response in 3D monoculture and 2D monoculture (92 % vs 40 %) (Figure 16a). A heatmap summarizes all the mean relative to DMSO-control values (%) and illustrates how the 3D co-culture was associated with the lowest sensitivity to drug treatment among cell culture models The most sensitive model was revealed to be 2D monoculture. Nevertheless, a suggested trend of 3D monoculture associated with higher sensitivity to FIIN1 single treatments but lower sensitivity to darolutamide single treatment when compared to 2D co-culture could be observed (Figure 16b).

In conclusion, cell viability analysed after drug response of darolutamide and FIIN1 combination was indeed affected by the TME and inclusion of CAFs. However, the effect becomes significant only when comparing two sufficiently different models, such as 2D monoculture and 3D co-culture.

a.)

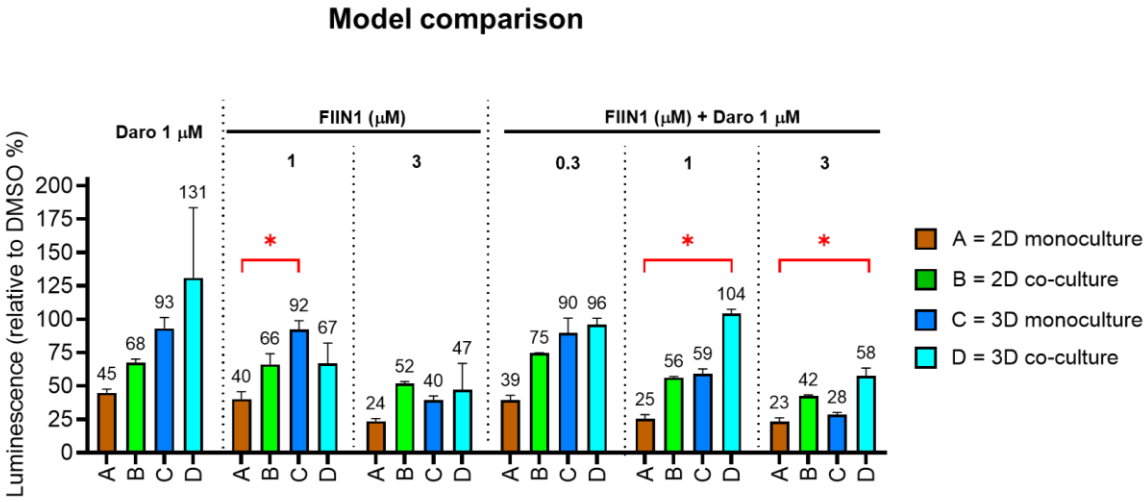

b.)

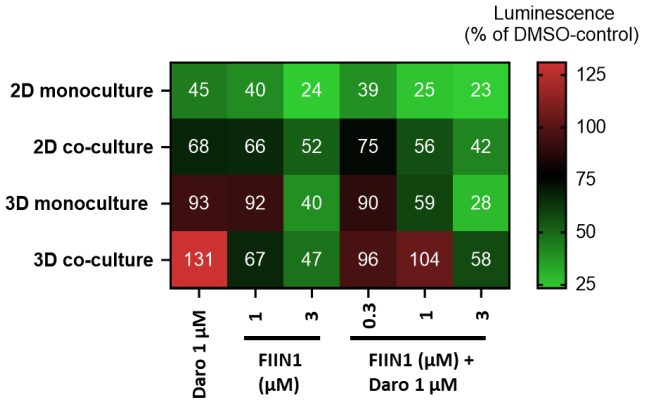

Figure 16. Drug sensitivity to Daro + FIIN1 1 µM and 3 µM combinations was significantly lower in 3D co-culture compared to 2D monoculture. Among models, 3D co-culture was the least sensitive to any type of drug treatment. Comparison of all experimental models in terms of cell viability including statistical analysis of significance. a.) The four experimental models were compared together by their relative to DMSO-control luminescence shown in % (shown above bars). Results presented according to the drug treatment given (annotated on top) and models annotated with the colour of bars (legend). Significance tested by Kruskal-Wallis and Dunn's post-hoc tests by comparing models within each drug treatment (separated by dotted line). Significancy level is represented as following * = P ≤ 0.05. b.) Model comparison summarized as a heatmap. Models represented according to a row and columns represent a type of drug treatment. Cell values illustrate mean luminescence value of each model.

4 Discussion

Prior to investigating the main questions of the current thesis, validation studies of AR expression in selected cell lines as well as darolutamide and FIIN1 sensitivity were performed. AR expression and activity were observed in VCAP prostate cancer cells and in CAFs, as indicated by a dose-dependent increase of PSA expression in VCaP as well as AR expression in both VCaP and CAFs. This was in line with previous studies (Bonollo et al., 2020 ; Dai et al., 2017 ; Sampson et al., 2013). Altogether, these preliminary results were supporting and validating the selection of VCaP and CAF as useful for the current study. VCaP cells showed sensitivity to ascending doses of both darolutamide and FIIN1 single treatments in terms of cell viability and, to a lesser extent, also to proliferation. These observations are in accordance with the literature regarding darolutamide (Fizazi et al., 2018 ; Sugawara et al., 2018) and FGFR-inhibitor effectivity as an anti-proliferative, and cell viability inhibiting agents in cancer cells and particularly in VCaP (Feng et al., 2012). FIIN1 was not previously tested in VCaP cells. However, taking into account previous studies testing sensitivity of VCaP cells to the older generations of selective- FGFR inhibitors, such as AZ8010, an anti-proliferative and viability inhibiting effect of FIIN1 was expected (Feng et al., 2012).

4.1 Combinatorial treatment was not superior to single treatment in any of *in vitro* models

The first aim of the current thesis was to evaluate the effectivity of combining both AR and FGFR-pathway inhibitions by the use of second-generation antiandrogen darolutamide and FIIN1 inhibitors simultaneously in VCaP cells. We decided to test single and combinatorial drug treatments in simplistic 2D monolayer culture, as well as more *in vivo*-like cultures and organotypic 3D models of tumour cells co-cultured with CAFs embedded in extracellular matrix.

Results from the current 2D monoculture, 2D co-culture, 3D monoculture and 3D co-culture *in vitro* models suggest that darolutamide in combination with FIIN1 did not significantly reduce the viability of prostate cancer cells compared to single darolutamide or single FIIN1 treatment, using a defined dose concentration. Nevertheless, in 2D monoculture, a combinatorial treatment with 1 μM of each drug reduced cell viability, but the effects were not statistically significant. There was, however, a small additive effect and the inhibition was slightly more pronounced when compared to darolutamide or FIIN1 single treatments at 1 μM. This could suggest that a combination of both AR and FGFR-second-generation inhibitors may at least exhibit additive therapeutical effect, at least in 2D monoculture. The additive effect from combinatorial treatment could theoretically arise from the

possibility that both Androgen-dependent (AF-2-activated) as well as the RTKs-specific Androgen-independent (AF-1-activated) signalling pathways are blocked by the combination of drugs, as used in this study (Antonarakis et al., 2016 ; Tan et al., 2014). The individual blockage of both the FGFR and the AR-signalling pathways by themselves was previously attributed to reduced cancer activity, proliferation and progression both *in vitro* as well as in xenograft models (Feng et al., 2012; Fizazi et al., 2018), but no studies have yet administered inhibitors targeting both pathways simultaneously, and in combination. However, there was also indication that FGFR-inhibitors given together with other anti-tumour drugs may improve the therapeutical effect of these chemotherapeutic agents indirectly. This might occur by increasing the sensitivity of cancer cells to treatments with agents against which the cells may have initially been resistant. This includes other RTKs inhibitors, particularly against EGFR inhibitors in breast cancer (Chae et al., 2017). Moreover, evidence of FGFR and AR-signalling interplay in PC has been described (Giacomini et al., 2021). Also, another possibility is that specifically in 2D monoculture, the combinatorial drug therapy is indeed more effective compared to single treatment. This is indicated by lowered reduced cell viability but was not detected statistically due to high degree of experimental variation observed within drug treatment replicates. As a result, the high variability of the results reduces the statistical power of the replicates and the experiment as a whole (McKillup, 2012).

It is still highly possible that the combination of an FGFR-inhibitor like FIIN1 and an anti-androgen like darolutamide is not particularly effective in VCaP cells. VCAP cells generally show low sensitivity to many growth-inhibiting drugs, which is explained by the low proliferation rate of these cells in culture. The current study utilized the FGFR/AR combinatorial therapy for the first time in VCaP cells, which is also one of the few PC cell lines that contain wild-type AR (Sampson et al., 2013), although AR is highly amplified and overexpressed in these cells. Another possible reason for the observation that FIIN1 and darolutamide in combination were not as effective as we initially expected is the potential that the treated cells (VCaP) may harbour FGFR-gatekeeping mutations or express certain AR- variations and *de novo* mutations. Moreover, even when both pathways are effectively inhibited, there is the possibility that alternative cell survival mechanisms in PC cells exist that may bypass the sensitivity to the drugs used in this study, such as other RTK-activated signalling pathways, increased LSD1 activity which leads to epigenetic changes in PC cells and silencing of genes that may cause drug sensitivity. Another alternative is the possibility of N-MYC overexpression with simultaneous loss of *PTEN* (Makino et al., 2021) which both occur in PC, and which may also serve as a potential bypass mechanism related to AR- and also FGFR signalling. Despite the statistical limitations and the high variability of the experimental results, we observed that the

difference between combinatorial and single treatment in 2D monoculture was already minor in 2D co-cultures, and completely disappeared in the 3D models. This is suggesting that the sensitivity or lack of sensitivity of the cells may be partially influenced by the presence or absence of an ECM and TME which both are not present in 2D cultures. In 3D cultures, however, they have a strong effect on tumour cell proliferation, growth, and survival.

The results from our quantitative proliferation assays (endpoint assays) and phenotypic analyses (AMIDA image analysis program), based on confocal live-cell imaging on the other hand, did not detect any visible differences between the combinatorial and the single drug treatments. Moreover, quantitative measurements of cell proliferation in 2D models did not indicate a clear dose-dependent trend that could have been observed by measuring how fast the cell cultures reach confluence, which is a simple measure of how fast cells grow in culture. Nevertheless, reduced cell growth in 2D and increased cell stress in 3D monoculture were both observed in response to higher doses of drug treatments, compared to the controls. All in all, my data suggest low sensitivity of VCaP cells and their proliferation in 2D cultures in response to both darolutamide and FIIN1 within a 72-hour period. On the other hand, morphometric results from 3D monoculture based on AMIDA image analyses detected a more pronounced trend in which higher treatment doses were associated with smaller organoid size and a higher degree of cell stress. This could support the idea that more optimizations may be needed for meaningful 2D- proliferation studies, particularly longer drug treatment incubation which should allow the accumulation of more significant differences in growth over an extended period of time, as well as the application of morphology-based assays in 3D models for precise quantifications of small differences, particularly the AMIDA program or any other phenotypic analysis tools.

4.2 Reduced sensitivity to combinatorial and single treatment was observed in VCaP models with an *in vivo*-like ECM and TME

The second aim of the thesis study was to investigate if combinatorial treatment effectivity was affected when administered to cell cultures of PC cell lines under conditions that include more TME-characteristics, so-called *in vivo*-like models. One of the most relevant elements of such organotypic models is the presence of a physiologically relevant ECM, such as collagen type I, or Matrigel, a laminin-rich basement membrane extract. To statistically investigate differences in cell viability between models, control viability values relative to each of the models used were analysed.

Despite the observed therapeutical effect from single and combinatorial treatment on cell viability in 2D co-culture, lower sensitivity of co-cultures and especially of 3D co-cultures to overall drug

treatment compared to monoculture was observed in terms of cell viability. This could be explained by the presence of stromal-epithelial interaction, originating from the inclusion of cancer-associated fibroblasts or CAFs in 2D co-culture. The presence of fibroblasts or CAFs represents one of the key components in TME. CAFs are generally promoting the growth of PC cells, their proliferation and survival under various stress conditions, thus they are contributing to cancer progression and acquired therapy resistance. (Fontana et al., 2020; Bonollo et al., 2020). Moreover, reduced sensitivity in 2D co-culture goes in line with general trend of the current study, where reduction of single and combinatorial treatment effectivity is observed in response to more TME-components simulated *in vitro*. Particularly, significant differences between 2D monoculture and 3D co-culture sensitivity were observed in the current study. Important to notice is that a minor reduction of cell viability observed by single treatment of darolutamide was limited to the simple, 2D monolayer models of VCaP monoculture and co-culture and totally disappeared in 3D organotypic models. According to Joseph et al. (2019) improved resistance of cancer to anti-tumour treatment is expected in 3D *in vitro* cultures compared to 2D. It was suggested that the 3D organotypic model could improve resistance to drug treatment, due to inclusion of TME-features that are absent in 2D models. Specifically, this is the polarity and differentiation of cells in organoids, the presence of complex cell-cell interactions such as gap- and tight junctions forming between tumour cells within an organoid, and finally, the support of cells by the ECM (Fontana et al., 2020 ; Åkerfelt et al., 2015). Moreover, increased resistance of cancer cells to drug treatment in 3D conditions, and particularly to antiandrogens such as darolutamide compared to 2D- culture models has been previously reported. Specifically, it was found that 3D models of cancer were often associated with overall improved resistance to anti-cancer therapy including response to antiandrogens, such as enzalutamide and anti-taxanes compared to a single cell culture model with unassembled organoids (Hemelryk et al., 2021). All of this is suggesting that 3D-modelling reduces the drug effectivity regardless of the drug target mechanism. This may be related to the protective effects of dense multicellular aggregates, especially organoids, which form tight cell-cell-interactions that may impede the uptake of drugs and the effectivity of these drugs. Results of previous studies are in line with the current thesis, as in addition to darolutamide single treatment, also FIIN1 was ineffective when cells were introduced to 3D modelling.

In a more physiologic 3D co-culture model – especially when combined with CAFs, the resistance of cancer cells to drug treatment was even more pronounced concerning the exposure to darolutamide and combinatorial treatment accordingly. However, in contrast to darolutamide, FIIN1 single treatment effectivity was not different in 3D monoculture compared to 3D co-culture model. Thus, it cannot be concluded that improved cancer resistance occurs in more *in vivo*-like model regardless of

the MoA of a drug. As a result, the reason of reduced response to combinatorial treatment in 3D-co-culture compared to 3D monoculture and more simplistic models, could result from improved resistance to specifically darolutamide and not FGFR-inhibition, which will be discussed in further section of discussion. Nevertheless, as discussed in the literature, sensitivity to combinatorial treatment in 3D-co-culture was the lowest among all the models tested. This could suggest that 3D co-culture resembled the most to a genuine in vivo-like environment. All in all, suggesting that as a preclinical early-stage drug screening model, a 3D monoculture is not sufficiently predictive concerning the drug response to chemotherapy. In this case, this is illustrated by the response to FIIN1 and darolutamide in VCaP. A possible conclusion is that a 3D co-culture model would be more robust tool to evaluate effectivity of inhibitors in PC *in vitro*.

4.3 Targeting the interaction of CAFs and tumour cells as part of the TME as the future treatment strategy?

As FIIN1 is targeting mainly FGFRs and their phosphorylation, current results suggest that FGFR targeted inhibition may have therapeutical potential specifically in a co-culture model. Previously, the importance of FGFR-signalling on survival of VCaP and CAF cells has been described (Feng et al., 2012 ; Hegab et al., 2019). In addition, other co-culture studies have found that antiandrogens were less effective in PC that were grown in a 3D model together with CAFs, such as the 3D-culture of DuCaP cells with CAF (Eder et al., 2016). DuCaP cells were established from the same patient as VCaP but show different characteristics, since they were isolated from different metastases. Intriguingly, similar study found that 3D monoculture associated with more favourable antiandrogen effectivity compared to 3D co-culture, in which CAFs responded to antiandrogens even in a stimulatory manner. Additionally, they have found that spheroids in the 3D co-culture were associated with stronger expression of E-Cadherin, Vimentin and showed a lower expression AR. This may suggest that CAFs promote the AR-independent signalling of PC by certain de-differentiation pathways that are characteristic of epithelial tumours. It is also evident that these particular processes occur only in 3D-models, but not in 2D monolayer culture in which the cells are mainly engaged in cell proliferation but do not show strong indication of differentiation. This leads to the hypothesis that the main mechanisms and components in TME that drive AR-bypass are not only related to the presence of CAFs, but also to the consequences of culturing cells in a 3D microenvironment and the presence of a functional ECM. However, in one previous study (Eder et al., 2016), PC cells were grown as spheroids without external ECM and connective proteins, which might suggest that 3D-structures are differentiated to a different phenotype when cultured with CAFs, and their phenotype in co-culture is strongly supported by CAFs. Coming back to the current results, FGFR-inhibition

seems still to be effective in 3D co-cultures. However, the observed importance of combining both 3D modelling and CAF-component for PC *in vitro* study, signifies the role of stroma-ECM and stroma-organoid interactions. Suggesting that future therapies potentially could target not only the PC and stromal cells, but also ECM proteins.

There are several ECM-related drug targets and potential agents that could be further evaluated. Specifically, structural composition of the matrix degrading agents like anti-hyaluronidase and heparinase, strategies targeting CAF-ECM signalling, such as integrin signalling inhibitors (like inhibitors of focal adhesion kinase or FAK). Alternatively, agents could be used that specifically target the ECM-secreted factors that affect the development of the characteristic cancer and stromal phenotypes. This could be another area for future drug discovery and development in PC (Maia et al., 2021). However, the ECM remains as a crucial part of also a healthy microenvironment, and it cannot be solely targeted or inhibited. Yet, instead it could be modified to reduce its tumorigenic potential, such as invasion and metastasis. Moreover, it has been earlier described in PC and solid tumours that ECM undergoes modifications, such as changes in matrix compositions, structural remodelling, and increased stiffness, which were all together shown to promote cancer progression. Particularly, *in vivo* and *in vitro* studies found that collagen fibres cultured with tumour cells were actively remodelled to a preferred radially aligned orientation, which subsequently promoted invasion of tumour cells (Luthold et al., 2022). Clinical findings found that patients that had stiffer collagen structure within the tumour tissue experienced more aggressive PC progression; this is related to the frequently observed problem that some tumours are highly fibrotic. In line with this, an association was observed between increased tumour stiffness mediated by the presence of collagen type I (which is characteristic of tumour fibrosis) and increased Gleason scores (Osorio et al., 2019). Another study observed also *in vitro* an improved resistance of PC to taxane-therapy when cultured in a stiffer matrix (Yong et al., 2017). All in all, this confirms that there is also a distinct cancerous phenotype related to the activity of the ECM, particularly increased matrix stiffness, or matrix remodelling, which could be potentially targeted. Agents targeting ECM-stiffness are currently under evaluation. By MoA, they target the collagen composition itself, by depleting collagen composition in ECM directly or disturbing the collagen folding and assembly. Alternatively, there are agents inhibiting the inducers of ECM- remodelling and stiffness, like mechanotransducers and mechanosensors, whose inhibition could also have a broader anti-tumour effect (Jiang et al., 2022). These ECM-targeted potential therapies for PC could be also combined with an actual anti-tumour drug, such as antiandrogens or FGFR-inhibitors for example. Taking in count that ECM is also one of the protective components of

cancer in response to external molecules, as its connective proteins were observed to provide a protective barrier for cancer from the arriving drug treatment molecules (Maia et al., 2021).

4.4 *In vivo*-like model development and optimization

Another goal of the current thesis was to develop a more *in vivo*-like model, which could combine both 3D modelling, ECM, and stromal components of the TME, specifically in 3D co-culture with CAFs. It can be concluded that 3D co-culture optimization was not completed as planned, but I could show that it is still reliable for investigating the drug response in terms of cell viability of the co-culture as a whole. As observed by Calcein AM staining, organoids in 3D co-culture were still viable and significant morphological differences were evident in organoid formation, especially due to drug treatment and dosages. Particularly, it was found that control samples and darolutamide single treatment samples associated with more solid co-culture organoid formation and growth, but single FIIN1 treatment as well combinatorial treatment samples inhibited the co-culture organoid growth. These observations suggest that cell viability results were comparable to live-cell imaging and confocal microscopy results of the 3D co-culture. In addition, organoids in 3D models were observed with non-viable organoid core, suggesting a possible hypoxia in the middle of the organoid, as illustrated from the Calcein AM staining. Possible hypoxic core of the organoid was not as evident in 3D co-culture as in 3D monoculture, but it could be attributed to different imaging conditions as well as CAFs own fluorescent signal as interference. Hypoxic core is one of the *in-vivo* characteristics of tumours and one of the distinguishing features of the 3D organotypic model from our previously utilized 2D cell models (Fontana et al., 2020). All in all, suggesting that 3D monoculture and 3D co-culture models of the thesis harboured the main TME -characteristics and are applicable for the drug treatment sensitivity studies.

Interestingly, 3D co-culture optimization faced issues related to gel contraction, and limitation regarding morphology analysis. Particularly, due to unexpected and individual gel contraction occurrence, it was impossible to analyse the morphology of the co-culture organoid due to both dense CAF – ECM network as well as destruction of the gel and dislocation of the organoid from the focal location. Gel contraction is not a novel event in co-culture models, as it was previously described to be the result of ECM remodelling driven by CAFs for further migration and development of new connective protein so-called tracks (Ergodan et al., 2017). Due to the gel contraction, shorter pre-treatment incubation compared to 5 days in 3D monoculture was utilized, so the co-culture organoid would not grow as rapidly. The initially tested 70% of Matrigel/ 50 % of Collagen ratio led to higher rates of contraction than subsequently utilized 1:1 gel ratio, which might suggest that Matrigel is the

main PC migration and ECM plasticity driving scaffold material. Nevertheless, Collagen is known to be preferred for fibroblasts and CAFs for proliferation and elongation (Åkerfelt et al., 2015). The more profound contractility and cell migration properties by Matrigel compared to Collagen were previously observed in a study, which compared different Collagen and Matrigel ratios in terms of cancer migration and cell forces (Anguiano et al., 2020).

4.5 Study limitations

The current study has following main limitations: high variations within drug treatment groups, leading to a lower statistical power, limited applicability of live-cell imaging assays in VCaP, gel contraction of 3D co-culture model, absence of cell-specific quantifications in co-culture models, and limited assays for the drug testing. High variation within drug treatment groups, which resulted from uncomplete model optimization, as well as sparse sample sizes, all together decreased the statistical power of cell viability analyses. Practically, it required to utilize a non-parametric alternative of ANOVA, Kruskal-Wallis test, which is not as sensitive in detecting differences in smaller sample sizes (McKillup, 2012). Limitations were associated also with 3D co-culture studies, as current model encountered gel contraction at further time-points, suggesting that more optimizations would be necessary prior to quantitative morphological analyses could be utilized for the model. Moreover, VCaP cells were found to proliferate in a slow rate, which challenged to detect changes between treatment groups in live-cell imaging analyses, which suggest more optimizations for the 2D-model proliferation studies in VCaP.

Additionally, in the current study, cell viability was quantified for the co-culture as a whole, and not cell-specified, which led to open questions regarding CAF- and VCaP-specific drug treatment responses. Moreover, in the current study, in addition to morphology, proliferation and cell viability, no other assays were utilized for investigating the combinatorial treatment.

4.6 Future perspectives

There is a high potential for further studies focused on cell-specific and TME-component-specific response to second-generation FGFR and AR- inhibitors in PC. As it was observed that more TME-component recapitulating models, such as co-culture as well as models with 3D-architecture, were associated with a weaker inhibitory effect of darolutamide single treatment, the AR by-pass mechanisms could be investigated in cell-specific manner, particularly CAFs. Particular studies would require quantifiable tools to segment the cell-specific drug treatment response or alternatively ECM-specific response in co-culture models. Subsequently, it remains an open question which TME-

specific components or features in 3D organoids are the main drivers of increased VCaP and PC resistance to second-generation AR- and FGFR-inhibitors. The answer could provide potential novel drug targets for future combinatorial therapies, targeting PC and specifically AR- bypass mechanisms, not limited to AF-1 and AF-2 Androgen-signalling pathways.

In addition, as there was no clear evidence of FIIN1 and darolutamide combination superiority to inhibitors given separately, it remains unknown whether the lack of significant results is due to the actual VCaP and CAF resistance to treatment or it is due to the high variations within replicates leading to low statistical power. Therefore, another research-track for the future could be more studies with *in vivo*-like models that recapitulate both epithelial-stroma interactions as well as ECM and 3D-architecture. In particular, suggesting more validating studies as well as further *in vitro* co-culture and 3D model optimizations to avoid high variations between samples and enable morphometric and further assay quantifications.

Furthermore, these *in vivo*-like *in vitro* disease models could be developed to recapitulate specific diseases, disease-stages, as well as patient-specific phenotypes, to provide even more precision and personalization of preclinical studies. All in all, facilitating also biomedical research, as the demand for time- and cost-effective models with a robust predictive value cannot be overestimated in early drug screening.

5 Conclusions

It can be summarized that drug sensitivity of *in vitro* VCaP culture, which was confirmed to be sensitive to both AR- as well as FGFR- second-generation inhibitors, was not significantly different in single treatment compared to combinatorial darolutamide and FIIN1 treatment. Despite the lack of significant evidence of combinatorial therapy superiority to single inhibitor therapy, an association between the drug sensitivity and utilized *in vitro* model was found. It was found that overall reduction of drug therapy effectivity was associated with the TME-, and stroma-epithelium interaction harbouring models. Specifically, a significantly more viable PC cells were observed in 2D-monoculture of model of VCaP in response to combinatorial therapy compared to *in vivo*-like 3D co-culture model. Moreover, results suggest that not until CAFs and ECM scaffolding structures are modelled in 3D, darolutamide remained effective in certain extent. Suggesting further studies targeting not only tumour and stromal cells, but also ECM and stroma-ECM interactions in order to inhibit AR-independent PC progression. In addition, a trend was observed where an increased resistance to treatment was evident in 2D co-culture, 3D monoculture and 3D co-culture in ascending order compared to the 2D monoculture model. Concluding that when employing a more in TME resembling components, such as CAFs and ECM structure, there is a reduction of PC responsiveness to combinatorial therapy.

Current thesis project provides a novel insight on VCaP 3D organotypic culture response to darolutamide and FIIN1 combination regarding morphology and cell viability. Moreover, a more in vivo-like preliminary VCaP and CAF co-cultured 3D organotypic *in vitro* model was developed, which provided not only an alternative preclinical drug screening *in vitro* model for VCaP, but also an estimation of PC viability in response to darolutamide and FIIN1 combinatorial treatment. Taking in count, the importance of a 3D-architecture with cell polarization, ECM support, and stroma-epithelium interaction for PC natural architecture, particular 3D co-culture model could have a high predictive value for further preclinical drug screening studies prior to *in vivo* and clinical trials. On the contrary, large variation between replicates, limitations of morphometric analysis for 3D co-culture, and limitations of live-cell imaging analysis for 2D in VCaP, signifies the need for further model optimizations. Additionally, lack of cell-specific quantifiable studies in co-culture models as well as sparse assays for drug testing were current study limitations.

In the future, investigation of TME-specific mechanisms (CAFs, ECM, VCaP) in 3D co-culture microenvironment when responding to FGFR and AR- signalling pathway inhibition could potentially provide a novel drug resistance mechanisms and AR-alternative drug targets for PC.

Taking in count applicability of *in vivo*-like models, such as 3D co-culture model of the current study, further development of TME-recapitulating *in vitro* models would possess a high clinical value for PC and CRPC preclinical research.

6 Materials & Methods

6.1 Cell culture

6.1.1 Cell lines and conditions

VCaP and PF179T GFP CAF cell lines were received as a gift from Varda Rotter´s laboratory, Weizmann Institute, Israel. Cell lines were cultured in Dulbecco's Modified Eagle Medium (DMEM) obtained from Gibco, ThermoFisher Scientific, USA. DMEM was supplemented with 10 % fetal calf serum (FBS) (Gibco, ThermoFisher Scientific, USA), and 1 % penicillin/streptomycin (Gibco, ThermoFisher Scientific, USA). Cell lines and culture models were incubated at 37˚C with 5 % CO_2.

6.1.2 2D culture models

For the 2D monoculture, VCaP cells were seeded with a seeding density of 12 000 cells / well. Subsequently, 2D co-culture plates were seeded with 9000 VCaP cells and 600 CAF cells / well. Both models utilized 96-well flat bottom, clear polystyrene, Tissue Culture -treated microplates (Corning®, USA).

6.1.3 3D organotypic models

6.1.3.1 3D organotypic optimization

CELLSTAR® 96-well Suspension culture, U-Shape plate (Greiner Bio-One, Austria) and non-adherent 100 mm Petri dish (Thermofisher Scientific, USA) were tested as organoid pre-growth methods. For the U-Shape plate, seeding densities within a range of 500-3000 VCaP cells / well were studied. For the Petri dish, 7 million VCaP cells were seeded and were mixed by pipetting up and down on a daily manner from the day when cell cluster chains were formed (Figure 11) to make clusters rounder shaped. On the 5th day, organoids were seeded from the U-shape plate and Petri dish with 20 and 40 organoids/well densities to the 15 well µ-slide angiogenesis plate (Ibidi, Germany). Matrigel (Growth Factor Reduced (GFR) Basement Membrane Matrix, Corning®, USA) was utilized as the gel material and was polymerized to the well as usual.

6.1.3.2 3D monoculture

Two Petri dishes with 7 million VCaP cells / dish were utilized as pre-growth method with analogous protocol as in optimization except for 7-day incubation instead of 5 days. On the 7th day of pre-growth, organoid suspension was transferred from Petri dishes into two 15 ml Falcon tubes and

separated by fractionation for collecting organoids of 50-200 µm diameter. Two-time fractionation was executed as following; 1.) Falcon tubes were gently mixed by pipetting up and down and settled for 2 minutes, 2.) upper half of suspension was discarded, 3.) remaining half was similarly mixed and settled for 2 minutes, and finally, 1 ml of the pellet area was harvested from each tube for gel seeding. Manual counting was performed from a smaller organoid sample with further extrapolation and confirmed with the organoid size by Inverted phase contrast microscope (Olympus, Japan).

4 mg/ml dense bottom gel was prepared by mixing Matrigel (Corning®, USA) with DMEM medium, and was seeded into 96-well µ-plate angiogenesis (Ibidi, Gernmany) occupying 1/3 of total well volume. Combination of anagenesis µ-plate properties with the denser bottom gel layer compared to the upper gel, allowed organoid formation in a certain altitude or focal-plane, which aided with further imaging and avoided the meniscus formation. Plate was centrifuged at 200 G for 10 minutes and incubated at + 37 C ° up to 1 hour. Upper gel density of 2 mg/ ml included also organoid suspension and was seeded on top of polymerized bottom gel occupying the remaining volume of the wells with 80 VCaP organoids/well of pre-selected diameter. 1X PBS (Cityva, USA) was added into edges and reservoir of the plate for avoiding the evaporation. Centrifugation at 100 G for 15 minutes was followed by incubation at + 37 C ° for 4 hours. After gel polymerization, culture medium was added on top of each well.

6.1.3.3 3D- co-culture

Following otherwise analogues protocol to 3D monoculture, co- culture utilized Collagen type 1 (BD Biosciences, USA) / Matrigel gel mixture with the ratio of 1:1. Collagen pH was neutralized prior to the mixture preparation (see Appendix 3.1.5). Gel densities were following; bottom gel with a 0.75 mg/ml of Collagen, 2 mg/ml of Matrigel and upper gel with a 0.375 mg/ml of Collagen and 1 mg/ml of Matrigel. Cell suspension with single cells of CAF was mixed with the upper gel suspension including VCaP organoids. Co-culture was cultured with 2000 CAF cells + 80 VCaP organoids/ well.

6.2 Inhibitor treatments

6.2.1 Inhibitor molecules

FGFR; FIIN1 (Tocris Bioscience, UK) and AR inhibitors; Darolutamide (Selleck Chemicals, USA) and Enzalutamide (AdooQ® Bioscience, USA) were utilized as the drug treatment. Darolutamide and FIIN1 were given in a 3-fold dose-ascending manner as following; 0.3, 1, 3 and 10 µM. Inhibitors were given separately in a single treatment experiment and together with a fixed dose of darolutamide

in combinatorial treatment experiments. Inhibitor dilutions were prepared with DMSO (Sigma-Aldrich, USA). Prepared inhibitor dilutions were stored at -20 ˚C.

6.2.2 Immunofluorescence inhibitor treatment

VCaP 2D monoculture and co-culture models were treated with 1 µM Enzalutamide after 48-hours from cell seeding. A second-generation antiandrogen Enzalutamide treatment was given to act for 72 hours until the cell cultures were fixed and permeabilized.

6.2.3 Single and Combinatorial treatment experiments

Single and Combinatorial inhibitor treatment was given to cells at a 48-hour time-point from cell culture seeding in 2D models. In 3D monoculture, combinatorial treatment was given on a 5^{th} day from cell seeding to the gel and in 3D co-culture, at a 48-hour time-time point from co-culture seeding to the gel. Combinatorial treatment was given to act for 72 hours in 2D models and for 6 days in 3D models, while incubating. Treatment medium was changed once in the middle of the combinatorial treatment duration. 0,2 % DMSO was utilized as the negative control for the combinatorial treatment experiments. Each drug treatment, including DMSO-control was represented in 96-well plate as triplicates. Both 2D and 3D models were monitored by the IncuCyte S3 2020A (Sartorius, Germany) live-cell imaging system. At the endpoint of the combinatorial treatment experiments, cell viability assay for both models and additionally, confocal imaging with morphometric analysis for 3D models was carried as illustrated in the Figure 17.

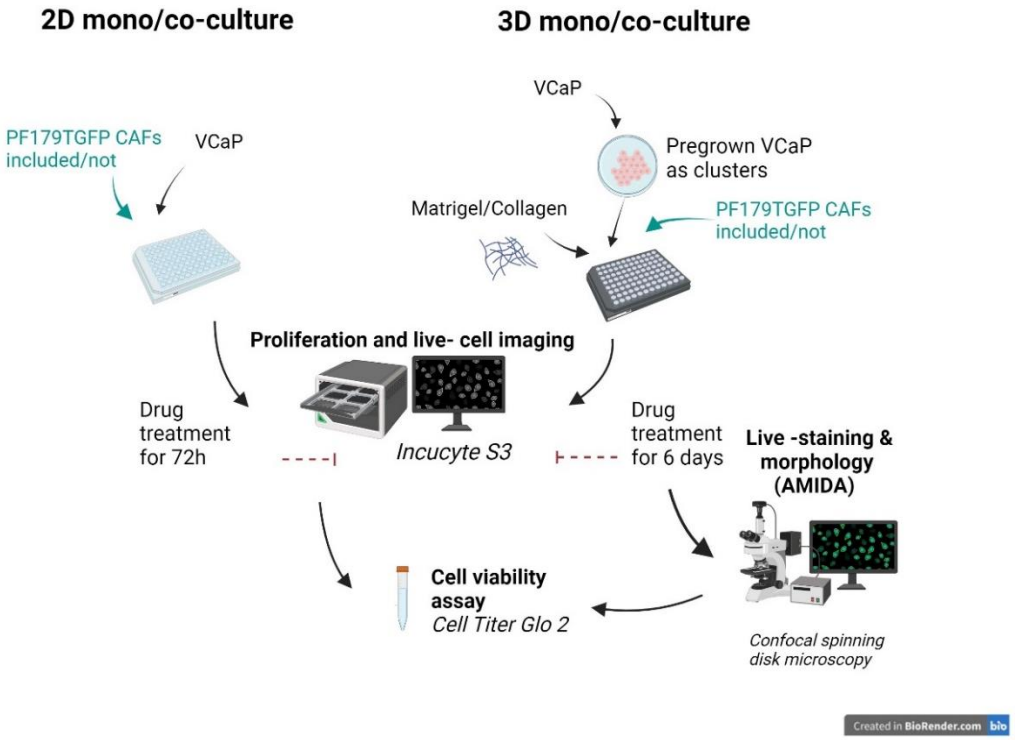

Figure 17. Visual illustration of the experimental workflow of the study. Four cell models were investigated in total: 2D monoculture, 3D monoculture, and co-culture models of both 2D and 3D. Created with BioRender.com.

6.3 Immunofluorescence

At the end of the immunofluorescence inhibitor treatment, cells were fixed and permeabilized with 4% Paraformaldehyde in 0.5% Triton X100 solution (Sigma-Aldrich, USA) (see Appendix 3.1.1) and incubated at room temperature for 10 minutes. After the incubation, cells were washed for 5 minutes three times in 1X PBS (Cityva, USA). In order to prevent non-specific antibody and intermolecular binding, which could result in high background signal, cells were blocked with 3% Bovine Serum Albumin (BSA) (Biowest, USA) in PBS solution for 10 minutes at room temperature. Blocked cells were washed again three times for 5 minutes with PBS.

Primary antibody for AR (AR 441) was diluted accordingly (Table 1.) in 3% BSA + PBS and incubated at a room temperature for 1,5 hour. Afterwards, three times of 5 minutes PBS washes were performed. Secondary antibody was incubated for 1 hour in a room temperature together with a Hoechst- nuclear stain according to the Table 1. Before imaging, another three times of 5 minutes PBS washes were performed. Brightfield and Fluorescence images were acquired by the Operetta CLS High-Content Analysis System (Perkin Elmer, USA) under 60X objective. Following excitation

channels were acquired; 630/20 nm channel for the AR visualization (red), 475/30 nm for the GFP visualization (green) and 380/40 nm for the Hoechst- nuclear stain (blue).

6.4 Immunoblotting

6.4.1 Cell harvesting and lysis

0,8 million VCaP cells were seeded into 35 mm x 10 mm Tissue Culture -treated culture dish (Sarstedt, Germany) were incubated for 5 days. Prior to collection of cells, medium was aspirated out from the culture dish and cell pellet was gently washed with PBS. Addition of 100 µl of Cell lysis buffer (see Appendix 3.1.2) into the dish was followed with scraping the pellet out by the cell scraper (Celltreat Scientific, USA) which enabled transferring cells in lysis buffer into fresh Eppendorf tube. Protease and phosphatase inhibitors (ThermoFisher Scientific, USA) as well as Sodium Metavanadate ($NaVO_3$) were included in the cell lysis buffer. The Eppendorf tube was next vortexed and left at +4 C° for 20 minutes with additional vortex turn after 10 minutes and just before centrifugation. Centrifugation at 13 000 RPM and + 4 C ° for 20 minutes was further performed. Finally, supernatant was collected from the tube for protein quantity measurement.

6.4.2 Cell lysis and protein measurement

Prior to the assay run, the cell lysates were 5-fold (1/5 of total volume) diluted with a cell lysis buffer. Protein quantity was measured by the bicinchoninic acid (BCA) assay provided by the Pierce™ BCA Protocol Assay kit (ThermoFisher Scientific, USA). BCA assay was prepared by mixing 1 part of Reagent B with 49 parts of Reagent A, so 1/50 ratio in a total sample volume. 200 µl of reagent solution was mixed with a 10 µl of a diluted protein sample or an equal volume of cell lysis buffer in a blank sample. Subsequently, samples were light covered, gently mixed, and incubated at + 37 C ° for 30 minutes. Absorbance was measured by spectrophotometry at 570 nm wavelength / 1 s measurement time, utilizing Victor X4 plate reader (PerkinElmer, USA). Measurements of bovine serum albumin (BSA) standard dilutions, supplied by the kit, generated the standard curve, which was extrapolated for the protein calculations. Western blotting samples were prepared by diluting protein stock in cell lysis buffer, and addition of 4X Laemmli Buffer (Bio-Rad, USA) and β-mercaptoethanol (Sigma-Aldrich, USA) mixture (see Appendix 3.1.3) that constituted ¼ of the total sample volume. The sample mixture was then denatured at + 95 C ° for 5 minutes.

6.4.3 Western blotting

Hand-made 8 % acrylamide gel was prepared (see Appendix 3.1.4) for the western blotting. Prior to lysate addition into wells, the gel was pre-run on 65 V for 15 minutes. After sample and BlueStar Plus MWP04 ladder addition into the gel (Nippon Genetics, Germany), gel was run first on 70 V for 15 minutes and on 100 V for 1 hour. Wet transfer was performed on 80 V for 2 hours and samples were transferred into nitrocellulose membrane. Blocking was performed by 5 % milk in 1X TBST for 1 hour and 15 minutes. Membrane was incubated with the primary antibodies (Table 1.) overnight at in 4 C °. Three washes for 5 minutes with 1X TBST were done before the secondary antibody (Table 1.) incubation at a room temperature for 1 hour. Both primary and secondary antibodies were diluted in 5 % BSA and 1X TBST. After similar 1X TBST washes, membrane was imaged by the Odyssey® CLx system (Li-Cor, USA). Quantification of protein fluorescence signal was enabled by the Image Studio™ software (Li-Cor, USA).

Table 1. Antibodies and nuclear stain utilized for western blotting and immunofluorescence. Application annotation in the first row: IF= immunofluorescence and WB= western blotting.

Application	Type	Reactivity	Dilution	Product origin
IF	Primary antibody	Anti-AR	1 / 200	Santa Cruz Biotechnology, USA
IF	Secondary antibody	Anti-mouse	1 / 300	Invitrogen, ThermoFisher Scientific, USA
IF	Nuclear stain	Hoechst 33342	1 / 600	Invitrogen, ThermoFisher Scientific, USA
WB	Primary antibody	Anti-PSA	1 / 1150	Abcam, UK
WB	Primary antibody	Anti-AR	1 / 1000	ThermoFisher Scientific, USA
WB	Primary antibody	Anti-alfa-tubulin	1/ 5000	Abcam, UK
WB	Secondary antibody	Anti-rabbit	1 / 8000	Li-Cor, USA
WB	Secondary antibody	Anti-mouse	1 / 2500	Li-Cor, USA

6.5 Live-cell imaging

6.5.1 IncuCyte imaging system parameters

All the experimental plates were monitored by the IncuCyte® S3 live-cell imaging system (Sartorius, Germany). Experimental plates of the 2D models were imaged every 12 hours utilizing scan definitions by the IncuCyte S3 2020A (Sartorius, Germany) software. Phase contrast imaging channel was defined for the monoculture scans, and its combination with Green- fluorescence filter for the co-culture model, since CAFs are labelled with GFP. For the 3D models, multi-spheroid scan setting by the software was utilized. Identically with 2D studies, Phase contrast and Green- channels were selected for monoculture and co-culture. Scans of 3D plates were taken every 24 hours. Scans above utilized 10X objective. Whole well imaging scans with 4X objective was also performed for the 3D co-culture.

6.5.2 Live-cell imaging segmentation and proliferation analysis

Proliferation analysis was conducted for the 2D cultures. The analysis was conducted by the IncuCyte S3 2020A (Sartorius, Germany) software with analysis definition of confluence quantification in percentage (%). The analysis segmentation was identical between the monoculture and co-culture, with following parameters; Background = 0.8., Minimum object area filter = 100 μm^2 (Figure 18). In co-culture both VCaP and CAF cells were included into the segmentation and proliferation analysis accordingly (Figure 18b). Generated confluence (%) data from the analysis was normalized and converted into trend presenting proliferation curve with following equation; where Cx = confluence value of the certain time-point within a sample, Cstart= confluence value of the first time-point within a sample, Cmin= minimum observed value:

$$(Cx - (Cstart - Cmin(\ Cstart\ values\ of\ all\ the\ samples))$$

a.)

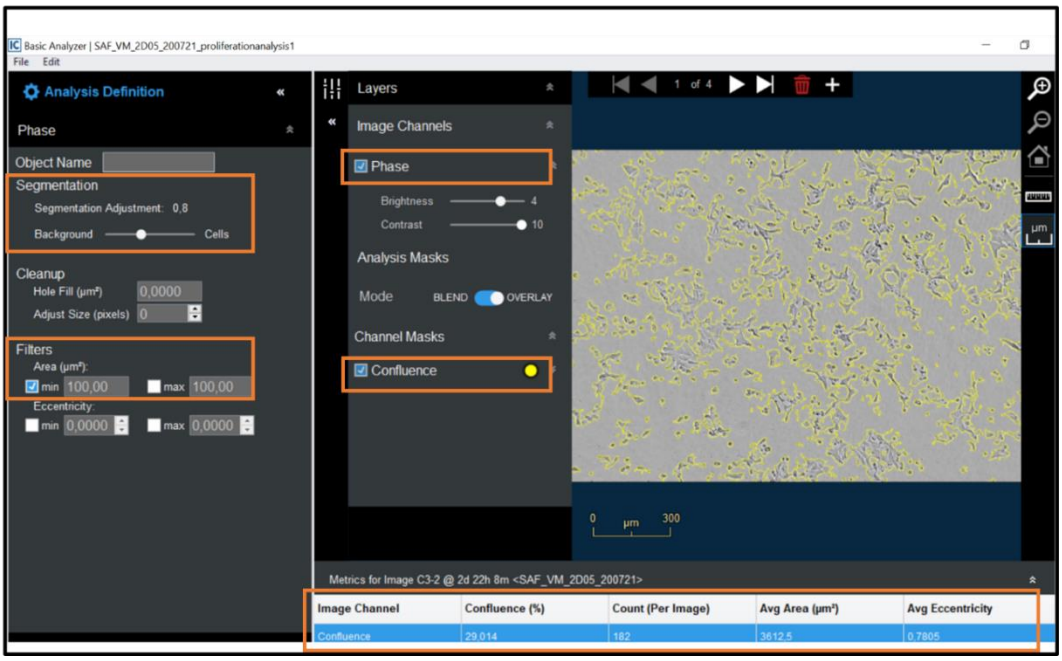

b.)

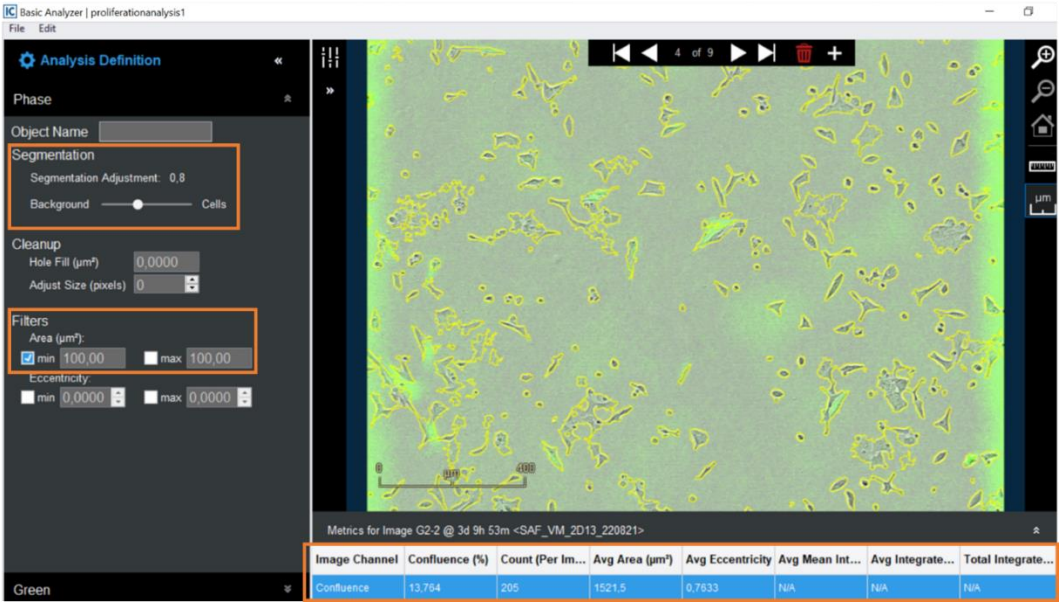

Figure 18. Segmentation parameters for live-cell imaging successfully captured all the tumour cells without artifacts in 2D models. 2D monoculture (a.) and 2D co-culture (b.) images were segmented accordingly prior to the proliferation analysis. The captured image was taken from the IncuCyte S3 2020A (Sartorius, Germany) software, analysis definition window. The framed information indicates the background filter, object area filter, image mask channels, as well as generated results (bottom framed panel).

6.6 Confocal imaging and morphological analysis

6.6.1 Confocal imaging

Prior to organoids were stained, Calcein AM (Invitrogen, ThermoFisher Scientific, USA) and Ethidium Homodimer (EtHD) (Invitrogen, ThermoFisher Scientific, USA) were diluted 1/1000 in DMEM culture medium. At the endpoint of the 3D culture, cell staining was performed with Calcein AM to stain and visualize alive cells and EtHD (Invitrogen, ThermoFisher Scientific, USA) to visualize dead cells in the organoids. Medium of the experimental wells was aspirated and filled with the diluated stains. Plates were incubated at + 37 C ° for 45 minutes. Confocal imaging was conducted with Spinning disk confocal microscope (Zeiss Axiovert-200M, microscope) utilizing the CSU22 spinning disk confocal unit (Yokogawa, Japan). Images were acquired by laser excitation under 488nm for Calcein AM detection and 561nm for EtHD detection. As a results, alive cells were visualized as green and dead cells as red. Images were captured under 5X objective. Acquired images were converted to a maximum intensity projection and batch renormalization was applied in SlideBook 6 software (3i Intelligent Imaging Innovation, USA).

6.6.2 Morphological analysis by AMIDA

Morphological analysis was performed by the AMIDA program (Härmä et al., 2014). Prior to the analysis, images were segmented and filtered by set-up values for accurate organoid identification. The segmentation filters were following; Sensitivity= 20, Threshold=1, Smallest object= 100 (Figure 19). Morphometric data quantified by the AMIDA was visualized as a box and whisker plots generated by RStudio software and statistically analysed. The generated morphometric data was presented by various parameters, which could be divided into three main categories; 1.) Basic morphological parameters, such as average size of the organoid, 2.) Phenotypical parameters, such as invasiveness of the organoid and 3.) Functional parameters, which indicate various statistical appearances of results, e.g., the number of cells per structures, deviation within green or red channel etc. (Härmä et al., 2014). The main parameters of focus in the current study were “roughness” parameter (%), which indicates the proportion of surface roughness of the segmented structure and the “area” parameter indicating the size (in pixels) of the segmented structure (Härmä et al., 2014).

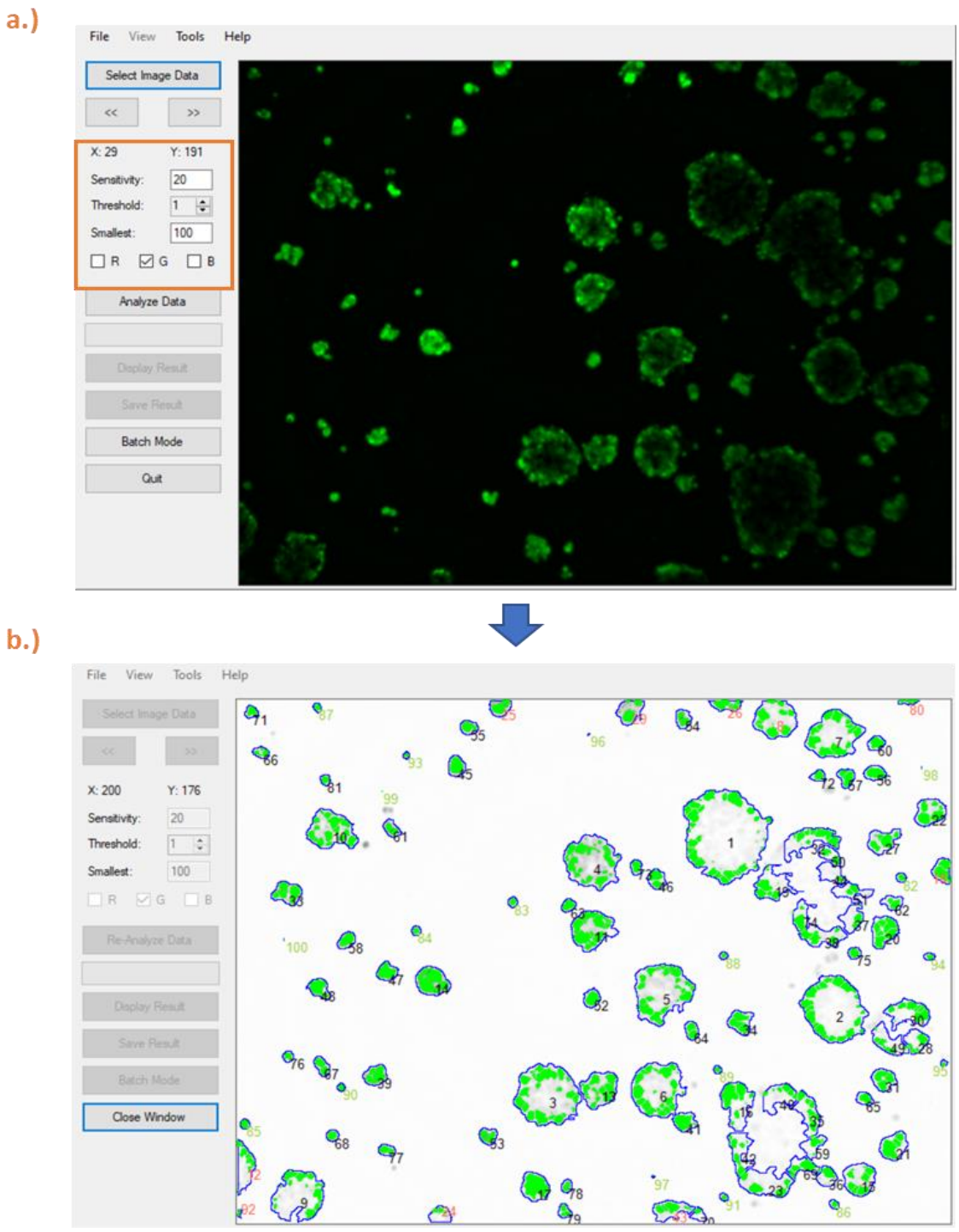

Figure 19. Segmentation set-up values of acquired confocal images of 3D monoculture (a.) and generated segmented organoid identification (b.). Segmented data was then run by AMIDA for morphometric results. The illustrated segmentation was taken for one of the DMSO 0.2 % negative-control wells of 3D monoculture experiment.

6.7 Cell viability assay

Cell viability assay as the last assay for each experiment was conducted by the CellTiter Glo 2.0® reagent (Promega, USA) according to the manual provided by the manufacturer. The CellTiter Glo

reagent was added into each experimental well with a volume equal to the one of the culture medium/well in 2D models or equal to gel suspension/well in 3D models. Experimental plates were shaken by the orbital shaker, variable speed setting for 2 minutes (Delfia®, PerkinElmer, USA). The luminescence signal was quantified by Victor X4 Plate Reader (Perkin Elmer, USA).

6.8 Statistical analysis

GraphPad Prism 9 software was used for the cell viability statistics. Prior to analysis, raw data of the cell viability was background subtracted and baseline-corrected for presenting it as the relative to DMSO-control value in percentage. Relative to DMSO-control sample values were statistically analysed by the Kruskal-Wallis and Dunn's post-hoc test in comparison to DMSO-control, single treatment of each cell culture model, and between all the models as the final comparison. Normality of the data was tested prior to statistical analysis. Morphometric data generated by the AMIDA was statistically analysed with RStudio software by the Mann- Whitney U test with Bonferroni correction as a post-hoc test in comparison to DMSO-control.

Acknowledgments

First of all, I would like to express my sincere gratitude to Matthias Nees and Malin Åkerfelt for their constructive supervision and encouragement, as well as giving me the possibility to work, gain knowledge, skills, and complete a thesis in a wonderful research group. I would like to greatly thank my practical supervisor Syeda Afshan for teaching me various new methods, as well as for the support and patience in guiding me throughout the entire thesis. My huge gratitude goes to the members of Nees research group, Mervi Toriseva, Jesse Mattsson Erica Långbacka, Shaoxia Wang and Jimmy Fagersund for helping in the practical work and sharing your scientific advice. I would want to specially thank Jesse Mattsson for his critical suggestions and assistance during the 3D- experiments. Also, I would like to acknowledge Saiganesh Sriraman, Verneri Virtanen and Antti Kukkula for their assistance in western blotting.

Finally, my warmest thanks to my family and friends for believing in me and supporting me during thesis.

List of abbreviations

ADT	Androgen deprivation therapy
AF-1	Activation Function 1
AF-2	Activation Function 2
AKT	Protein kinase B
AMIDA	Automated morphometric image data analysis
AR	Androgen receptor
ARE	Androgen response elements
ATCC	American Type Culture Collection
CAF	Cancer-associated fibroblast
CRPC	Castration-resistant prostate cancer
DBD	DNA- binding domain
DHT	Dihydrotestosterone
DNPC	Double-negative prostate cancer
ECM	Extracellular matrix
EMT	Epithelial-to-mesenchymal transition
FDA	Food and Drug Administration
FGF	Fibroblast growth factor
FGFR	Fibroblast growth factor receptor
FRS2	FGFR-substrate-2
GLOBOCAN	Global Cancer Observatory from World Health Organization
GnRH	Gonadotropin-releasing hormone

HSPG	Heparin/heparan sulphate proteoglycan
JAK	Janus kinase
LBD	Ligand- binding domain
LH	Luteinizing hormone
LSD1	Lysine-specific demethylase 1
MAPK	Mitogen-activated protein kinase
MoA	Mechanism of action
NE	Neuroendocrine
NSAA	Non-steroidal antiandrogen
NTD	N-terminal domain
OS	Overall survival
PC	Prostate cancer
PIA	Proliferative inflammatory atrophy
PIN	Prostatic intraepithelial neoplasia
PLCγ	Phospholipase C-γ
PSA	Prostate-specific antigen
PSCs	Prostate stem cells
RTK	Receptor tyrosine kinase
TK	Tyrosine kinase
TME	Tumour microenvironment

7 References

Aaron, L., Franco, O. E., & Hayward, S. W. (2016). Review of Prostate Anatomy and Embryology and the Etiology of Benign Prostatic Hyperplasia. *The Urologic clinics of North America*, *43*(3), 279–288. https://doi.org/10.1016/j.ucl.2016.04.012

Åkerfelt, M., Bayramoglu, N., Robinson, S., Toriseva, M., Schukov, H. P., Härmä, V., Virtanen, J., Sormunen, R., Kaakinen, M., Kannala, J., Eklund, L., Heikkilä, J., & Nees, M. (2015). Automated tracking of tumor-stroma morphology in microtissues identifies functional targets within the tumor microenvironment for therapeutic intervention. *Oncotarget, 6*(30), 30035–30056. https://doi.org/10.18632/oncotarget.5046

Alizadeh, M., & Alizadeh, S. (2014). Survey of clinical and pathological characteristics and outcomes of patients with prostate cancer. *Global journal of health science, 6*(7 Spec No), 49–57. https://doi.org/10.5539/gjhs.v6n7p49

Aly, M., Leval, A., Schain, F., Liwing, J., Lawson, J., Vágó, E., Nordström, T., Andersson, T. M., Sjöland, E., Wang, C., Eloranta, S., & Akre, O. (2020). Survival in patients diagnosed with castration-resistant prostate cancer: a population-based observational study in Sweden. *Scandinavian journal of urology*, *54*(2), 115–121. https://doi.org/10.1080/21681805.2020.1739139

Anguiano, M., Morales, X., Castilla, C., Pena, A. R., Ederra, C., Martínez, M., Ariz, M., Esparza, M., Amaveda, H., Mora, M., Movilla, N., Aznar, J. M. G., Cortés-Domínguez, I., & Ortiz-de-Solorzano, C. (2020). The use of mixed collagen-Matrigel matrices of increasing complexity recapitulates the biphasic role of cell adhesion in cancer cell migration: ECM sensing, remodeling and forces at the leading edge of cancer invasion. *PloS one*, *15*(1), e0220019. https://doi.org/10.1371/journal.pone.0220019

Antonarakis, E. S., Chandhasin, C., Osbourne, E., Luo, J., Sadar, M. D., & Perabo, F. (2016). Targeting the N-Terminal Domain of the Androgen Receptor: A New Approach for the Treatment of Advanced Prostate Cancer. *The oncologist, 21*(12), 1427–1435. https://doi.org/10.1634/theoncologist.2016-0161

Attardi, B. J., Hild, S. A., Koduri, S., Pham, T., Pessaint, L., Engbring, J., Till, B., Gropp, D., Semon, A., & Reel, J. R. (2010). The potent synthetic androgens, dimethandrolone (7α,11β-dimethyl-19-nortestosterone) and 11β-methyl-19-nortestosterone, do not require 5α-reduction to exert their maximal androgenic effects. *The Journal of steroid biochemistry and molecular biology*, *122*(4), 212–218. https://doi.org/10.1016/j.jsbmb.2010.06.009

Aw Yong, K. M., Sun, Y., Merajver, S. D., & Fu, J. (2017). Mechanotransduction-Induced Reversible Phenotypic Switching in Prostate Cancer Cells. *Biophysical journal, 112*(6), 1236–1245. https://doi.org/10.1016/j.bpj.2017.02.012

Barron, D. A., & Rowley, D. R. (2012). The reactive stroma microenvironment and prostate cancer progression. *Endocrine-related cancer, 19*(6), R187–R204. https://doi.org/10.1530/ERC-12-0085

Bissell, M. J., & Hines, W. C. (2011). Why don't we get more cancer? A proposed role of the microenvironment in restraining cancer progression. *Nature medicine, 17*(3), 320–329. https://doi.org/10.1038/nm.2328

Bjartell, A., Montironi, R., Berney, D. M., & Egevad, L. (2011). Tumour markers in prostate cancer II: diagnostic and prognostic cellular biomarkers. *Acta oncologica (Stockholm, Sweden), 50* Suppl 1, 76–84. https://doi.org/10.3109/0284186X.2010.531284

Bluemn, E. G., Coleman, I. M., Lucas, J. M., Coleman, R. T., Hernandez-Lopez, S., Tharakan, R., Bianchi-Frias, D., Dumpit, R. F., Kaipainen, A., Corella, A. N., Yang, Y. C., Nyquist, M. D., Mostaghel, E., Hsieh, A. C., Zhang, X., Corey, E., Brown, L. G., Nguyen, H. M., Pienta, K., Ittmann, M., … Nelson, P. S. (2017). Androgen Receptor Pathway-Independent Prostate Cancer Is Sustained through FGF Signaling. *Cancer cell, 32*(4), 474–489.e6. https://doi.org/10.1016/j.ccell.2017.09.003

Bonollo, F., Thalmann, G, N., Kruithof-de Julio, M., Karkampouna, S. (2020). The Role of Cancer-Associated Fibroblasts in Prostate Cancer Tumorigenesis. *Cancers, 12*(7):1887. https://doi.org/10.3390/cancers12071887

Borgmann, H., Lallous, N., Ozistanbullu, D., Beraldi, E., Paul, N., Dalal, K., Fazli, L., Haferkamp, A., Lejeune, P., Cherkasov, A., & Gleave, M. E. (2018). Moving Towards Precision Urologic Oncology: Targeting Enzalutamide-resistant Prostate Cancer and Mutated Forms of the Androgen Receptor Using the Novel Inhibitor Darolutamide (ODM-201). *European urology, 73*(1), 4–8. https://doi.org/10.1016/j.eururo.2017.08.012

Brawer M. K. (2005). Prostatic intraepithelial neoplasia: an overview. *Reviews in urology*, *7 Suppl 3*(Suppl 3), S11–S18.

Butler, W., & Huang, J. (2021). Neuroendocrine cells of the prostate: Histology, biological functions, and molecular mechanisms. *Precision clinical medicine, 4*(1), 25–34. https://doi.org/10.1093/pcmedi/pbab003

Chae, Y. K., Ranganath, K., Hammerman, P. S., Vaklavas, C., Mohindra, N., Kalyan, A., Matsangou, M., Costa, R., Carneiro, B., Villaflor, V. M., Cristofanilli, M., & Giles, F. J. (2017). Inhibition of the fibroblast growth factor receptor (FGFR) pathway: the current

landscape and barriers to clinical application. *Oncotarget, 8*(9), 16052–16074. https://doi.org/10.18632/oncotarget.14109

Chen, S. Y., Cai, C., Fisher, C. J., Zheng, Z., Omwancha, J., Hsieh, C. L., & Shemshedini, L. (2006). c-Jun enhancement of androgen receptor transactivation is associated with prostate cancer cell proliferation. *Oncogene*, *25*(54), 7212–7223. https://doi.org/10.1038/sj.onc.1209705

Chiodelli, P., Coltrini, D., Turati, M., Cerasuolo, M., Maccarinelli, F., Rezzola, S., Grillo, E., Giacomini, A., Taranto, S., Mussi, S., Ligresti, A., Presta, M., & Ronca, R. (2022). FGFR blockade by pemigatinib treats naïve and castration resistant prostate cancer. *Cancer letters*, *526*, 217–224. https://doi.org/10.1016/j.canlet.2021.11.030

Choi, E., Buie, J., Camacho, J., Sharma, P., & de Riese, W. T. W. (2022). Evolution of Androgen Deprivation Therapy (ADT) and Its New Emerging Modalities in Prostate Cancer: An Update for Practicing Urologists, Clinicians and Medical Providers. *Research and reports in urology, 14*, 87–108. https://doi.org/10.2147/RRU.S303215

Dai, C., Heemers, H., & Sharifi, N. (2017). Androgen Signalling in Prostate Cancer. Cold Spring *Harbor perspectives in medicine, 7*(9), a030452. https://doi.org/10.1101/cshperspect.a030452

Davey, R. A., & Grossmann, M. (2016). Androgen Receptor Structure, Function and Biology: From Bench to Bedside. *The Clinical biochemist. Reviews, 37*(1), 3–15.

Eder, T., Weber, A., Neuwirt, H., Grünbacher, G., Ploner, C., Klocker, H., Sampson, N., & Eder, I. E. (2016). Cancer-Associated Fibroblasts Modify the Response of Prostate Cancer Cells to Androgen and Anti-Androgens in Three-Dimensional Spheroid Culture. *International journal of molecular sciences, 17*(9), 1458. https://doi.org/10.3390/ijms17091458

Ehsani, M., David, F. O., & Baniahmad, A. (2021). Androgen Receptor-Dependent Mechanisms Mediating Drug Resistance in Prostate Cancer. *Cancers, 13*(7), 1534. https://doi.org/10.3390/cancers13071534

Ellem, S. J., De-Juan-Pardo, E. M., & Risbridger, G. P. (2014). In vitro modeling of the prostate cancer microenvironment. *Advanced drug delivery reviews, 79-80*, 214–221. https://doi.org/10.1016/j.addr.2014.04.008

Erdogan, B., & Webb, D. J. (2017). Cancer-associated fibroblasts modulate growth factor signaling and extracellular matrix remodeling to regulate tumor metastasis. *Biochemical Society transactions, 45*(1), 229–236. https://doi.org/10.1042/BST20160387

Feng, S., Shao, L., Yu, W., Gavine, P., & Ittmann, M. (2012). Targeting fibroblast growth factor receptor signaling inhibits prostate cancer progression. *Clinical cancer research : an official*

journal of the American Association for Cancer Research, 18(14), 3880–3888. https://doi.org/10.1158/1078-0432.CCR-11-3214

Fizazi, K., Smith, M. R., & Tombal, B. (2018). Clinical Development of Darolutamide: A Novel Androgen Receptor Antagonist for the Treatment of Prostate Cancer. *Clinical genitourinary cancer, 16*(5), 332–340. https://doi.org/10.1016/j.clgc.2018.07.017

Fontana, F., Raimondi, M., Marzagalli, M., Sommariva, M., Gagliano, N., & Limonta, P. (2020). Three-Dimensional Cell Cultures as an In Vitro Tool for Prostate Cancer Modeling and Drug Discovery. *International journal of molecular sciences, 21*(18), 6806. https://doi.org/10.3390/ijms21186806

Giacomini, A., Grillo, E., Rezzola, S., Ribatti, D., Rusnati, M., Ronca, R., & Presta, M. (2021). The FGF/FGFR system in the physiopathology of the prostate gland. *Physiological reviews, 101*(2), 569–610. https://doi.org/10.1152/physrev.00005.2020

Härmä, V., Schukov, H. P., Happonen, A., Ahonen, I., Virtanen, J., Siitari, H., Åkerfelt, M., Lötjönen, J., & Nees, M. (2014). Quantification of dynamic morphological drug responses in 3D organotypic cell cultures by automated image analysis. *PloS one, 9*(5), e96426. https://doi.org/10.1371/journal.pone.0096426

Hegab, A. E., Ozaki, M., Kameyama, N., Gao, J., Kagawa, S., Yasuda, H., Soejima, K., Yin, Y., Guzy, R. D., Nakamura, Y., Ornitz, D. M., & Betsuyaku, T. (2019). Effect of FGF/FGFR pathway blocking on lung adenocarcinoma and its cancer-associated fibroblasts. *The Journal of pathology*, *249*(2), 193–205. https://doi.org/10.1002/path.5290

Helsen, C., Van den Broeck, T., Voet, A., Prekovic, S., Van Poppel, H., Joniau, S., & Claessens, F. (2014). Androgen receptor antagonists for prostate cancer therapy, *Endocrine-Related Cancer, 21*(4), T105-T118. Retrieved Sep 15, 2021, from https://erc.bioscientifica.com/view/journals/erc/21/4/T105.xml

Hu, J. C., Nguyen, P., Mao, J., Halpern, J., Shoag, J., Wright, J. D., & Sedrakyan, A. (2017). Increase in Prostate Cancer Distant Metastases at Diagnosis in the United States. *JAMA oncology*, *3*(5), 705–707. https://doi.org/10.1001/jamaoncol.2016.5465

Jiang, Y., Zhang, H., Wang, J., Liu, Y., Luo, T., & Hua, H. (2022). Targeting extracellular matrix stiffness and mechanotransducers to improve cancer therapy. *Journal of hematology & oncology*, *15*(1), 34. https://doi.org/10.1186/s13045-022-01252-0

Joseph, J. S. , Malindisa, S. T. , & Ntwasa, M. (2018). Two-Dimensional (2D) and Three-Dimensional (3D) Cell Culturing in Drug Discovery. In (Ed.), *Cell Culture.* IntechOpen. https://doi.org/10.5772/intechopen.81552

Kirby, M., Hirst, C., & Crawford, E. D. (2011). Characterising the castration-resistant prostate cancer population: a systematic review. *International journal of clinical practice,* 65(11), 1180–1192. https://doi.org/10.1111/j.1742-1241.2011.02799.x

Labanca, E., Yang, J., Shepherd, P. D. A., Wan, X., Starbuck, M. W., Guerra, L. D., Anselmino, N., Bizzotto, J. A., Dong, J., Chinnaiyan, A. M., Ravoori, M. K., Kundra, V., Broom, B. M., Corn, P. G., Troncoso, P., Gueron, G., Logothethis, C. J., & Navone, N. M. (2022). Fibroblast Growth Factor Receptor 1 Drives the Metastatic Progression of Prostate Cancer. *European urology oncology, 5*(2), 164–175. https://doi.org/10.1016/j.euo.2021.10.001

Leung, J. K., & Sadar, M. D. (2017). Non-Genomic Actions of the Androgen Receptor in Prostate Cancer. Frontiers in endocrinology, 8, 2. https://doi.org/10.3389/fendo.2017.00002

Litwin, M. S., & Tan, H. J. (2017). The Diagnosis and Treatment of Prostate Cancer: A Review. *JAMA, 317*(24), 2532–2542. https://doi.org/10.1001/jama.2017.7248

Luthold, C., Hallal, T., Labbé, D. P., & Bordeleau, F. (2022). The Extracellular Matrix Stiffening: A Trigger of Prostate Cancer Progression and Castration Resistance?. *Cancers, 14*(12), 2887. https://doi.org/10.3390/cancers14122887

Maia, A., & Wiemann, S. (2021). Cancer-Associated Fibroblasts: Implications for Cancer Therapy. *Cancers*, *13*(14), 3526. https://doi.org/10.3390/cancers13143526

Makino, T., Izumi, K., & Mizokami, A. (2021). Undesirable Status of Prostate Cancer Cells after Intensive Inhibition of AR Signaling: Post-AR Era of CRPC Treatment. *Biomedicines, 9*(4), 414. https://doi.org/10.3390/biomedicines9040414

McKillup, S (2012). *Statistics Explained: An Introductory Guide for Life Scientists (2nd edition).* Cambridge University Press

McPhee, S. J., & Hammer, G. D. (2014). Pathophysiology of disease: An introduction to clinical medicine (7th edition.). New York: McGraw-Hill.

Mohler, J. L., Antonarakis, E. S., Armstrong, A. J., D'Amico, A. V., Davis, B. J., Dorff, T., Eastham, J. A., Enke, C. A., Farrington, T. A., Higano, C. S., Horwitz, E. M., Hurwitz, M., Ippolito, J. E., Kane, C. J., Kuettel, M. R., Lang, J. M., McKenney, J., Netto, G., Penson, D. F., Plimack, E. R., … Freedman-Cass, D. A. (2019). Prostate Cancer, Version 2.2019, NCCN Clinical Practice Guidelines in Oncology. *Journal of the National Comprehensive Cancer Network : JNCCN, 17*(5), 479–505. https://doi.org/10.6004/jnccn.2019.0023

Osorio, C. F. E. M., Costa, W. S., Gallo, C. B. M., & Sampaio, F. J. B. (2019). Expression of stromal elements of prostatic adenocarcinoma in different gleason scores. *Acta cirurgica brasileira*, *34*(10), e201901005. https://doi.org/10.1590/s0102-865020190100000005

Packer, J. R., & Maitland, N. J. (2016). The molecular and cellular origin of human prostate cancer. *Biochimica et biophysica acta, 1863*(6 Pt A), 1238–1260. https://doi.org/10.1016/j.bbamcr.2016.02.016

Parker, C., Castro, E., Fizazi, K., Heidenreich, A., Ost, P., Procopio, G., Tombal, B., Gillessen, S., & ESMO Guidelines Committee. Electronic address: clinicalguidelines@esmo.org (2020). *Prostate cancer: ESMO Clinical Practice Guidelines for diagnosis, treatment and follow-up. Annals of oncology : official journal of the European Society for Medical Oncology, 31*(9), 1119–1134. https://doi.org/10.1016/j.annonc.2020.06.011

Parsons, B. A., Evans, S., & Wright, M. P. (2009). Prostate cancer and urinary incontinence. *Maturitas, 63*(4), 323–328. https://doi.org/10.1016/j.maturitas.2009.06.005

Rebello, R. J., Oing, C., Knudsen, K. E., Loeb, S., Johnson, D. C., Reiter, R. E., Gillessen, S., Van der Kwast, T., & Bristow, R. G. (2021). *Prostate cancer. Nature reviews. Disease primers, 7*(1), 9. https://doi.org/10.1038/s41572-020-00243-0

Sampson, N., Neuwirt, H., Puhr, M., Klocker, H., & Eder, I. E. (2013). In vitro model systems to study androgen receptor signaling in prostate cancer. *Endocrine-related cancer, 20*(2), R49–R64. https://doi.org/10.1530/ERC-12-0401’

Sehn J. K. (2018). Prostate Cancer Pathology: Recent Updates and Controversies. *Missouri medicine*, *115*(2), 151–155.

Siegel, R. L., Miller, K. D., & Jemal, A. (2019). Cancer statistics, 2019. *CA: a cancer journal for clinicians,* 69(1), 7–34. https://doi.org/10.3322/caac.21551

Source: ECIS - European Cancer Information System
From https://ecis.jrc.ec.europa.eu, accessed on 17/April/2023
© European Union, 2023

Source: UroToday.com (2012). History of prostate cancer: Diagnosis and treatment timeline - 1904 to 2012. From https://www.urotoday.com/recent-abstracts/urologic-oncology/prostate-cancer/56112-prostate-cancer-treatment-timeline.html (accessed on 19 /July /2023)
© UroToday, 2012

Sugawara, T., Baumgart, S. J., Nevedomskaya, E., Reichert, K., Steuber, H., Lejeune, P., Mumberg, D., & Haendler, B. (2019). Darolutamide is a potent androgen receptor antagonist with strong efficacy in prostate cancer models. *International journal of cancer*, *145*(5), 1382–1394. https://doi.org/10.1002/ijc.32242

Sung, H., Ferlay, J., Siegel, R. L., Laversanne, M., Soerjomataram, I., Jemal, A., & Bray, F. (2021). Global Cancer Statistics 2020: GLOBOCAN Estimates of Incidence and Mortality

Worldwide for 36 Cancers in 185 Countries. *CA: a cancer journal for clinicians*, *71*(3), 209–249. https://doi.org/10.3322/caac.21660

Tan, L., Wang, J., Tanizaki, J., Huang, Z., Aref, A. R., Rusan, M., Zhu, S. J., Zhang, Y., Ercan, D., Liao, R. G., Capelletti, M., Zhou, W., Hur, W., Kim, N., Sim, T., Gaudet, S., Barbie, D. A., Yeh, J. R., Yun, C. H., Hammerman, P. S., Mohammadi, M., Jänne, P. A., Gray, N. S. (2014). Development of covalent inhibitors that can overcome resistance to first-generation FGFR kinase inhibitors. *Proceedings of the National Academy of Sciences of the United States of America, 111*(45), E4869–E4877. https://doi.org/10.1073/pnas.1403438111

Teishima, J., Hayashi, T., Nagamatsu, H., Shoji, K., Shikuma, H., Yamanaka, R., Sekino, Y., Goto, K., Inoue, S., & Matsubara, A. (2019). Fibroblast Growth Factor Family in the Progression of Prostate Cancer. *Journal of clinical medicine, 8*(2), 183. https://doi.org/10.3390/jcm8020183

Teo, M. Y., Rathkopf, D. E., & Kantoff, P. (2019). Treatment of Advanced Prostate Cancer. *Annual review of medicine,* 70, 479–499. https://doi.org/10.1146/annurev-med-051517-011947

Van Hemelryk, A., Mout, L., Erkens-Schulze, S., French, P. J., van Weerden, W. M., & van Royen, M. E. (2021). Modeling Prostate Cancer Treatment Responses in the Organoid Era: 3D Environment Impacts Drug Testing. *Biomolecules*, *11*(11), 1572. https://doi.org/10.3390/biom11111572

Vellky, J. E., & Ricke, W. A. (2020). Development and prevalence of castration-resistant prostate cancer subtypes. *Neoplasia (New York, N.Y.), 22*(11), 566–575. https://doi.org/10.1016/j.neo.2020.09.002

Wang, G., Zhao, D., Spring, D. J., & DePinho, R. A. (2018). Genetics and biology of prostate cancer. *Genes & development*, *32*(17-18), 1105–1140. https://doi.org/10.1101/gad.315739.118

Wang, L., Lu, B., He, M., Wang, Y., Wang, Z., & Du, L. (2022). Prostate Cancer Incidence and Mortality: Global Status and Temporal Trends in 89 Countries From 2000 to 2019. Frontiers in public health, 10, 811044. https://doi.org/10.3389/fpubh.2022.81104

Xie, Q., Liu, Y., Cai, T., Horton, C., Stefanson, J., & Wang, Z. A. (2017). Dissecting cell-type-specific roles of androgen receptor in prostate homeostasis and regeneration through lineage tracing. *Nature communications, 8,* 14284. https://doi.org/10.1038/ncomms14284

Xie, Y., Su, N., Yang, J., Tan, Q., Huang, S., Jin, M., Ni, Z., Zhang, B., Zhang, D., Luo, F., Chen, H., Sun, X., Feng, J. Q., Qi, H., & Chen, L. (2020). FGF/FGFR signaling in health and disease. *Signal transduction and targeted therapy, 5*(1), 181. https://doi.org/10.1038/s41392-020-00222-7

Xin L. (2013). Cells of origin for cancer: an updated view from prostate cancer. Oncogene, 32(32), 3655–3663. https://doi.org/10.1038/onc.2012.541

Yu Gang Kim (2021). The effects of the combination treatment of AR and FGFR inhibitors in prostate cancer. [Master's thesis, University of Turku]. UTUPub https://www.utupub.fi/handle/10024/152397

Yu, L., Toriseva, M., Afshan, S., Cangiano, M., Fey, V., Erickson, A., Seikkula, H., Alanen, K., Taimen, P., Ettala, O., Nurmi, M., Boström, P. J., Kallajoki, M., Tuomela, J., Mirtti, T., Beumer, I. J., Nees, M., & Härkönen, P. (2022). Increased Expression and Altered Cellular Localization of Fibroblast Growth Factor Receptor-Like 1 (FGFRL1) Are Associated with Prostate Cancer Progression. *Cancers, 14*(2), 278. https://doi.org/10.3390/cancers14020278

Yu, L., Toriseva, M., Tuomala, M., Seikkula, H., Elo, T., Tuomela, J., Kallajoki, M., Mirtti, T., Taimen, P., Boström, P. J., Alanen, K., Nurmi, M., Nees, M., & Härkönen, P. (2016). Increased expression of fibroblast growth factor 13 in prostate cancer is associated with shortened time to biochemical recurrence after radical prostatectomy. *International journal of cancer, 139*(1), 140–152. https://doi.org/10.1002/ijc.30048

Zhang, D., Zhao, S., Li, X., Kirk, J. S., & Tang, D. G. (2018). Prostate Luminal Progenitor Cells in Development and Cancer. *Trends in cancer*, *4*(11), 769–783. https://doi.org/10.1016/j.trecan.2018.09.003

8 Appendices

8.1 Ingredients

8.1.1 Fixation solution for the Immunofluorescence

4 % Paraformaldehyde (PFA)

- 100 % PFA (Sigma-Aldrich, USA)
- MiliQ- H_2O

0,5 % Triton X100 (10 ml)

- 100 % Triton X100 (Sigma-Aldrich, USA)
- 3 % BSA (Biowest, USA) in 1X PBS (Cityva, USA)

Fixation solution stored at room temperature.

8.1.2 Cell lysis buffer (base)

- MiliQ- H_2O = 174 ml
- 5 M NaCl = 4 ml
- 0,5 M NaF = 4 ml
- 1 M Tris-Cl (pH 7,4) = 4 ml
- 1 % Triton X-100 = 2 ml
- 0,5 M EDTA = 400 µl

Aliquot of the base mixed with inhibitors and Na_3VO_4 :

- 100mM Na_3VO_4 = 1 % = 1 mM from the total aliquot volume
- Phosphatase inhibitor cocktail (ThermoFisher Scientific, USA) = 1 Tablet
- Protease inhibitor cocktail (ThermoFisher Scientific, USA) = 1 Tablet

Cell lysis buffer stored at +4 C °.

8.1.3 4X Laemili Buffer + β-mercaptoethanol mixture for the western blotting

• 4X Laemili buffer (Bio-Rad, USA) = 9/10 of total volume

• β-mercaptoethanol (Sigma-Aldrich, USA), 1/10 of total volume

Mixture stored at room temperature.

8.1.4 Acrylamide gel (8 %) for the western blotting

Upper / Stacking gel (two gels)

- MiliQ-H_2O = 3,05 ml
- Acrylamide = 0,65 ml
- 4X Upper gel buffer = 1,25 ml
- 10 % APS = 30 µl
- Temed = 10 µl

Lower / Separation gel (two gels)

- MiliQ-H_2O = 7,25 ml
- Acrylamide = 4 ml
- 4X Upper gel buffer = 3,75 ml
- 10 % APS = 50 µl
- Temed = 10 µl

Gels strored at +4 C °.

8.1.5 Collagen type 1 pH neutralization (BD Biosciences, USA)

Preparation of 1000 µl of 3 mg/ml Collagen working stock:

- 800 µl of 3.8 mg/ml collagen stock

- 100 µl of 10 x RMPI CM (Roswell Park Memorial Institute (RPMI) 1640 Medium (Gibco, ThermoFisher Scientific, USA)
- 40 µl of 1M HEPES buffer
- 30 µl of sodium bicarbonate 7,5 %
- 16 µl of NaOH 1M
- 14 µl of sterile H_20